# FINAL REPORT: STUDY OF THE FEASIBILITY OF AN EARLY LUNAR FLARE

**JULY 1964**
**DOUGLAS REPORT SM-47954**

MISSILE & SPACE SYSTEMS DIVISION
DOUGLAS AIRCRAFT COMPANY, INC.
SANTA MONICA CALIFORNIA

DOUGLAS

# FINAL REPORT: STUDY OF THE FEASIBILITY OF AN EARLY LUNAR FLARE

JULY 1964
DOUGLAS REPORT SM-47954

PREPARED FOR HEADQUARTERS,
NATIONAL AERONAUTICS AND
SPACE ADMINISTRATION
CONTRACT NO. NAS 7-281

APPROVED BY: R.B. CANRIGHT
PROGRAM MANAGER, ELF

DOUGLAS MISSILE & SPACE SYSTEMS DIVISION

CONTENTS

# Section 1
# INTRODUCTION

In early 1963 the Missile and Space Systems Division of Douglas Aircraft Company, Inc. was asked to recommend the best method for obtaining early experimental information on the physical and chemical characteristics of the lunar surface material. The use of a chemical flare, composed of chlorine trifluoride and aluminum, had already been proposed in late 1962 by the Propellants Division of Amoco Chemicals Corporation. On the basis that any information, if it was to be obtained at an early date, should be both simply and economically obtained, Douglas recommended that the Amoco proposed flare be integrated with a spacecraft in Douglas Report SM-434201, dated 19 October 1963.

Subcontractors were brought together to form a capable investigating team, which included the Electro-Optical Division of Perkin-Elmer Corporation and Shock-Hydrodynamics, Inc. On 1 April 1964, this team was awarded a contract to investigate experimentally and analytically the feasibility of utilizing such a lunar-flare concept to analyze the chemical composition and physical structure of the moon's surface. Unfortunately, system feasibility considerations were not funded in this initial study.

Facts concerning chemical composition and the physical structure of the lunar surface will have a profound effect on current planning for the United States' space program. To cite a few examples; the determination that the dust layer on the moon's surface is more than 6 feet deep, and formed of very porous material, would certainly influence the design of the Lunar Excursion Module for Apollo; moreover, the discovery that chemically bound hydrogen is present on the moon might dramatically reduce the cost of interplanetary exploration by an order of magnitude. The results obtained thus far in the preliminary ELF studies seem to indicate that such questions can be resolved by an early flight program which utilizes the lunar-flare concept.

## Section 2
## SUMMARY

Several questions concerning the static and dynamic compatibility of flare structural materials with chlorine trifluoride have been answered. Air combustion tests indicate that a slightly aluminum-rich-mixture ratio gives the best performance if the aluminum is finely divided. These same tests as well as the vacuum tests show that increasing the soil dilution decreases the light yield from the flare. The vacuum tests of the flare indicate a fairly high degree of soil constituents excitation. Also, differentiation between calibration and soil shots as well as between three different soils is easily made from the resulting spectra. Conversion of chemical energy into light energy was approximately one-half of one percent for both the air combustion and vacuum impact tests. The peak temperature achieved in the tests was estimated to be roughly 5000°K. The impact tests proved impact ignition at lunar speeds in both hard and soft targets. The light output from the tests extrapolated to a full-size flare (50, 000 grams) on the moon was evaluated from an earth observational standpoint and found to be adequate for several classes of equipment and instrumentation (existing and proposed) which can be used to record and analyze spectroscopically and photometrically. Because of their varied capabilities a number of observatories in the southwest U. S. will be required to observe the event. Prediction of where and when the flare would impact the moon presents no unusual problems and can be easily accomplished by the Deep Space Net. Finally, an analysis of the impact event was made on high-speed computers and results indicate that a triorthogonal configuration has the greatest probability of successfully meeting all the requirements in a near-surface reaction against both hard and soft targets.

## Section 3
## EXPERIMENTATION

The purpose of all experimentation was to establish the technical feasibility of using a high-temperature chemical flare concept to determine approximate chemical and physical characteristics of simulated lunar surface materials. The experiments were to be simple, economical, and accelerated; however, as the program got underway it soon became obvious that these operational objectives would have to be compromised somewhat in order to obtain sufficient confidence in feasibility. The general technical objectives were: experimental definition of the impact phenomena to be expected, the time history of temperature and light intensity for the reactants chosen under varying conditions, and the spectral determination of the relative abundance of soil constituents admixed in an aluminum/chlorine trifluoride flame. The specific technical objectives of the experiments were:

1. To determine static and dynamic compatibility of candidate payload materials.
2. To determine the luminosity and temperature of the reaction.
3. To determine the scaling factors which would lead to the prediction of parameters for the full scale flare.
4. Determine whether the reaction chosen would activate simulated lunar soils spectroscopically.
5. To determine the effects of high speed impact on reaction initiation, luminosity, and soil involvement.
6. To determine spectroscopic correlation of relative abundance of soil constituents.

To accomplish these objectives the following experiments were planned and carried out.

## 3.1 COMPATIBILITY EXPERIMENTS

The objective of these tests was to determine whether or not basic flare materials were compatible under the anticipated environmental conditions.

### 3.1.1 Static Compatibility Tests

These tests were to determine the compatibility of candidate flare materials under static, elevated temperature conditions over a relatively long period of time. Results would be used to answer filling, sealing, and storage questions concerning the end-item flare.

#### 3.1.1.1 Summary

Eight small (5cc), heavy-wall, aluminum containers were filled with CTF and stored for seven days at 340°K (92 psi). One leaked empty and two others could not be opened. The other five showed very little corrosion in the container body. The threads of the one that leaked showed some corrosion.

#### 3.1.1.2 Test Setup

A standard temperature controlled oven located in a test bay at the Amoco facility at Seymour, Indiana was used.

#### 3.1.1.3 Instrumentation

Standard temperature gauge.

#### 3.1.1.4 Results

The containers were fabricated from 1100 and 6061 aluminum and five of the eight containers survived the test sufficiently well to conclude that massive aluminum is stable toward CTF (as received from the mfgr, $\approx$ 1% HF) under storage at 340°K. The seals remain a questionable item.

### 3.1.2 Dynamic Compatibility Tests

The purpose of these tests was to determine the compatibility of candidate flare materials in dynamic, elevated temperature environment for shorter periods of time consistent with expected flare launch and handling conditions.

### 3.1.2.1 Summary

Two small configuration vessels, one thin walled, were subjected to vibration, drop, and rifle fire impact tests. The thin-walled vessel contained aluminum powder and foil in a stoichiometric mixture ratio with CTF. Both vesseles were stable under all conditions tested.

### 3.1.2.2 Test Setup

For the vibration tests a standard uniaxial shaker with mount stem protruding thru a hole in the side of the temperature controlled oven was employed. A clamp on the end of the stem held each vessel during its test. The frequencies shown in Table 3-1 were scanned manually and when a resonance was observed the test was conducted at that point; if no resonance occurred a mid-range setting was employed for the duration of the test. All tests were run at 340°K.

Table 3-1
VIBRATION

| Frequency (cps) | Acceleration (g) | Duration (min.) | Simulation |
|---|---|---|---|
| 10 | 2 | 60 | Grount Transport |
| 5-50 | 2.3 | 10 | Launch |
| 50-500 | 11 | 10 | Launch |
| 500-2000 | 21 | 10 | Launch |
| 2000-3000 | 40 | 10 | Launch |
| 3000-5000 | 21 | 10 | Launch |

The drop tests were made to determine the sensitivity of flare configurations in case of an accidental drop. Two configurations were dropped from a height of 8 feet onto concrete resulting in estimated decelerations up to 50,000 g.

The two vessels that could not be opened after the static compatibility tests were subjected to .22 calibre rifle fire at room temperature.

#### 3.1.2.3 Instrumentation

A vibration scanner, clock, and standard temperature gauge were used in conjunction with visual observations.

#### 3.1.2.4 Results

In the vibration tests both vessels were stable under all conditions; no initiation occurred. In the drop test no initiation occurred, and the vessels were disposed of by rifle fire.

In the rifle fire tests the contents of both vessels ignited and burned including the lead bullet (which was contained in the aluminum shell). However, the vessel was substantially unaffected despite initiation of a lead-CTF flare.

## 3.2 COMBUSTION EXPERIMENTS

These experiments comprise some of the efforts of Amoco in establishing design parameters for optimum mixture ratio, configuration, scaling factor, effects of soil penetration, and vacuum compatibility of the chemical reaction chosen.

### 3.2.1 Mixture Ratio Tests

#### 3.2.1.1 Summary

These tests had three objectives; (1) to maximize the flame temperature (2) to maximize the light yield and (3) to ascertain the effect of departure from stoichiometric ratio, (which will certainly occur at impact). Also, since lunar soil will probably be reactive with CTF, it was felt excess CTF might be a priori desirable. The results are described as follows.

#### 3.2.1.2 Test Setup

The mixture-ratio tests were made using Configuration X, which is a small aluminum canister weighing from three to eight grams (depending on design) filled with high surface area aluminum (powder and shredded foil) premixed with CTF. The ignition system consisted of a Teflon cork fitted to the neck of the can thru which two aluminum lead wires were inserted. The ends of

the lead wire, terminating inside the cannister, were crimped over aluminum wool. The other ends were hooked to a low power arc welder.

3.2.1.3 Instrumentation

The instrumentation used had these specifications:

| | | | |
|---|---|---|---|
| Spectrograph: | Bausch & Lamb Model No. 11 | | |
| | Spectrum: | 3700 - 7400 Å | 1st order |
| | | 1850 - 3700 Å | 2nd order |
| | Dispersion: | 15Å/mm | 1st order |
| | | 7.5Å/mm | 2nd order |
| | Resolving Power: | 70,000 | 2nd order |
| | Grooves per mm: | 450 | |
| | Blaze: | 4900Å | 1st order |
| | | 2450Å | 2nd order |
| Film: | Kodak High Speed Infrared HIR 421-1 (Similar to type 1-N) | | |
| Camera: | Fastax DWF-3 16mm | | |
| | Film: Kodachrome II & Ektachrome ER | | |
| Pyrometer: | Land Pyrometers Ltd., from Atlantic Pyrometers. | | |
| | Response Speed - less than 0.001 sec. | | |
| | Accuracy - Black body ± 3/4% | | |
| | Uses a silicon cell. The voltage drop across a 2500-Ω resistor is measured with a type 304-A Dumont Oscillograph; the response is photographed with a Polaroid camera. | | |
| Photometer: | Solar Systems, Inc., Model SS300 silicon cell, response-20 microseconds or less; output direct to a Honewell Oscillograph Model 906 with V450-55B galvanometers with 55-Ω shunt-response of 460 cycles (full scale). | | |

3.2.1.4 Results

Test firings 3, 4, 5, 11 and 12 were made (see Table 3-2). Light yield varied from 4.4 to $10^6$ lumen seconds to 0.53 x $10^6$ lumen seconds; in general these shots suffered from variation due to erratic rupture of the rather thin

Ta

SUMMARY OF DATA C

| Flare | Casing (gm) | Foil (gm) | Powder (gm) | CTF (gm) | Temperature (°C) | Ligh ($10^6$ |
|---|---|---|---|---|---|---|
| 1/50 | 8.5 | 2.1 | 11.2 | 29.2 | - | |
| 2/50 | 4.1 | 7.0 | 0 | 41.3 | - | |
| 3/50 | 3.7 | 2.4 | 13.6 | 34.7 | 1890 | |
| 4/50 | 3.8 | 2.4 | 11.7 | 35.2 | >2625 | |
| 5/50 | 3.7 | 2.4 | 7.6 | 40.0 | 1680 | |
| 6/50 | 8.1 | 2.4 | 12.6 | 35.5 | >2590 | |
| 7/50 | 3.9 | 14.1 | 0 | 35.1 | 2375 | |
| 8/50 | 8.5 | 2.4 | 7.6 | 39.7 | 2325 | |
| 9/50 | 8.9 | 2.4 | 13.6 | 34.6 | >2640 | |
| 10/50 | 3.6 | 2.4 | 11.7 | 36.2 | >2600 | |
| 11/50 | 3.7 | 2.4 | 7.6 | 41.2 | >2640 | |
| 12/50 | 3.6 | 2.4 | 7.6 | 40.0 | 2025 | |
| 13/50 | 3.6 | 2.4 | 7.6 | 39.6 | 3000 | |
| 14/50 | 3.3 | 2.4 | 7.6 | 39.9 | 2025 | |
| 15/50 | 9.7 | 10.0 | 0 | - | - | |
| 16/50 | 33.4 | 6.5 | 7.5 | 36.0 | - | |
| 1/500 | 73.1 | 140.1 | 0 | 370.0 | <2715 | |

ble 3-2

)N FLARE TESTS (AMOCO)

| t Yield lumen sec.) | Light Peak ($10^7$ lumens) | Duration (msec.) | Comments |
|---|---|---|---|
| - | - | - | Configuration X vibration and drop test |
| 0.90 | 3.8 | 112 | Configuration test all foil |
| 4.36 | 3.8 | 247 | Mixture ratio test aluminum rich |
| 1.04 | 13.0 | 18 | Mixture ratio test Stoichiometric |
| 0.89 | 1.1 | 79 | Mixture ratio test CTF rich |
| 2.55 | 17.4 | 63 | Configuration test heavy casing |
| 2.19 | 2.1 | 174 | Configuration test repeat 4/50 all foil |
| 0.90 | 1.9 | 95 | Configuration test repeat 5/50 heavy casing |
| 1.51 | 15.5 | 23 | Configuration test repeat 3/50 heavy casing |
| 1.36 | 13.8 | 78 | Configuration test repeat 4/50 at -78° |
| 0.97 | 2.9 | 84 | Mixture ratio test plus gabbro 44 microns |
| 0.53 | 0.6 | Estimated 53 msec. | Mixture ratio test Gabbro 44 microns in can |
| 1.5 | 4.8 | 45 | Burial test 1/2 diameter dirty sand |
| 0.35 | 0.39 | Estimated 262 msec. | Burial test 1 diameter dirty sand |
| - | - | - | Accidental ignition during loading |
| - | 3.0 | - | CTF and aluminum separated, rifle initiation |
| 9.3 | 120.0 | 18.8 | 500 gram spherical flare 3003 aluminum |

Tab

| Flare | Casing (gm) | Foil (gm) | Powder (gm) | CTF (gm) | Temperature (°C) | L (1 |
|---|---|---|---|---|---|---|
| Shot-gun No. 2 | 38.5 | 0.15 | 2.1 | 4.3 | - | |
| 18/50 | 9.6 | 14.1 | 0 | 38.4 | 3760 | |
| 19/50 | 9.7 | 14.1 | 0 | 37.1 | >3660 | |
| 20/50 | 9.7 | 14.1 | 0 | 37.0 | 1960 | |
| 20/50 | 9.7 | 14.1 | 0 | 37.0 | 1960 | |
| 21/50 | 9.8 | 14.1 | 0 | 39.4 | - | |
| 24/50 | 3.8 | 2.4 | 7.6 | 40.4 | - | |
| 28/50 | 19.3 | 7.0 | 7.0 | 37.9 | >3440 | |
| 32/50 | 9.1 | 14.0 | 0 | 38.7 | - | |
| 1/5000 | 696.4 | 1405 | 0 | 3666 | - | |
| 31/10 | 3.4 | 3.0 | 0 | 6.7 | - | |

le 3-2 (Cont)

| ight Yield $0^6$ lumen sec.) | Light Peak ($10^7$ lumens) | Duration (msec.) | Comments |
|---|---|---|---|
| 0.47 | High | 8.2 | CTF and Al separated by 1 mil Al foil ignited on acceleration |
| 5.6 | 11.5 | 28 | Burial test gravel 1/2 diameter |
| 0.47 | 15.6 | 9.7 | Burial test gravel 1 diameter |
| 0.28 | 0.28 | (Est) 160 | Burial test gravel 6 inches deep |
| 0.28 | 0.28 | (Est) 160 | Burial test gravel 6 inches deep |
| 0.35 | 0.37 | (Est) 160 | Vacuum test, 22 mm of mercury |
| 0.02 | 0.03 | (Est) 50 | Burial test, 6 inches deep dirty sand |
| 0.30 | 10.6 | 4.9 | 2 inch sphere, 1/2 burial Indiana soil |
| 0.27 | 10.1 | 4.8 | 1/2 diameter burial 1/2 foil, 1/2 fine wire |
| 71 | 778 | 11.8 | 5000 gram spherical vessel |
| 0.021 | 0.12 | 164 | Vacuum test 10 mm of mercury |

flare cases used. (Use of heavier cans was studied in the configuration tests and gave a shorter, more consistent reaction time). Firing 3 gave a very high light yield (calculated yield 87,000 lumen seconds per gram of flare). Efficiency of reaction (based on average wave length of 4200Å) was estimated as 1.3% conversion of thermal energy into light. It was concluded from these tests, that efficiency based on light measured by photocell, ranges from 0.3 - 1.3% and also that aluminum rich flares give the most light. Stoichiometric fuel ratios give the fastest reaction. These tests yielded useful information for further flare design but must be used with caution in view of their being air-immersed static shots. Tests 11 and 12 demonstrated an important point; both contained powdered gabbro and yielded about thirty new and fairly intense emission lines. (See Figures 3-1 through 3-5.) A microdensitometer run of a spectrogram on one of the control shots (9/50) is superimposed on Figures 3-1 through 3-5). Flare temperatures as measured by an absolute brightness pyrometer were only 1,950-2900°K for this series. These suspiciously low temperatures are possibly incorrect; otherwise it must be concluded that the rich short wave length emission is not blackbody radiation.

### 3.2.2 Flare Configuration Factor Tests

#### 3.2.2.1 Summary

Preliminary results of the compatibility tests and mixture ratio tests prompted a change in the basic flare design. These results showed that massive aluminum participates in flare reaction only to a small extent. To participate effectively in a flare reaction, the aluminum must be in the form of a fine powder fine wire or shredded foil which is thinner than 1 mil.

#### 3.2.2.2 Test Description

Six 50-gm flare tests were made to test the relative reactivity of aluminum sheet, foil, shredded foil, and powder. Two shotgun tests were made, one of which, Test 2 initiated in the barrel and burned up in the flight. Tests 2, 6, 7, 8, 9, and 10 used two thicknesses of aluminum casings (8 mil and 20 mil) and aluminum charges of aluminum powder, brand 1-131, and flash foil (0.5 mil shredded foil) in various ratios.

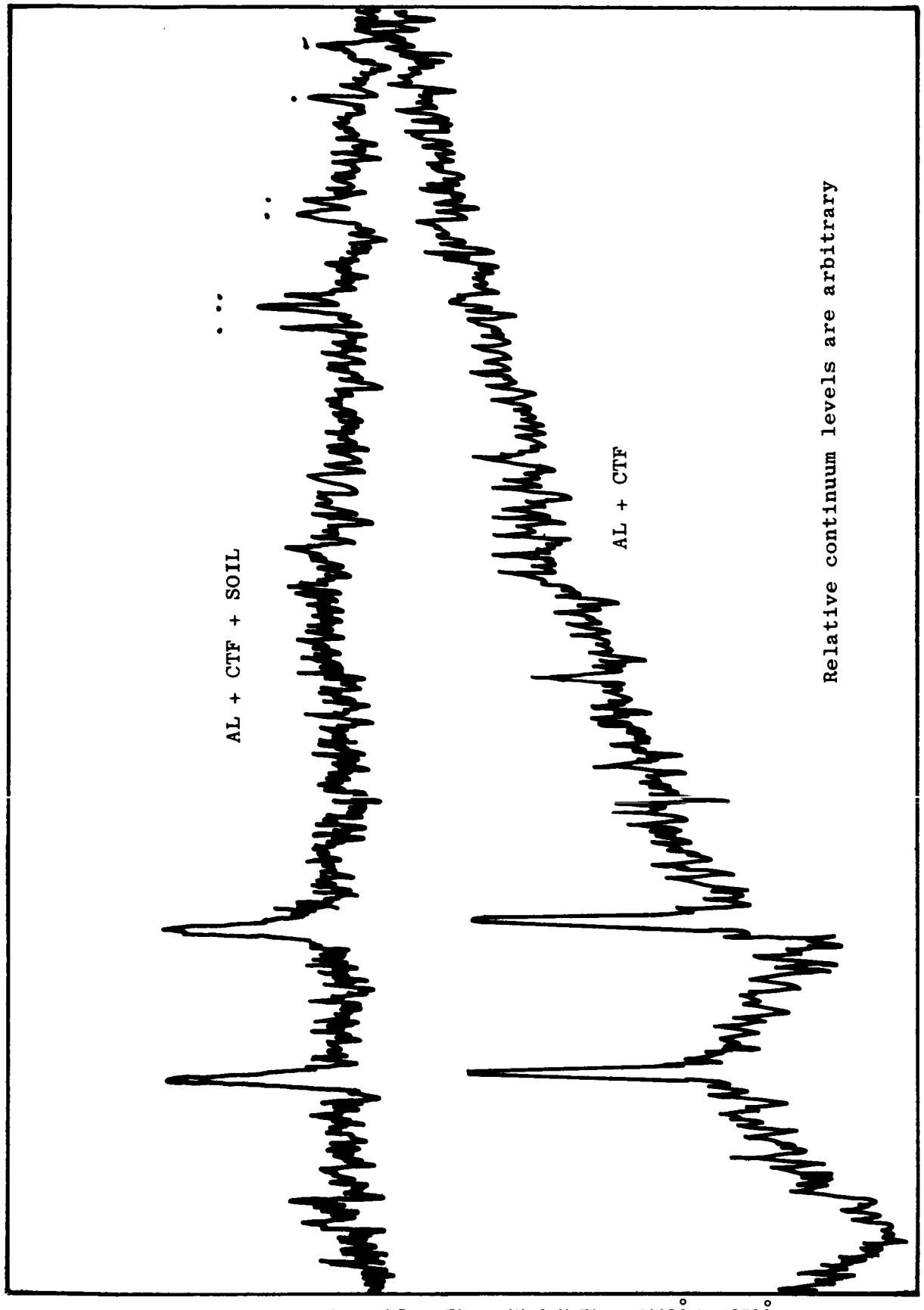


Figure 3-1 Comparison of Pure Flare with Soil Flare, 3920Å to 4070Å

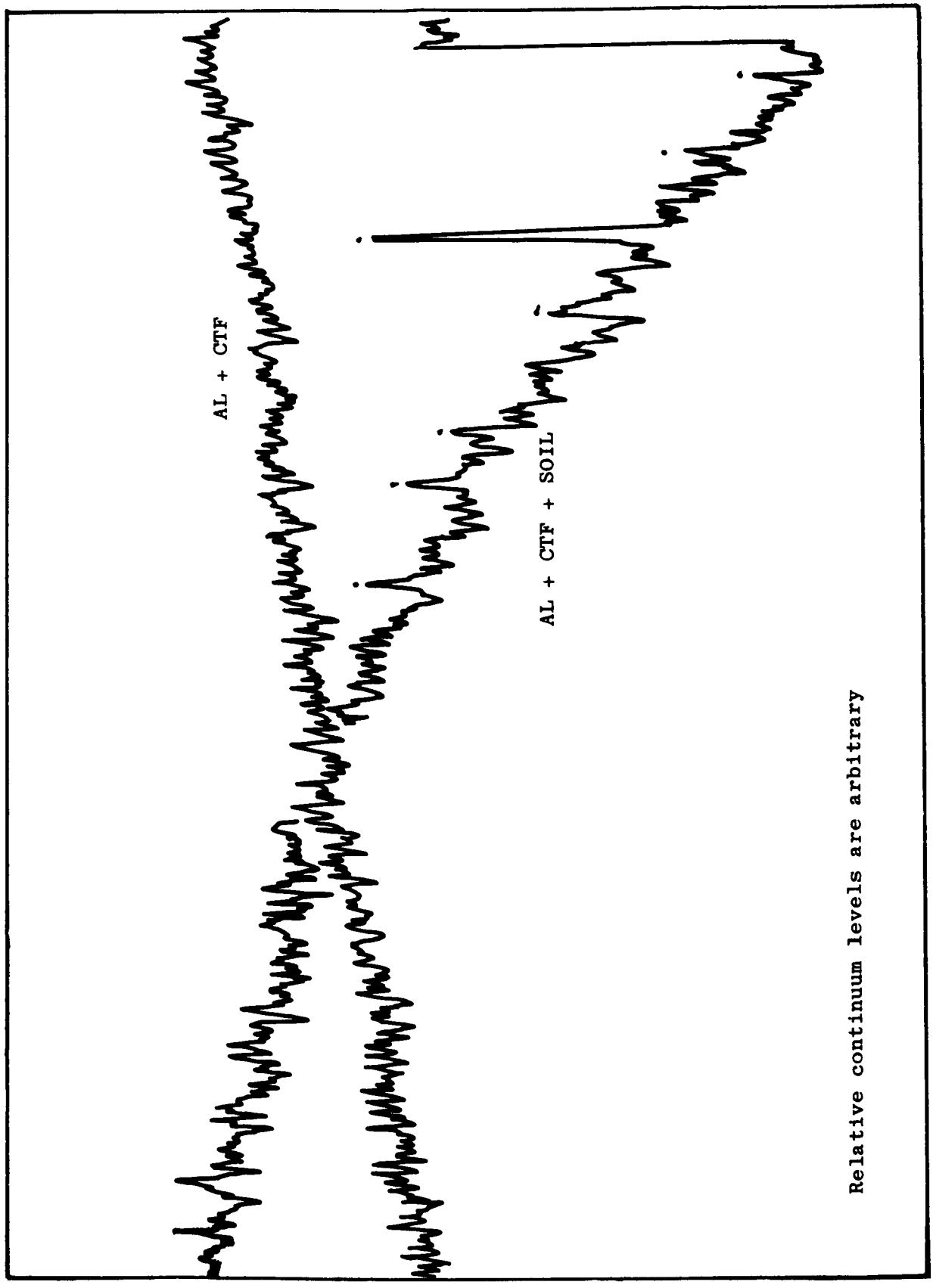


Figure 3-2 Comparison of Pure Flare with Soil Flare, 4040Å to 4200Å

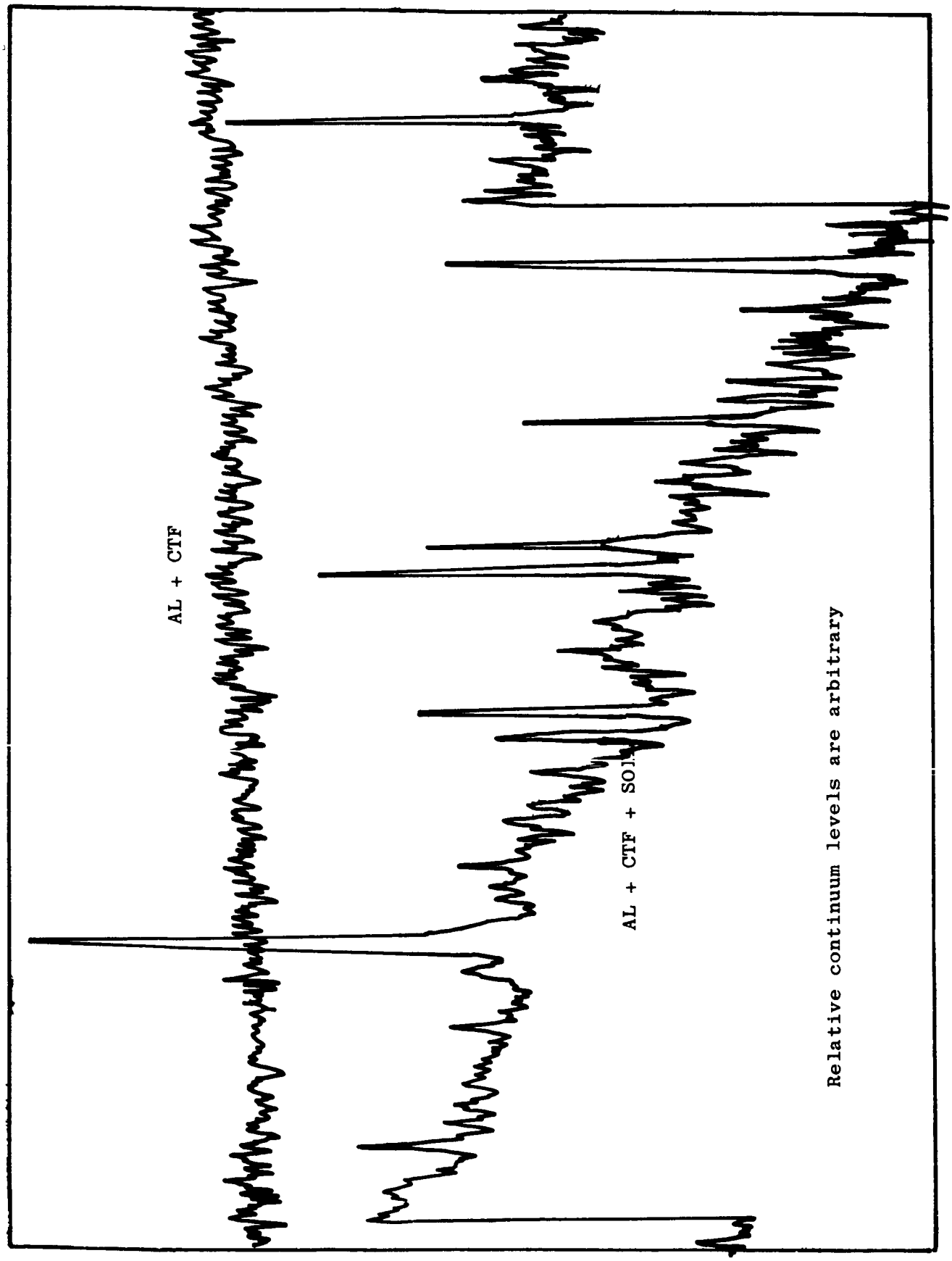


Figure 3-3 Comparison of Pure Flare with Soil Flare, 4200Å to 4320Å

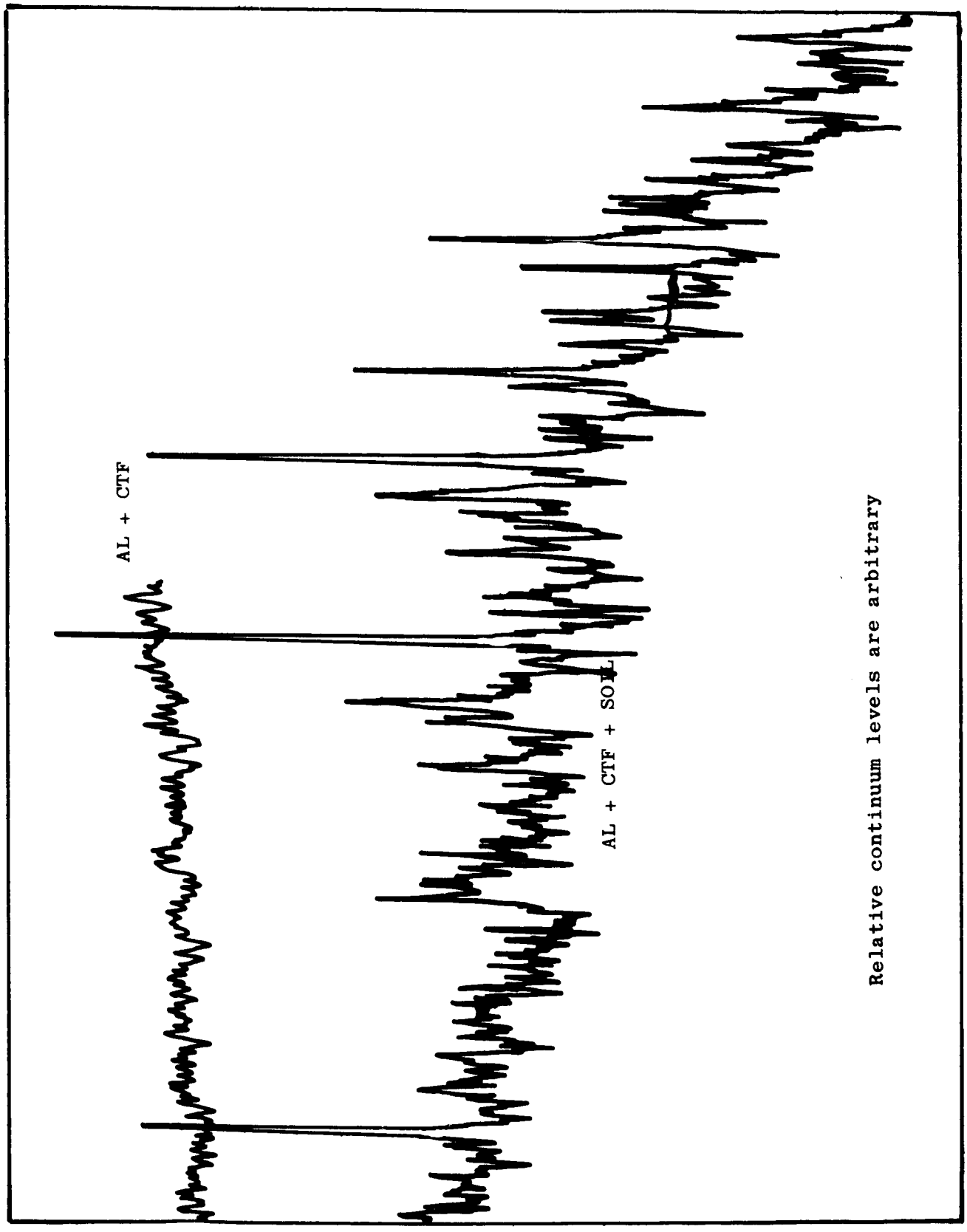


Figure 3-4 Comparison of Pure Flare with Soil Flare, 4350Å to 4480Å

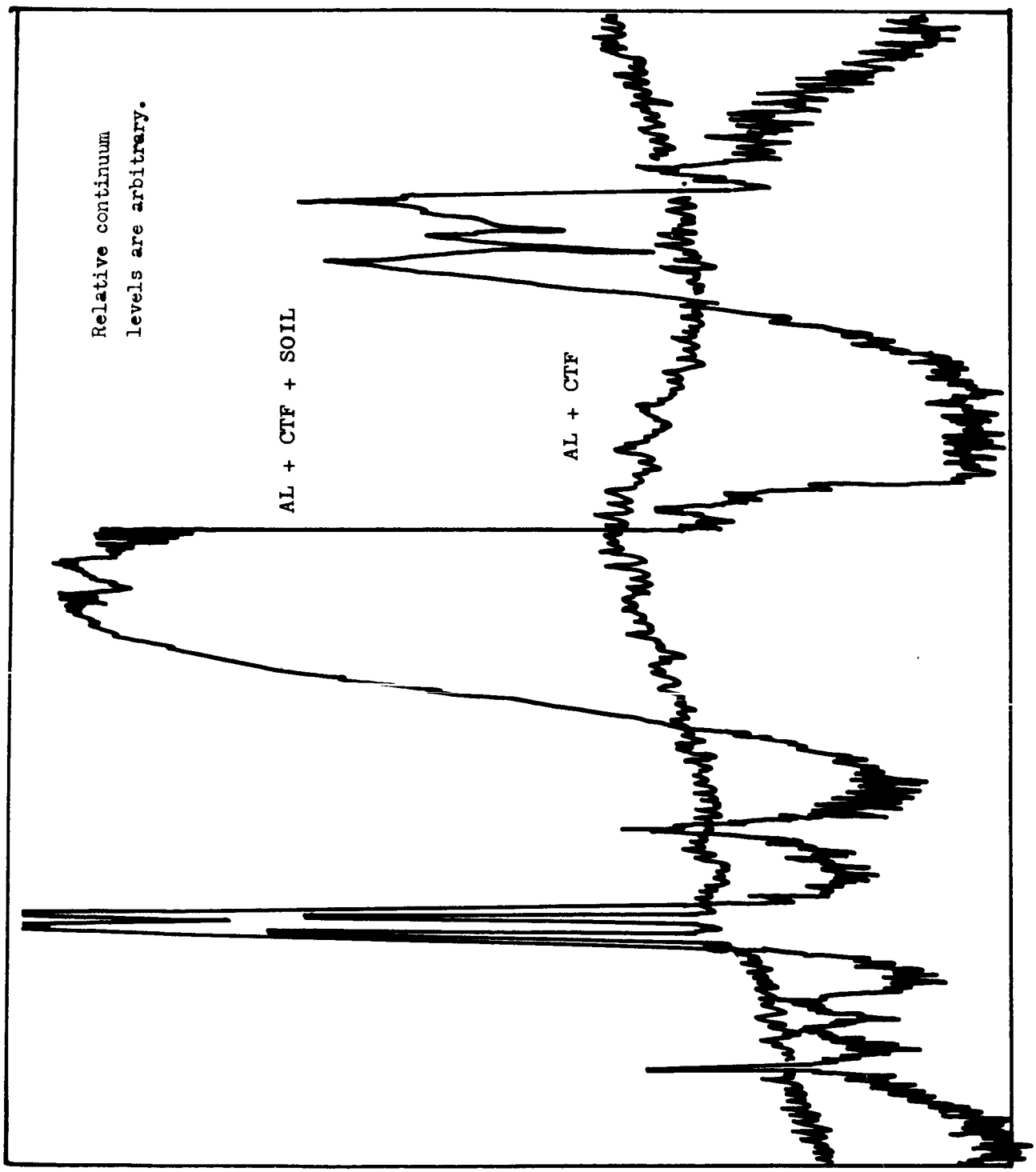


Figure 3-5 Comparison of Pure Flare with Soil Flare, 5800Å to 6300Å

The ignition system for the static tests was the same as for the mixture ratio tests.

3.2.2.3 Instrumentation

Same as used in mixture-ratio tests (paragraph 3.2.1.3) except for the spectrograph.

3.2.2.4 Results

In general, stoichiometric loadings of aluminum to CTF gave a rapid reaction estimated to be 1 millisecond or less with the total period of light emission being about 100 milliseconds. Vigorous shock waves were generated; conversion of energy into shock may reduce light yield.

The use of a heavier casing was not completely conclusive. Test 9 had a reaction time of 23 m sec. with a heavy casing, while Test 3 with a thin casing had a reaction time of 247 m sec. On the other hand, Tests 5 and 8 had about the same duration, though Test 8 had a higher indicated temperature and a higher peak luminosity.

Changing the aluminum loading from mostly powder to all foil (Test 2 and 7) had the effect of changing reaction rate to longer times. These same tests indicated that combining a light casing with foil results in a somewhat slower reaction.

For best results it appears the actual impact flares should consist of a charge of aluminum foil primarily with CTF and rely on rapid reaction, rather than impact containment, for as effective a reaction as possible.

Shotgun tests of small flares, made at a velocity of about 1000 ft/sec., show that CTF, aluminum powder and flash foil in contact with each other (Test 1) did not show a measurable light yield upon impact with a cement target, and the aluminum powder and foil was not consumed. In a Test 2, the CTF was separated from the aluminum powder and flash foil by a 1 mil. aluminum membrane. It initiated upon acceleration within the gun barrel and burned in flight, and did not hit the target due to aerodynamic instability of the

ruptured case. These tests show that ignition occurs much more readily when CTF and fine aluminum are suddenly placed in contact. These results indicate that ignition occurs either due to impact shock or due to sudden admixture of unpassivated aluminum with CTF.

The flare for Test 15 exploded prematurely. Although this configuration has been shown to be immune to shock or vibration, the test 15 flare, which had just been loaded, initiated a detonation type (1 millisecond) reaction while awaiting transfer to the firing stand. Initiation was traced to a drop of water falling from a condenser onto the flare, causing a CTF-water flame which propagated.

### 3.2.3 Scaling Factor Test

#### 3.2.3.1 Summary

The object of these tests was to gain information based on a diversified but small scale program that could be extrapolated into a full-scale flare design. Utilizing pertinent tabular data, with the necessary averages drawn at the 50 gram size, a correction factor for burial and vacuum extrapolations to the larger sizes was obtained and applied to the larger shots. Results indicate that a lunar flare of 50,000 gms may be expected to yield at least 8000 lumen-sec/gram while partially buried (diluted with soil) in a vacuum.

#### 3.2.3.2 Test Description and Results

In this series three tests were made using spherical vessels of Configuration X at masses of 50 gms, 500 gms, and 5000 gms. The three tests are described in the following paragraphs. The first scale-up test was the 500-gm flare. It was fired from a two foot tripod and resulted in a very strong shock wave. In order to minimize the shock wave and to simulate the lunar impact situation better, the large 5000-gm flare was fired while partially (50%) buried in soil. A 50-gm flare of spherical configuration was also fired while partially buried (50%) in soil to provide a basis for comparison between the 50-gm and the 5000-gm flares. Due to the extreme hazard involved in loading a large flare, in which CTF is in contact with finely divided aluminum, the flares

were loaded remotely by means of nitrogen pressure. In this way, the hazards were minimized during the loading of the large flares.

50 Gram Flare (28/50)

In this test a spherical aluminum vessel 0.032" thick was used. It was loaded with a stoichiometric ratio of 50% coarse aluminum powder (20 micron particle size) and 50% flash foil plus an appropriate amount of CTF. The CTF was added to the aluminum sphere remotely and the sphere was fired while partially buried (50%) in dry Indiana clay soil. The reaction was very fast, lasting only 4.9 m sec. No moderation in the reaction rate was gained by using coarse aluminum powder. The light yield was low, $0.3 \times 10^6$ lumen seconds or 6,000 lumen seconds per gram of flare, but both temperature and peak luminosity were high. The fireball from the flare was at least six feet in diameter.

500 Gram Flare (1/5000)

The first scale-up test was made in a 0.054-in-thick spherical aluminum vessel. The flare loading was all flashfoil aluminum at a stoichiometric ratio of aluminum to CTF. It was fired from a tripod which stood twenty-four inches above the ground level. CTF was loaded in the aluminum vessel remotely just before the firing. It resulted in a fast reaction (18.8 msec.) and a low light yield. The low light yield was probably because of the fast reaction ($9.3 \times 10^6$ lumen seconds or 18,600 lumen seconds per gram of reactants.) The shock wave from the flare was strong at a distance of about 200 ft. The fireball generated by the flare appeared to be 10-20 ft in diameter in relation to an eight foot high screen which was set up to shield a nearby house from the direct light of the flare.

5000 Gram Flare (1/5000)

This was the largest flare of the series, and it was necessary to find a location which would be removed from all roads and houses by at least 1500 ft. A suitable location was found in a cornfield adjacent to Amoco's Freeman Field Facility. The control room for the test was located about 750 ft. from the flare location. Considerable set-up time was involved in laying cables for lights and instrumentation. To prepare for the remote possibility

that normal ignition would fail to ignite the flare, a 30 caliber rifle with a scope sight was signted-in on the flare to provide backup ignition.

Since it was at this time believed desirable to slow the reaction somewhat to obtain a better light-yield, a small 50-gm flare (32/50) was loaded with a fifty-fifty mixture of flashbulb foil and fine aluminum wire (0.004 in diameter) but this mixture failed to give a slower reaction. Therefore an all flash foil loading was chosen for the 5,000-gm flare at a stoichiometric ratio of aluminum to CTF. The aluminum vessel for the flare was a nine-inch diameter sphere 0.062 in. thick. It was partially buried (50%) in local soil and was remotely loaded with CTF just before firing. A light yield of 71 x $10^6$ lumen seconds or 14,000 lumen seconds per gram was obtained. Reaction time was fast (11.8 m. sec). The flare fireball appeared to be 20-40 feet in diameter and the sound of the explosion was a dull boom. A crater about twelve inches deep and five feet in diameter (approximately 1500 pounds of soil) was displaced by the flare. A comparison of light-yields obtained from the 50-gm flare and the 5000-gm flare tests both were half buried, shows a scale-up in light yield per grm of flare of more than two times. A decrease in light yield per gm was noted in going from the 5000-gm flare to the 500-gm flare, but these are not comparable since the 500-gm shot was made above ground.

All three tests were monitored for light-yield with a chemical actinometer. The 50-gm and 500-gm flares indicated a light yield approximately ten times greater than those obtained from photocell measurements. However, a more accurate measurement obtained from the 5000-gm test gave 100 x $10^6$ lumen seconds. Since the chemical actinometer measures light from 5000 Å to 2000 Å, it seems likely that a correction to the photocell reading for ultra violet light would result in about a two-fold increase in light-yield over that measured by the photocell. Actinometric measurements are still being developed but as yet are not acceptable standards.

The ignition system was generally the same as for the mixture-ratio tests.

3.2.3.3 Instrumentation

The instrumentation was the same as that used in the configuration Factor Tests. However, a chemical actinometer of an experimental-type was employed.

## 3.2.4 Penetration Effect Tests

### 3.2.4.1 Summary

The object of these tests was to determine the effect of burial, in simulated lunar soil, on light output and to also determine whether adequate spectroscopic involvement of soil elements was possible.

The results of these tests indicate, or might be expected, that increasing depth of penetration of the flare in soil decreases the light yield. Spectrograms also indicate considerable soil constituent emission. (See Figure 3-6 for spectrograms of Test 20/50 as well as 9/50, calibration run, and 12/50 showing soil involvement.)

### 3.2.4.2 Test Description and Results

The first series, consisted of partially burying a CTF-rich loading at various depths, in feldspathic sand (supplied by Douglas). Depths were 0.5 dia, 1 dia, and 6 in for 50-gm flare tests (13, 14, and 24). Results showed a steadily decreasing light yield corresponding with depth. Soil involvement in the flare was good, spectrograms showed that line emission from soil elements was substantial. In the second series a hotter loading (stoichiometric) was buried at 0.5 dia, 1 dia, and 6 in respectively in crushed granite rock (about 3/4 inch pieces), (Tests 18, 19 and 20). Very high temperatures were observed (3920-4033°K) and light yield decreased much more slowly with depth than it did with the sand. Examination of the exposed crushed rock showed its surface to be attacked despite the short exposure, (10 - 30 milliseconds). Detailed examination did not show silicate melting, however. The ignition system was generally the same as for the mixture-ratio tests.

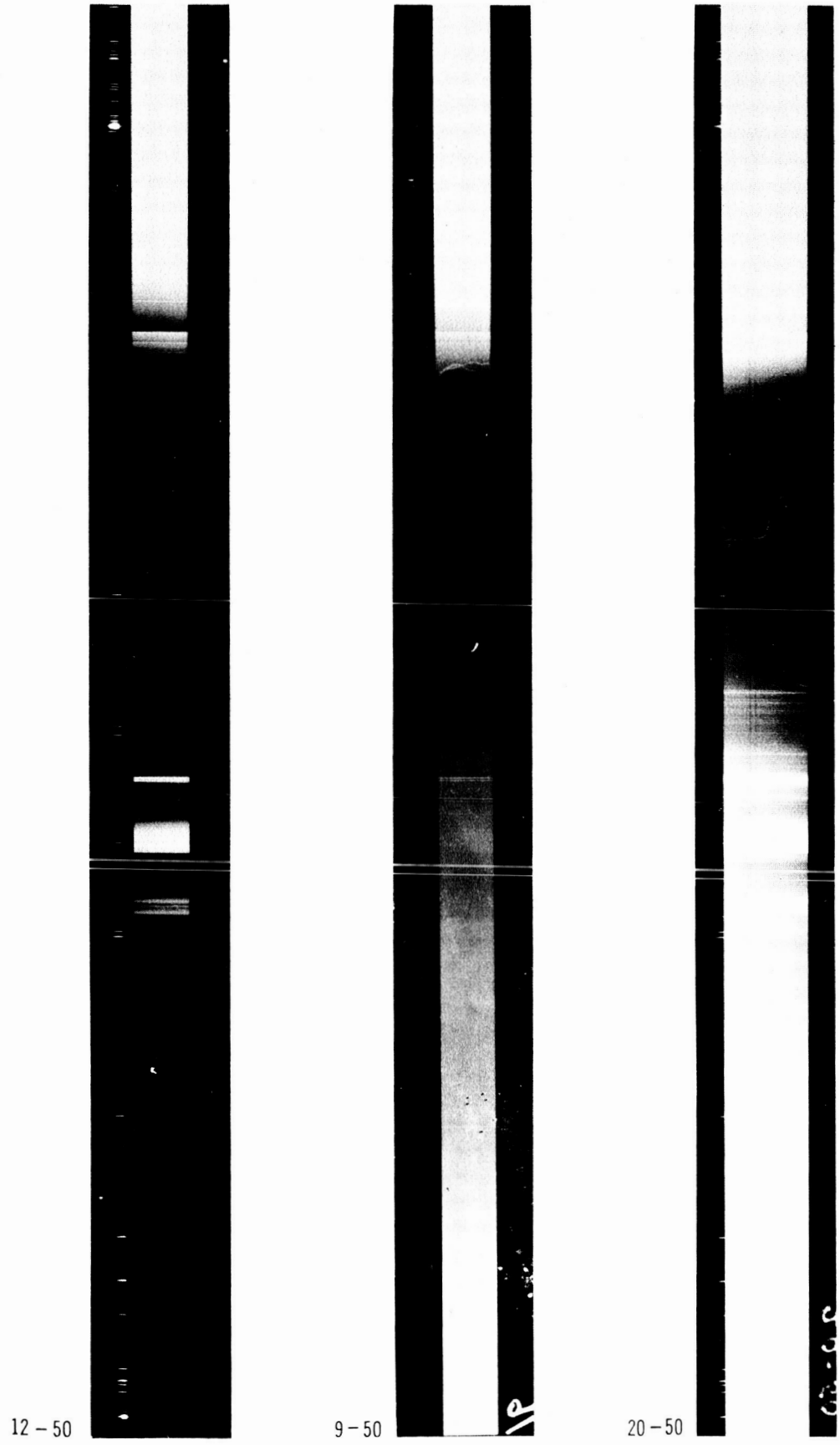


Figure 3-6 Amoco Spectrograms

3.2.4.3 Instrumentation

Same as for the mixture-ratio tests.

## 3.2.5 Vacuum Compatibility Tests

### 3.2.5.1 Summary

The objective of these tests was to determine the effect of pressure on light yield.

Only two of the six shots were successful and the results were not sufficient to be conclusive.

### 3.2.5.2 Test Description and Results

Six attempts to fire vacuum tests were made, two tests, one at 22 mm. and one at 10 mm., were successful. Test 21 resulted in a low light yield as measured through a tank port. Since the reaction lasted for about 250 milliseconds, it is recommended that the test be corrected for an extended source. This should be pursued because light yield was $9.3 \times 10^7$ lumen seconds, the highest obtained from a 50-gm flare. Duplicate tests at 7 mm pressure lost CTF and failed to fire. In an effort to settle the light-yield question four more tests were made, using a close-up photocell and five to ten gm charges. Two failed to initiate adequately, and one leaked out. The fourth and successful test was a 10-gm flare (31/10) which was initiated successfully under a vacuum of 10 mm. of mercury. It gave a high initial peak of $1.2 \times 10^6$ lumens followed by a slow reaction which lasted for about 200 milliseconds. Total light yield was low, $2.1 \times 10^4$ lumen seconds. Flares initiated under vacuum conditions seem to give a fast initial reaction followed by a slow reaction.

Extrapolation to zero pressure would seem to indicate that adequate initiation will give an initial high luminosity detonation. In vacuum, the gas will expand, but in the absence of inert gases, it may continue to react for approximately one second. Total light yield with a well-designed flare may be better than air-flare yields, based on the 50-gm test. Efficiency appears to increase with flare mass.

The ignition system employed here was generally the same as for the mixture-ratio tests adapted to the vacuum tank.

3.2.5.3 Instrumentation

Generally the same as for the configuration tests.

## 3.3 IMPACT EXPERIMENTS

Impact experiments were conducted at both Amoco and Douglas. The initial tests were conducted at Amoco in order to obtain early results and to determine if typical launch accelerations caused any detrimental effects on the projectile (e.g., premature initiation of the reaction in the gun barrel). The Douglas light-gas gun tests are discussed in 3.3.2.

### 3.3.1 Amoco Tests

In these tests, aluminum projectiles (1.5 in O.D., 2.3 in length) loaded with CTF, aluminum powder, and aluminum foil were launched at velocities up to 960 fps in air and light intensity upon impact measured.

The internal aluminum was separated from the CTF by means of a thin (0.012 in) diaphragm (Figure 3-7) which ruptured upon impact. A summary of these tests is given in Table 3-3.

Test 3, which was fired at the lowest velocity, gave the highest light yield perhaps due to a more thorough mixing of CTF and aluminum. Both tests 2 and 3 gave light yields comparable to those obtained in static tests. Cratering was very slight in these tests and only surface chipping was noted. although considerable cracking of the test slabs occurred.

The light yields obtained in tests 4 and 6 were somewhat lower than those obtained in the static tests. The gravel test (No. 5) gave no light yield. This was possibly due to a slower deceleration in gravel than in either rock or sand. A spectrogram taken during test 6 showed spectral lines due to soil involvement. The effect of target hardness is ambiguous since the sand target of test 6 gave a better light yield than the granite target of test 4. However, the test did establish that impact tests in sand are not quenched.

T

SUMMARY OF

| Test No. | Target | Casing Weight (gm) | Foil Weight (gm) | Al Powde Wt. (gm |
|---|---|---|---|---|
| 1 | Gabbro slab | 129 | 1.0 | 13.0 |
| 2 | Granite slab | 127 | 1.0 | 13.0 |
| 3 | Granite slab | 129 | 1.0 | 13.0 |
| 4 | Granite slab | 113 | 1.0 | 13.0 |
| 5 | Gabbro & Granite gravel | 110 | 1.0 | 13.0 |
| 6 | Gabbro & Granite sand | 106 | 1.0 | 13.0 |

able 3-3

MOCO IMPACT TESTS

| CTF Weight (gm) | Velocity (fps) | Peak Luminosity ($10^7$ lumens) | Light Yield ($10^6$ lumen-sec.) |
|---|---|---|---|
| 35.5 | 930 | 3.9 | 0.10 |
| 36.0 | 960 | 3.9 | 0.56 |
| 35.5 | 300 | 13.6 | 1.23 |
| 36.3 | 860 | 0.51 | 0.02 |
| 35.9 | 860 | - | - |
| 35.4 | 860 | 2.6 | 0.13 |

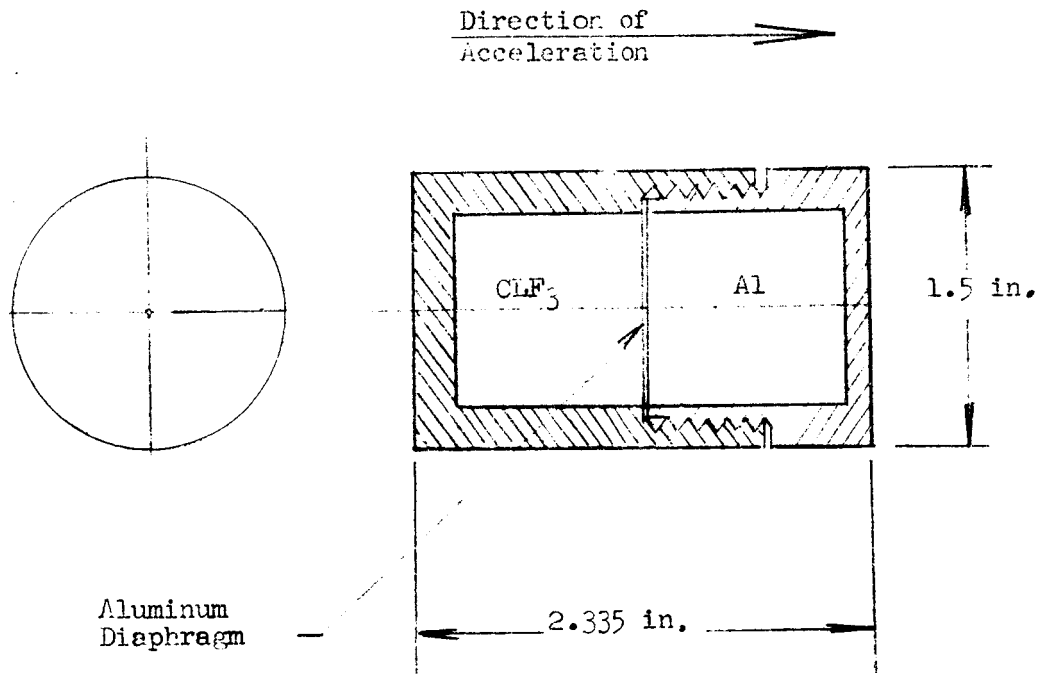


Figure 3-7 Configuration of Projectile Used in AMOCO Impact Tests

### 3.3.2 Light-Gas-Gun Tests

#### 3.3.2.1 Summary

During these tests, aluminum projectiles loaded with CTF and aluminum powder were launched at velocities (typically 8400 fps) approximating a lunar-impact speed. The projectiles impacted targets which simulated the estimated extremes of lunar surface physical characteristics. The tests were conducted at as low an ambient pressure as feasible (on the order of 5mm hg) in order to simulate, at least partially, the low pressure of the lunar surface. The reaction on impact was recorded with a fastax camera, a spectrograph, and photometric instrumentation.

A total of eleven firings were made. Two model configurations were planned; one a hollow aluminum sphere, the other a hollow conical model (Figure 3-8). The latter simulated the triorthogonal configuration recommended by

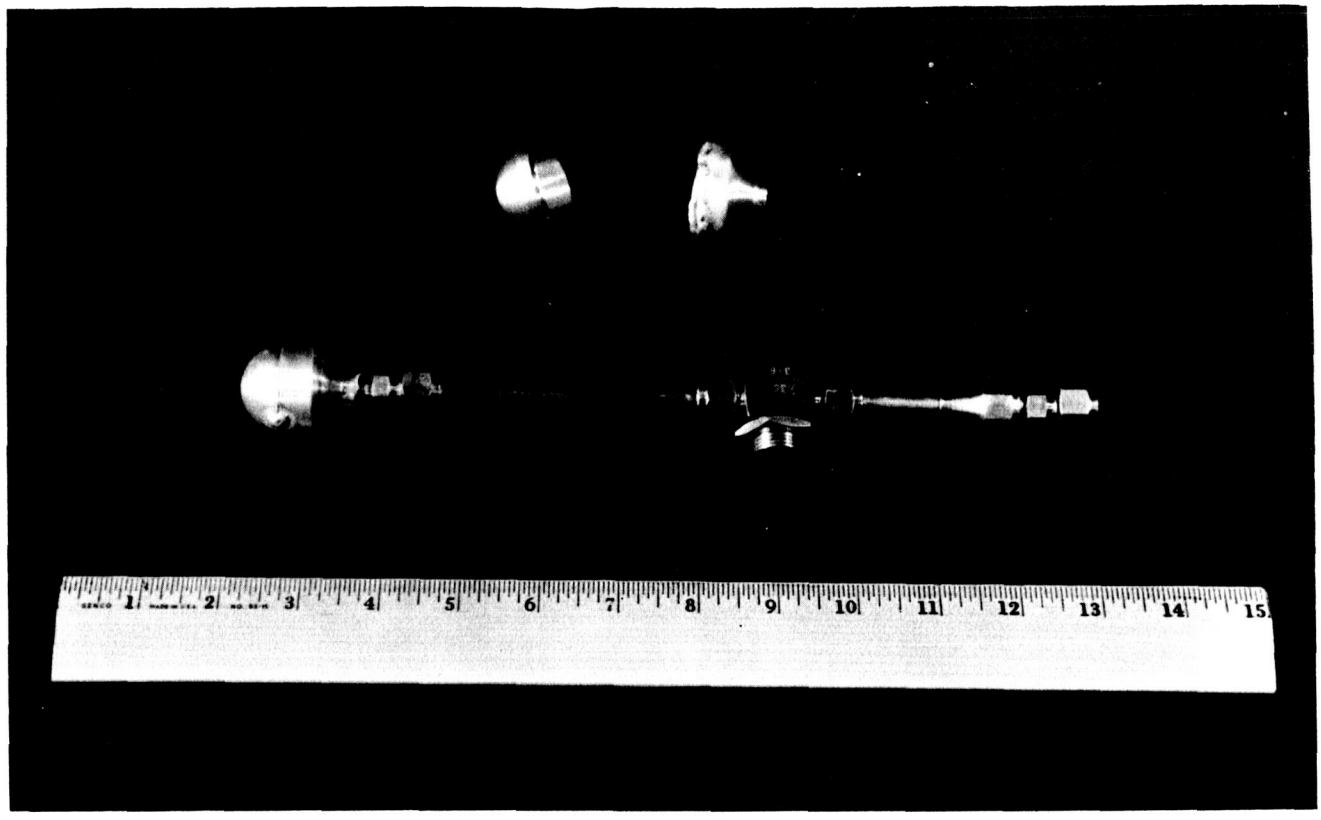


Figure 3-8 Light Gas Gun Components

Shock-Hydrodynamics. Analyses of the impact processes have shown this configuration to be superior to a spherical one, primarily because it does not penetrate as deeply. However, problems were encountered in the fabrication and loading of the conical model. These prevented the launch of a loaded model of this configuration prior to the end of the program.

The following results were obtained from these tests:

1. Impact ignition occurs for both hard and soft (dust-like) targets.
2. Both the peak luminosity and total quantity of light produced in the reaction are of the same order as those produced in static tests in air.

3.3.2.2 Test Setup

Impact tests were conducted in the light-gas-gun/ballistic-range facility of the DAC Aerophysics Lab (see Figure 3-9). The facility consists of a

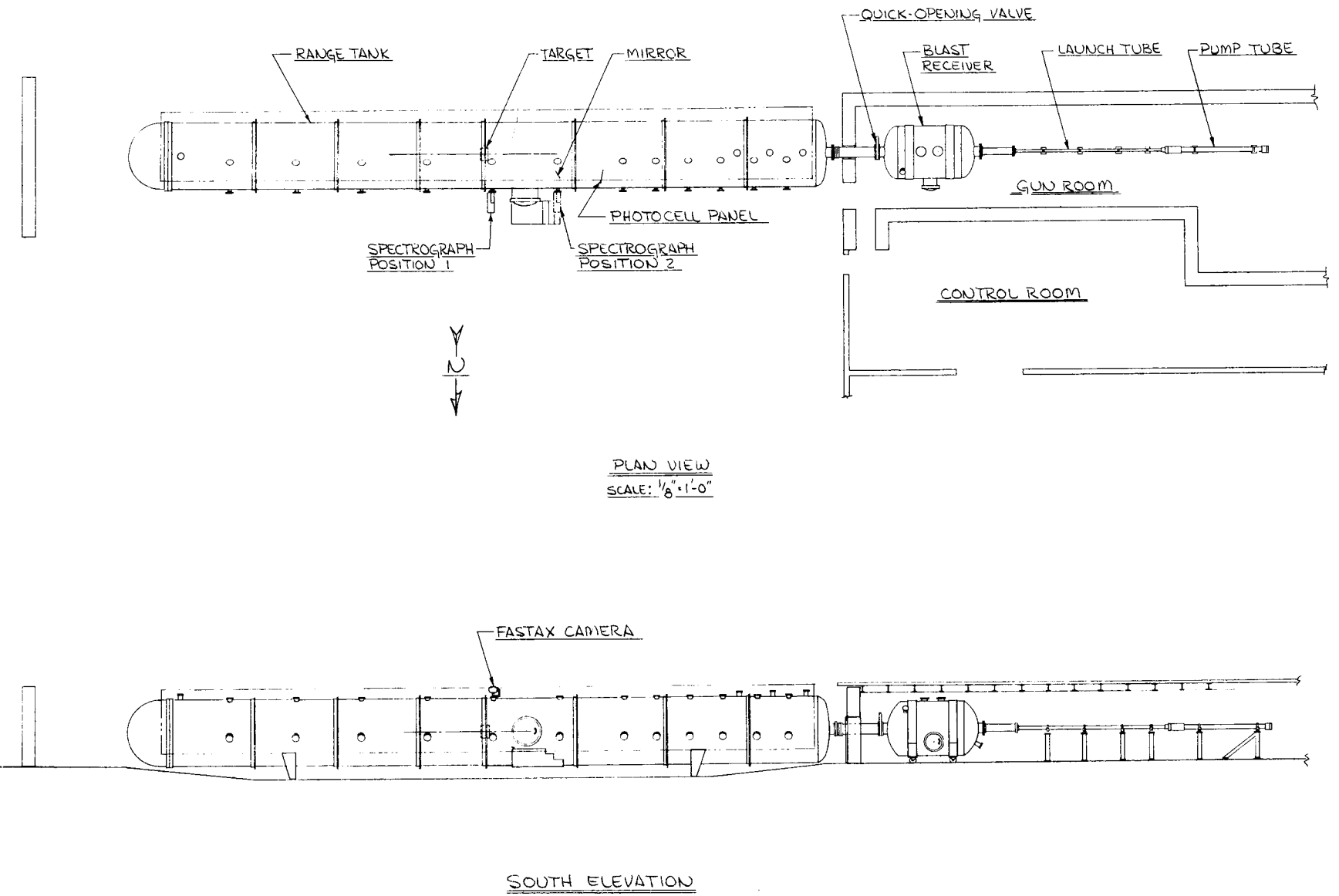


Figure 3-9 Light Gas Gun/Ballistic Range Setup

controlled atmosphere tank (the ballistic range), a blast receiver, and the light gas gun. The launcher used is a 1.5 in diameter-bore single-stage gun. Energy is supplied by initiation of gun powder in a Helium pre-pressurized breech. This ruptures a burst diaphragm just uprange of the model. Non-spherical or non-cylidrical shapes are launched by use of a sabot which is separated aerodynamically from the model in the blast receiver after leaving the launch tube. The ballistic range is 10 ft in diameter and 100 ft in length. The target for these tests is located approximately mid range, about 12 in down range from an observation station. Two view ports are provided at the observation station, one oriented vertically and one horizontally. The horizontal port was used for spectroscopic observation, while the vertical port was used for Fastax photographic coverage of the impact event. Photometric instrumentation is located inside the range, 17 ft forward of the target and 4 ft off the line of flight facing the target. Three spark discharge shadowgraph units are mounted at stations along the flight path for the purpose of obtaining photographs of the model in flight.

All operations which involved handling or transferring of chlorine-trifluoride were performed at the Douglas Astropower test site.

Preparing and loading the models was generally the same as the ampules of the Spectroscopic Tests.

3.3.2.3 Instrumentation

Velocity and Shadowgraphs

Photocell pickups are used to trigger two spark units at each of three shadowgraph stations for illumination of the projectile. The output from a spark unit of each station triggers two electronic timers. The pulse from the first station initiates both timers, the pulse from the second unit stops the first counter and the pulse from the third spark discharge unit stops the second counter so that two redundant projectile velocity measurements are obtained. The counter is a 10mc Beckman time-interval counter.

Photometric

Light intensity in five wavelength regions was measured with five photocells:

| Cell No. | Wavelength (Å) | Type of Cell |
|---|---|---|
| 1 | 3550 | Selenium - Int. React. Corp. Model B2M |
| 2 | 4350 | Silicon - Int. React. Corp. Model S3M |
| 3 | 5100 | Silicon - Int. React. Corp. Model S3M |
| 4 | 6500 | Silicon - Int. React. Corp. Model S1M |
| 5 | 7400 | Silicon - Int. React. Corp. Model S1M |

A Wratten filter and an interference filter were used with each cell; the resulting wavelength band for each region was approximately 600Å. The cells were mounted together on a panel and covered with a protective quartz window. The photocell outputs were amplified using an Astrodata model 885 wide-band DC amplifier; a C.E.C. oscillograph (Type 5-114-P4-18) was used to record the photocell output. Type 7-326 galvanometers were used with the exception of one 7-361 type. The oscillograph paper speed was 115 in per sec. Two amplifiers, operating at different gains, were used with each photocell (with the exception of cell no. 3, where only one amplifier was used).

Photographic

A fastax camera (model WF4S) was operated at approximately 6500 frames per second to obtain coverage of the flare event. A 12 mm wide angle lens was used with the camera. The field of view at the target was approximately 3-1/2 ft. in diameter, limited by the size of the observation port in the range tank.

Spectroscopic

The spectrograph (shown in Figure 3-10) used in these tests was the same one used in the Douglas static spectroscopic tests. The spectrograph was mounted outside of and immediately adjacent to the range tank. A quartz viewing window was provided for observation. The spectrograph slit was approximately 6 ft from the target in the first test. The spectrograph was later moved forward of the target position and used with a mirror to observe the flare from a direction perpendicular to, rather than parallel to, the surface of the target (Figure 3-9).

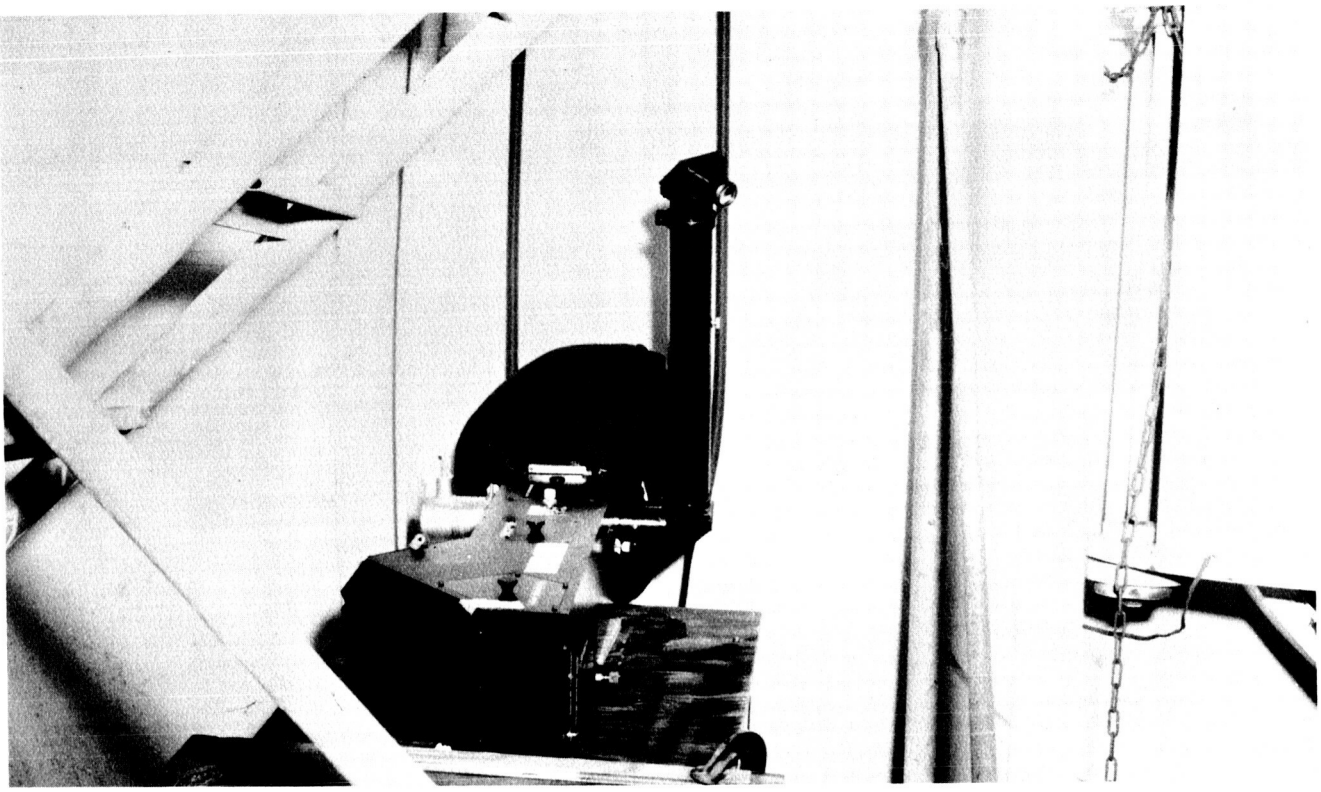

Figure 3-10 Spectrograph Set up Adjacent to the Range Tank at an Observation Port

The spectrograph is a Cassegrainian mounted, grating (600 lines per mm) type. It has a dispersion of approximately 120Å per mm. The wavelength region employed was 3200Å - 5400Å (except for the first live test where the wavelength ranged from 4200Å - 6700Å). The camera employed a folded Schmidt system and Kodak 1030a-0 plates are used. (Type 103a-F plates were used in the first live test.) A step filter, covered the slit in order to provide three different simultaneous exposures (approximately 100%, 10%, and 1% of the incident light).

Gas Samples

An evacuated bottle was used to sample atmosphere in the range following a test. The contents of the bottle were then analyzed to determine atmospheric constituents. The instrument used for analysis was a Perkin-Elmer model 521 infrared spectrophotometer.

3.3.2.4 Test Results

Eighteen tests were run in this phase of the program. Table 3-4 summarizes the conditions under which these tests were conducted and results of the firings. Of the eighteen firings, twelve were developmental and were conducted for the purpose of proving model integrity and/or sabot separation. Five were conducted with projectiles which contained CTF. Two projectile configurations were employed. Type 1 was a hollow aluminum sphere (see Figure 3-11A) and type 2 (see Figure 3-11B) a hollow aluminum cone. The design of model type 2 simulated the triorthogonal configuration considered in the analysis of the impact process. Several dummy launches were made to perfect the sabot design and separation technique for this model. The technique of aerodynamically stripping the sabot in the blast receiver while using a quick-opening valve between the blast receiver and the ballistic range appears to be satisfactory. The developmental problems encountered in perfecting the launch technique, however, coupled with difficulties experienced in loading the model with CTF prevented a live test of this configuration prior to completion of the program.

The condition of the projectiles following launch was determined by shadowgraph photography. Figure 3-12 shows typical in-flight photographs of both types of projectiles.

Two types of targets were used in the tests. For the competent rock-type target, large granite slabs were used. One of these targets is shown in Figure 3-13, as it appeared after impact in test No. 14. The face of the target is approximately 2-1/2 ft x 3 ft. In firing No. 11, a smaller slab (6 in x 6 in x 3 in) was used as a target. In this test, the granite target was totally pulverized, no large pieces were recovered. In firing No. 12, a slab 24 in x 24 in x 10 in was used; it was shattered upon impact.

Next a deep, powdery surface was simulated as shown in Figure 3-14 (before impact). A trough, 2-1/2 feet in diameter, was used to hold a garnet dust (average of 5$\mu$ grain size) which was sifted into place. A thin (1 mil) mylar diaphragm was used on the forward face to hold the dust in a near vertical position. A porosity of roughly 75% was achieved.

able 3-4

IT GAS GUN IMPACT TESTS

| hoto-ell ata | Spectro-graph | Fastax | Sabot | Purpose | Remarks |
|---|---|---|---|---|---|
| | | | None | Determine effect of of launch on model integrity | Model broke up |
| | | | 5 Piece | Test technique of aerodynamic sabot separation in blast rec. | Model launched successfully; sabot base followed model |
| | | | 5 Piece | Same as Run No. 2 but higher press in blast rec. | Same result as Run No. 2 |
| | | | 4 Piece | Same as No. 3 but sabot base eliminated | Quick opening valve between blast rec and range failed; sabot separation uncertain |
| | | | 4 Piece | Same as Run No. 4 | Model launched successfully, sabot separated but pins used to hold 4 pieces together followed model |
| | | | 1 Piece cut | Same as Run No. 5 but 1 piece sabot (precut) to eliminate pins study hypersonic stability of simulated Bjork-Jack | Good sabot separation; model unstable and hit baffles in blast rec |
| | | | 1 Piece cut | Same as Run No. 6 | Same as Run No. 6 |
| | | | 1 Piece cut | Same as Run No. 6 | Same as Run No. 6 |
| | | | None | Same as Run No. 1 | Completely successful |

RUN SUMMARY - LIGH

| Run No. | Date | Range Press | Blast Rec Press | Target | Model Config. | Velocity (FPS) | P c D |
|---|---|---|---|---|---|---|---|
| 1 | 4/14 | 5mm | 5mm | - | 1.5"O.D., water-filled, high-purity Al sphere | 7980 | |
| 2 | 5/11 | 14.5mm | 2psia | - | Sphere | 7500 | |
| 3 | 5/11 | 8.5mm | 5psia | - | Sphere | Not Recorded | |
| 4 | 5/20 | 5.3mm | 95mm | - | Sphere | 6730 | |
| 5 | 5/25 | 7.0mm | 200mm | - | Sphere | 7400 | |
| 6 | 5/26 | 7.0mm | 200mm | - | 1-1/8" base diam cone fired base first | - | |
| 7 | 5/27 | 4.0mm | 100mm | - | 1-1/4" base diam cone fired base first | - | |
| 8 | 5/28 | 4.5mm | 80mm | - | 1" base diam cone fired base first | - | |
| 9 | 6/3 | 10mm | 10mm | - | 1.5" O.D., $CCl_4$-filled, high-strength Al sphere | 8300 | |

ble 3-4 (cont)

| Photo-cell Data | Spectro-graph | Fastax | Sabot | Purpose | Remarks |
|---|---|---|---|---|---|
| | | | 4 Piece | Determine effect of launch on model integrity and check sabot separation | Completely successful windshield (hemisphere) makes base first cone hypersonically stable |
| X | X | | None | Obtain data for impact of CTF-filled model on hard target | Model launched successfully, |
| X | X | | None | Same as Run No. 11 | Same as Run No. 11 |
| | X | X | None | Obtain data for impact of CTF-filled model on soft target | Model launched successfully Electrical malfunction caused failure to record photometric data; fragments of model penetrated dust target 18" |
| X | X | X | None | Same as Run No. 11 | Successful except for a partial loss of CTF due to leakage before launch |
| X | | | None | Obtain data for impact of empty model on hard target | Successful |
| | | | 4-Piece | Determine effect of launch on model integrity and check sabot separation | Successful |
| | | | None | Obtain data for impact of CTF-filled model on soft target | Unsuccessful; model broke up on launch apparently because it was undersize |
| | | | 4-Piece Interlocking | Obtain data for impact of CTF-filled cone sphere model on soft target | Model not fired due to difficulties experienced in loading CTF. Program ended this date. |

bts.

Ta

| Run No. | Date | Range Press | Blast Rec Press | Target | Model Config. | Velocity (FPS) |
|---|---|---|---|---|---|---|
| 10 | 6/4 | 17mm | 100mm | - | Cone-sphere | 8600 |
| 11 | 6/8 | 6.0mm | 6.0mm | Solid Granite | CTF filled-sphere (See Fig. ) | 8300 |
| 12 | 6/12 | 5.0mm | 5.0mm | Solid Granite | Same as Run No. 11 | 8534 |
| 13 | 6/17 | 5.2mm | 5.2mm | Garnet Dust 5 75% Porosity | Same as Run No. 11 | 8710 |
| 14 | 6/18 | 7.3mm | 7.3mm | Solid Granite | Same as Run No. 11 | 8550 |
| 15 | 6/19 | 7.2mm | 7.2mm | Solid Granite | Same as Run No. 11 without CTF | Not Recorded |
| 16 | 6/24 | 28mm | 100mm | - | Cone-sphere (see fig ) filled with dense inert fluid | 8780 |
| 17 | 6/29 | 6.0mm | 6.0mm | Garnet Dust 5 75% Porosity | Same as Run No. 11 | - |
| 18 | 6/29 | | | Same Dust as 17 | CTF-filled cone-sphere | - |

Note: Land Camera Schlieren photographs obtained on all successful sh

Figure 3-11 Light Gas Gun Model Configurations

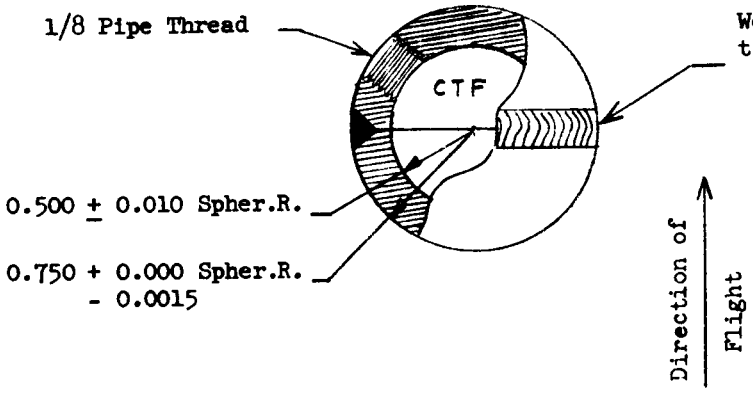


Notes:
1. Material 6061-T6
2. Weight of empty Model = 58 gm
3. Weight of internal Al dust = 4.4 gm
4. Weight of CTF = 12 gm
5. Loaded Model weight = 74.4 gm

(a)

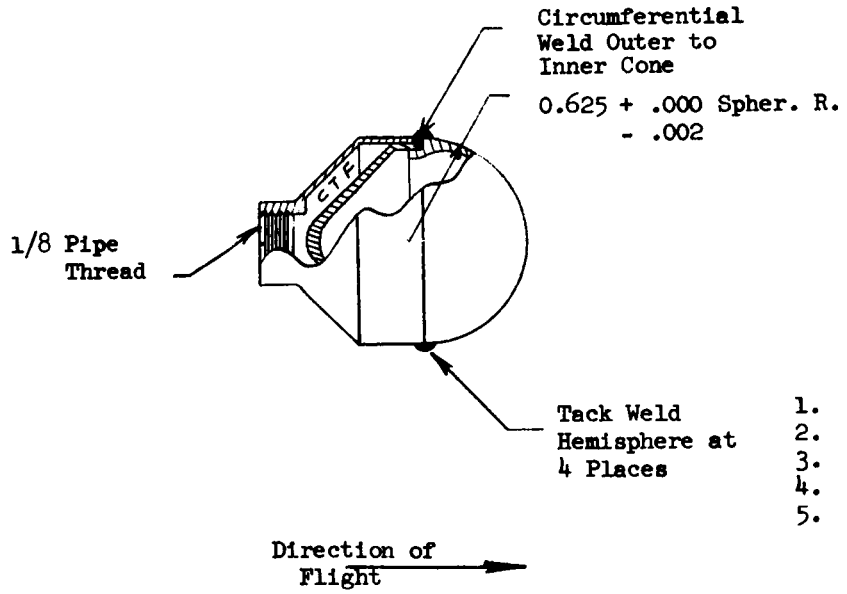


Notes:
1. Material 6061-T6
2. Weight of empty Model = 21 gm
3. Weight of internal Al = 2 gm
4. Weight of CTF = 5.4 gm
5. Loaded Model weight = 28.4 gm

(b)

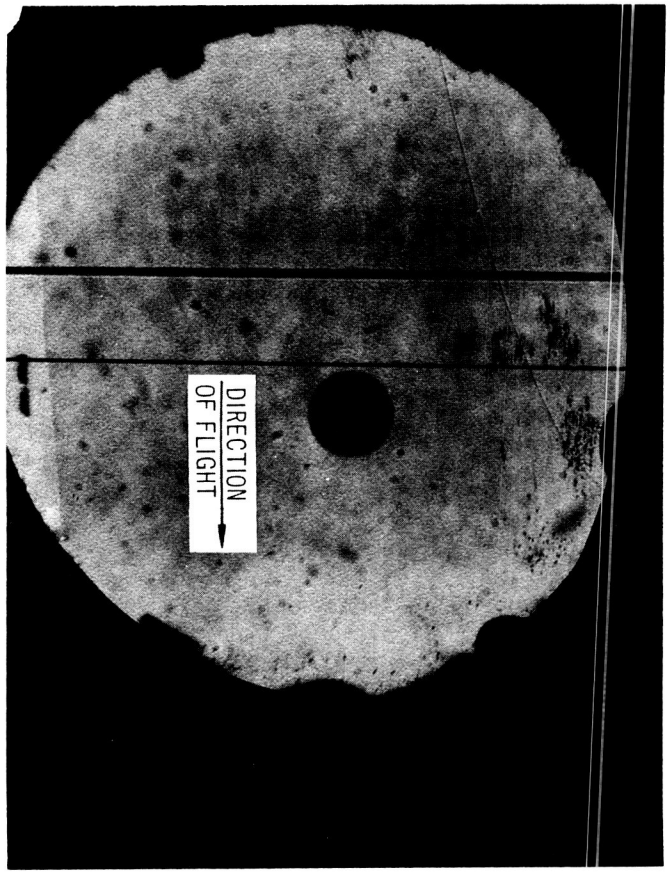


Type 1

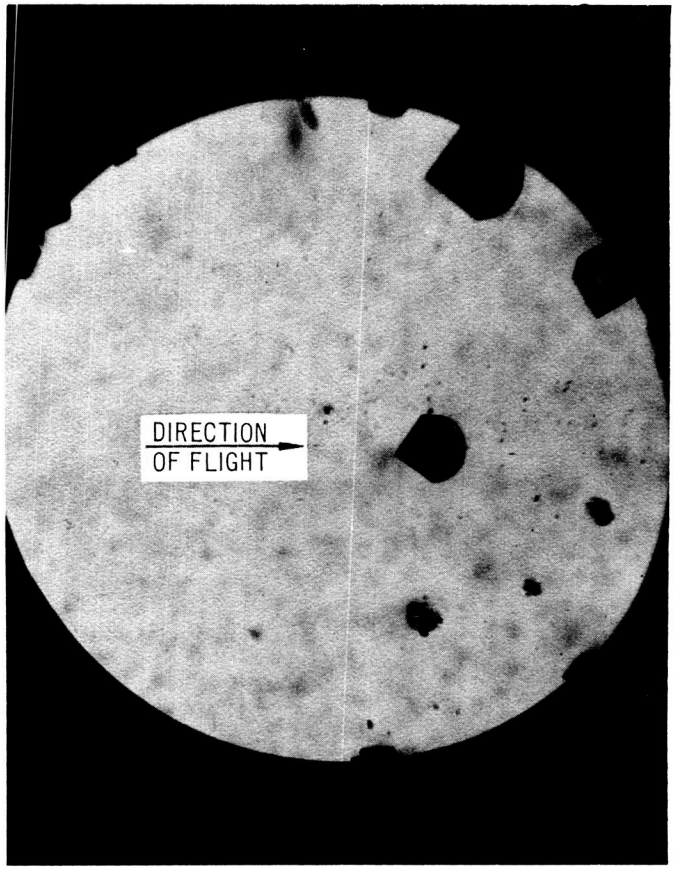


Type 2

Figure 3-12 Photographs Of Model Types 1 And 2 In Flight In Firings No. 11 And 16, Respectively

Figure 3-13 Large Granite Target After Impact

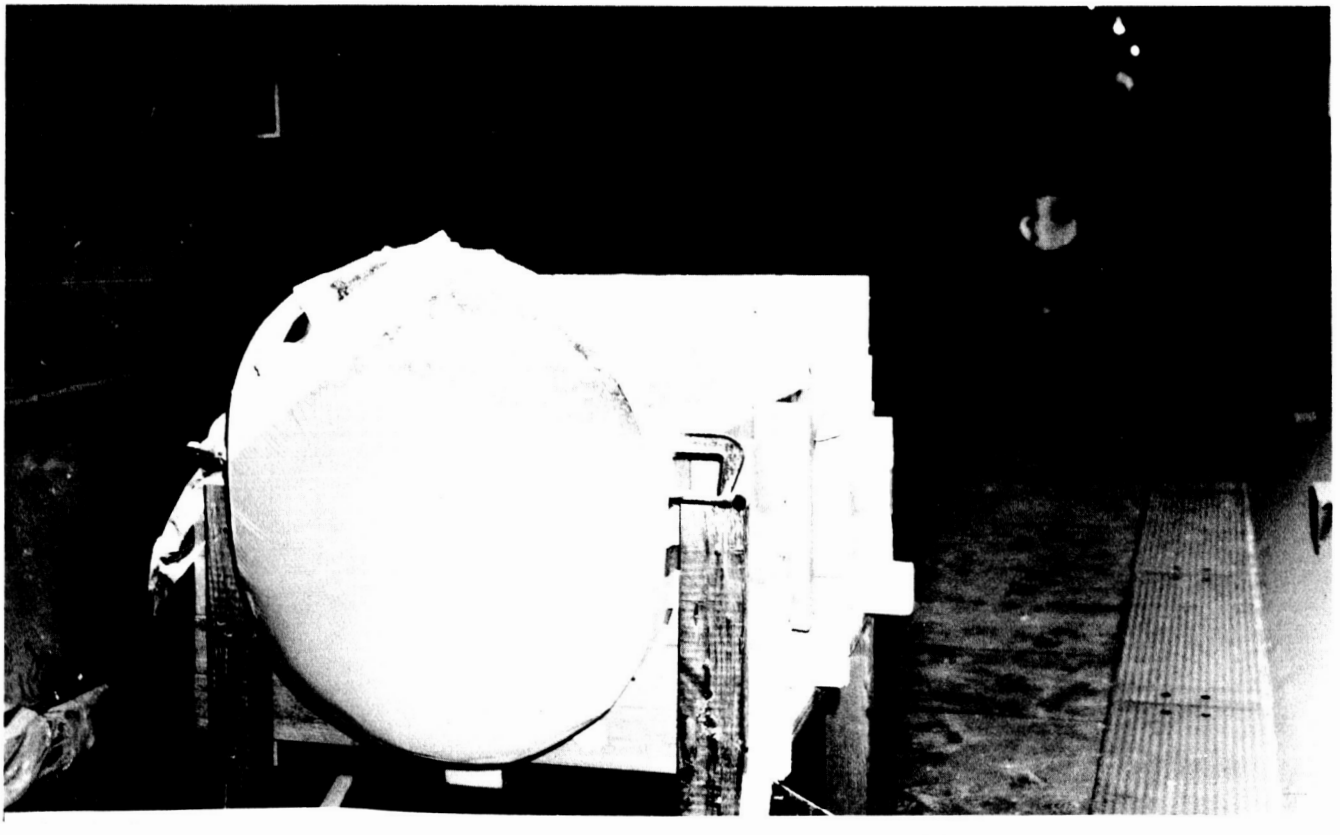

Figure 3-14 Dust-Like Target Before Firing

Photometric data were obtained in runs Nos. 11, 12, 14 and 15. From these data it is clear that flare initiation occurred upon impact. Photocell output traces obtained in runs 11 and 15 are presented in Figures 3-15 and 3-16 as being representative (omit the 3550Å traces in Figure 3-15). Runs Nos. 11 and 15 are basically the same with the exception that the projectile in 11 was loaded with CTF and aluminum powder, while the projectile in 15 was empty. Light obtained in 15, as indicated in Figure 3-16, is solely due to impact flash. Comparison of Figures 3-15 and 3-16 therefore indicates that the additional light obtained was due to the presence of reactants. In the case of a competent rock target, the maximum light intensity, with reactants present, occurred approximately 4-5 msec after impact. The duration of the event was on the order of 20 msec.

In Table 3-5 the data from output traces, like those presented in Figures 3-15 and 3-16, is summarized for the calibration source and runs nos. 11, 12, 14 and 15.

A photoflash lamp (G.E. #5B, with the plastic stripped) was used for calibration purposes because of its relatively high-color temperature and because the output of individual bulbs are highly consistent. The output from these bulbs is closely approximated by a 3800°K full radiator. Its peak luminous flux is $1.45 \times 10^6$ lumens. Calibration was also attempted with a tungsten lamp calibrated by the National Bureau of Standards; however, its output was insufficient to cause a noticeable output from the photocells at 3550Å and 4350Å. At other wavelengths, the results obtained using a tungsten lamp as a calibration source were consistent with results obtained using the photoflash lamp.

When using the photoflash lamp as a calibration source, it was assumed that the radiating area of the lamp was equal to its physical area. This assumption

T

PHOT

| | $\delta$ peak/G (in)[1] | | | | |
|---|---|---|---|---|---|
| Wavelength (Å) | 3550 | 4350 | 5100 | 6500 | 74 |
| Run no. | | | | | |
| Calibration | 0.18/3000 | 0.38/3000 | 0.83/1000 | 1.4/1000 | 1. |
| 11 (2) | 0.04/30 | 0.54/3 | off scale | 1.52/10 | C Sa |
| 12 | - | 0.19/30 | 0.28/10 | 0.86/30 | 1. |
| 14 | 0.45/1000 | 0.21/100 | 0.25/30 | 0.48/30 | 2. |
| 15 | 0.10/1000 | 0.30/1000 | 0.27/100 | 0.28/100 | 1. |

(1) $\delta$ = galvonometer deflection, G = amplifier gain, dt = incremental

(2) Target-to-photocell distance = 96 in; all others are 204 in.

able 3-5

OCELL DATA

| | $\int \delta dt/_G$ (in-msec)[1] | | | | |
|---|---|---|---|---|---|
| 00 | 3550 | 4350 | 5100 | 6500 | 7400 |
| 75/100 | 1.92/3000 | 5.77/3000 | 12.8/1000 | 19.4/1000 | 24.8/100 |
| ll<br>turated | 0.26/30 | 3.98/3 | off scale | 15.5/10 | Cell<br>Saturated |
| 41/10 | - | 1.03/30 | 1.8/10 | 5.25/30 | 13.1/10 |
| 59/30 | 0.90/1000 | 0.37/100 | 0.90/30 | 0.51/30 | 11.8/30 |
| 79/30 | 0.051/1000 | 0.37/1000 | 0.51/100 | 0.37/100 | 3.2/30 |

ime

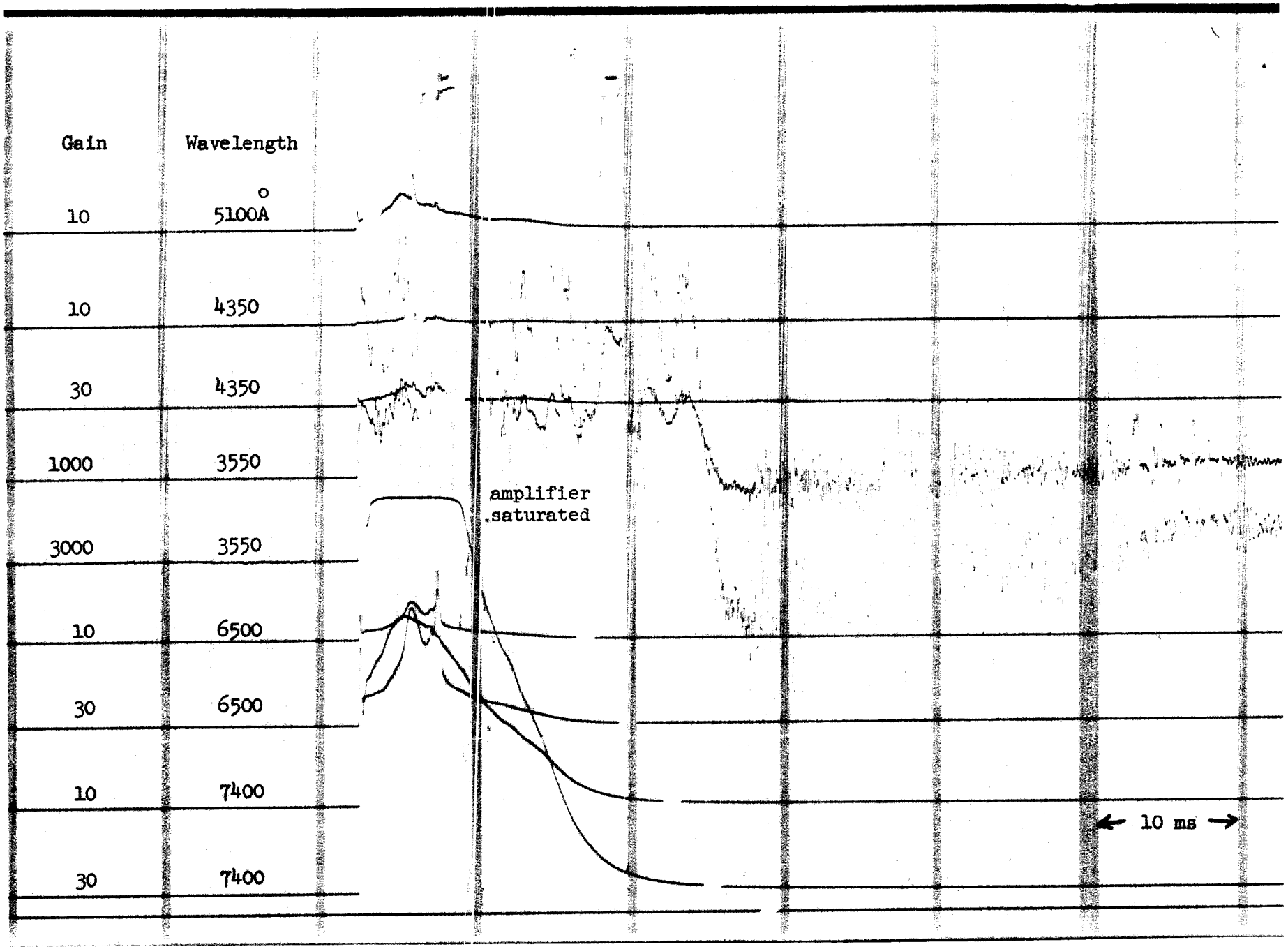


Figure 3-15 Photocell Outputs –Run No. 11

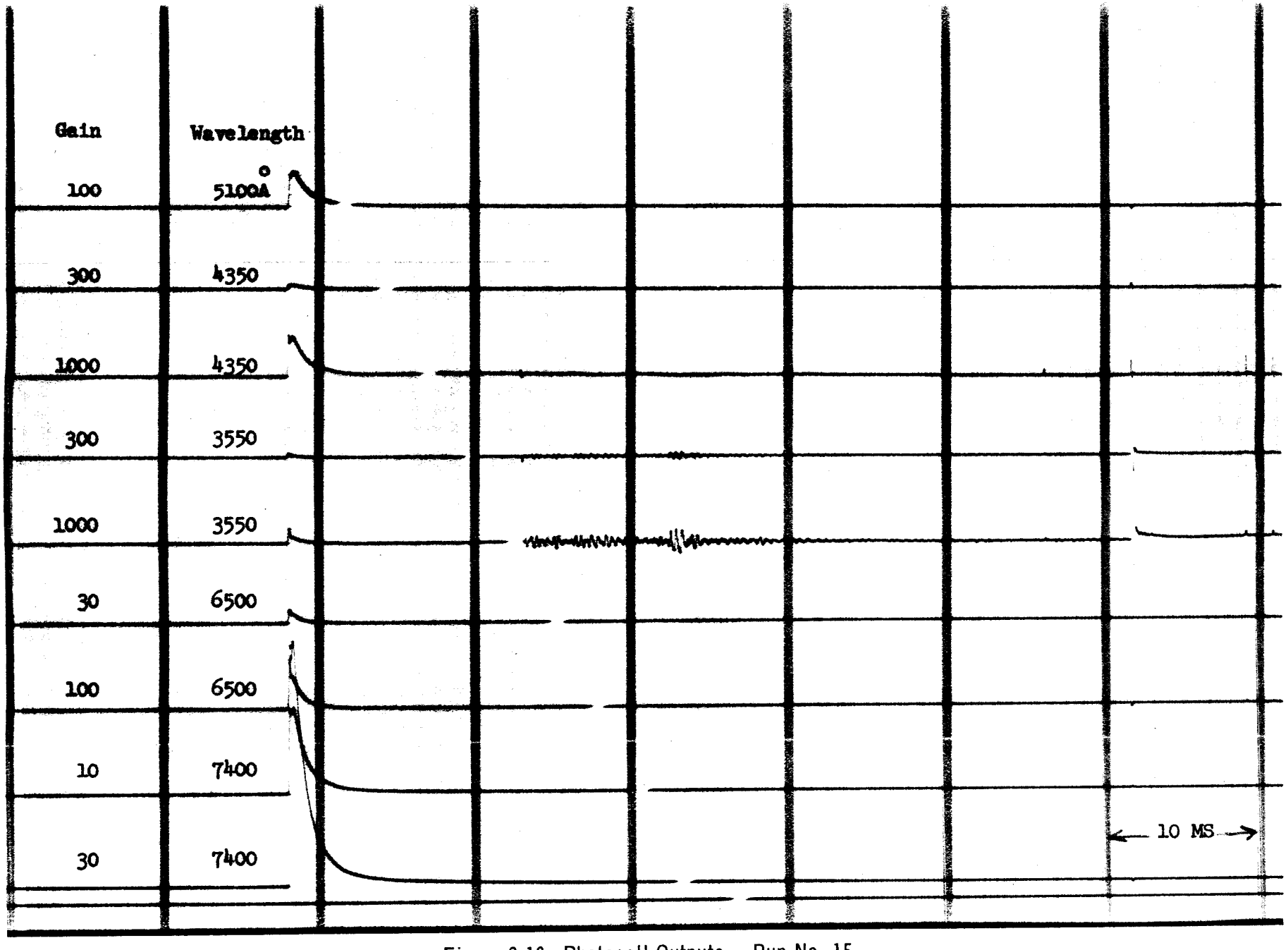


Figure 3-16 Photocell Outputs – Run No. 15

was checked by calculating the luminous flux and it was found to be $1.48 \times 10^6$ lumens, which is compatible with the value of $1.45 \times 10^6$ lumens.*

The calibration data are given in Table 3-6.

Figure 3-17 shows the peak irradiance values (watts/Å) from firings 11, 12, 14 and 15, that were obtained by using the data of Table 3-5 and the conversion derived from above. Figure 3-18 presents the total radiant-energy-per-unit wavelength (watt-sec/Å), again obtained using the data of Table 3-5 and the conversion above. In these figures, the high values shown for run 11 at 4350Å appear to be caused by strong Aℓ0 emission. The source of Aℓ0 could be an aluminum fixture which was used to hold the target in place during run 11 but not used during any other runs.

In order to compare the results obtained in the impact tests, with those obtained in the static tests, the luminous flux and quantity of light was estimated for run 12. The photocell outputs from this run were compared with the output from the photoflash lamp. The comparison was made at 4350Å, 5100Å, and 6500Å. The following values represent an average of the values at the three wavelengths. (The photoflash lamp output was assumed to be $1.45 \times 10^6$ lumens peak and 20,000 lumen-sec.) The values were $3.2 \times 10^6$ lumens per gram of reactants and $1.66 \times 10^4$ lumen-secs per gram. The luminous flux was comparable to several high values obtained in the static tests; the quantity of light was comparable to typical values achieved in static tests.

An attempt was made to calculate the flare temperature, several times during its duration, by a ratio of radiant intensities at two wavelengths. The wavelengths used in the calculation were close together because the assumption of

---

* Luminous flux, measured in lumens, is calculated as follows: The spectral distribution of the radiation from the lamp is found from its temperature using Planck's radiation formula: $J_\lambda(\text{watts cm}^{-2}\ \text{cm}^{-1}) = C_1 \lambda^{-5} / e^{C_2/\lambda T} - 1)$ where $C_1 = 3.74 \times 10^{-12}$ watt. $\text{cm}^2$ and $c_2 = 1.438$ cm. deg. The total luminous flux is given by $\int K\lambda J\lambda d\lambda$ where $K\lambda$ is the luminous efficiency of radiation and depends on wavelength. $K\lambda$ is a maximum for radiation of wavelength 5550Å and the value for any other wavelength is found by multiplying this maximum value (K max = 682 lumens per watt) by the relative luminous efficiency for that wavelength (a curve of relative luminous efficiency is given, in Photometry by J. W. T. Walsh, Figure 44).

Table 3-6

CALIBRATION DATA

| $\lambda$(Å) | $J_\lambda$ (watts/Å)* | Deflection, $\delta$ (in)** gain | $J_\lambda/\delta$ (Watts/Å/in)*** |
|---|---|---|---|
| 3550 | 0.377 | 0.18/3000 | 6290 |
| 4350 | 1.200 | 0.38/3000 | 9460 |
| 5100 | 1.93 | 0.83/1000 | 2320 |
| 6500 | 2.78 | 1.4/1000 | 1990 |
| 7400 | 2.97 | 1.75/100 | 170 |

* Theoretical irradiance from a 3800°K full radiator (29 $1c_2$)

** From Table 3-5

*** For unity gain

Figure 3-17 Radiant Flux Achieved in Impact Tests

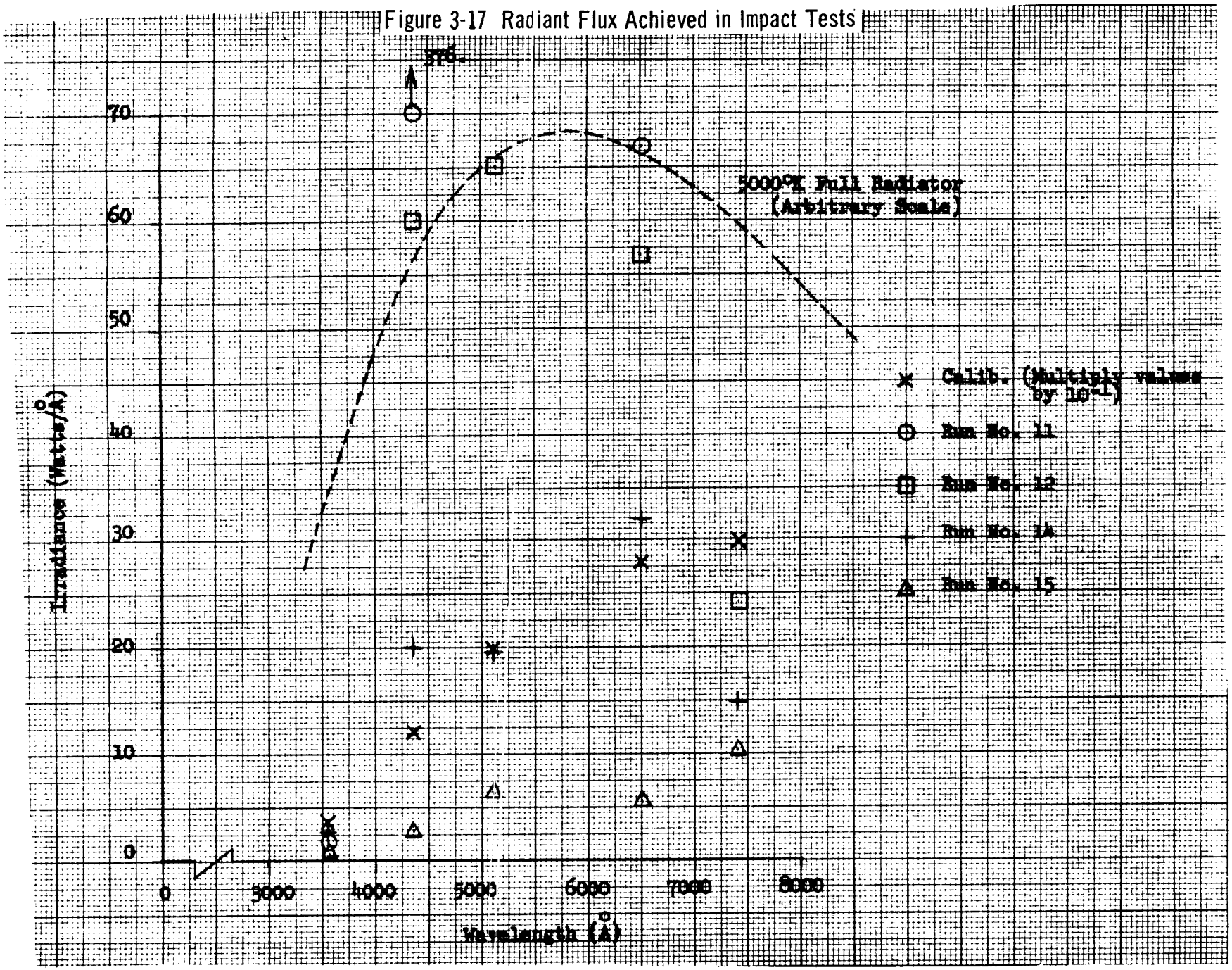

Figure 3-18 Radiant Energy Achieved in Impact Tests

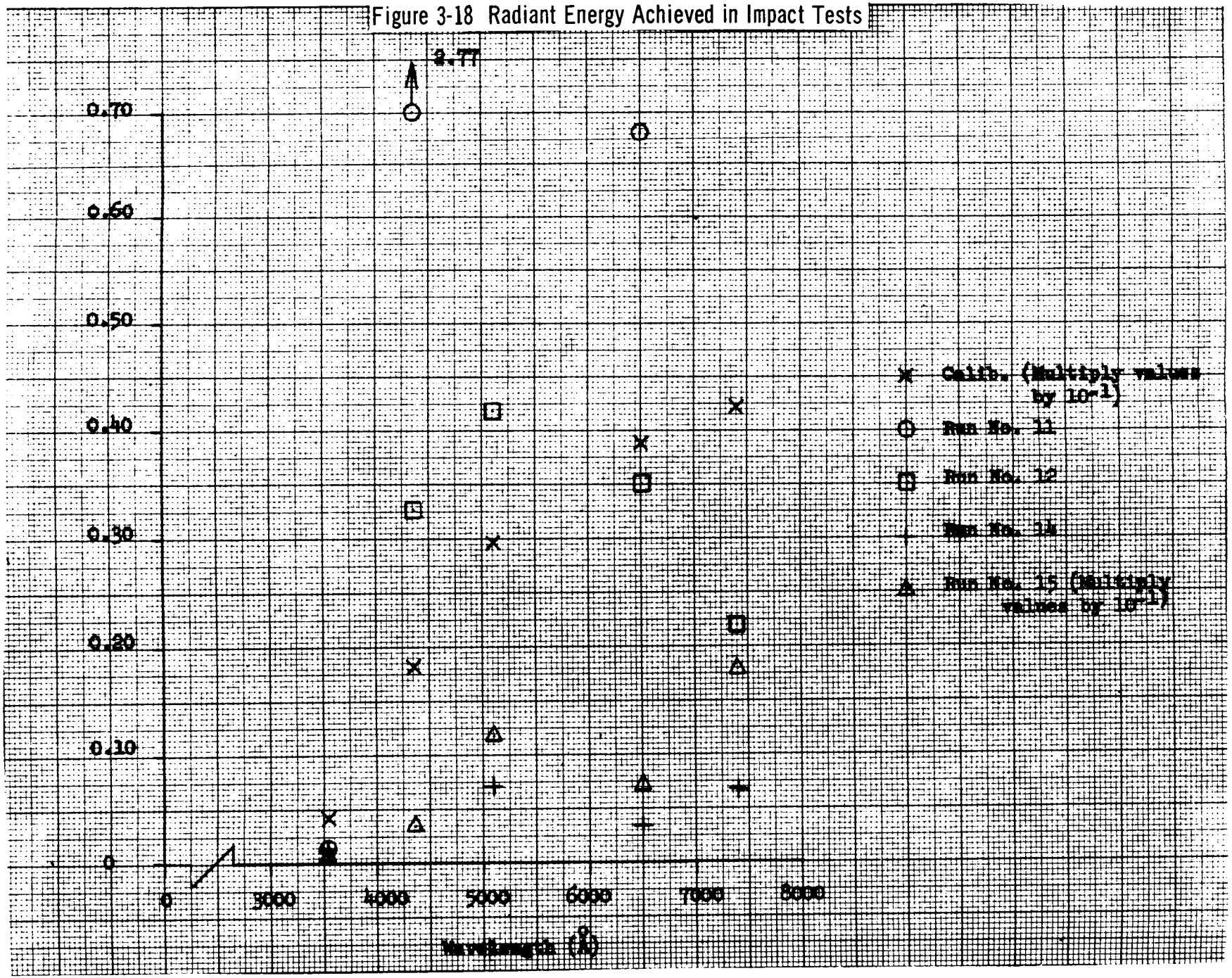

equal emittance values at the two wavelengths is generally more valid for a narrow spectral interval than for a wide one.

Temperatures calculated in this manner were erratic, indicating that spectral distribution of the flare radiation varies considerably from "graybody" conditions. This is also indicated in Figure 3-17 when spectral distribution of the flare intensity is compared with the ideal 5000°K curve. At long wavelengths, relative intensity is much less than what it would be for a full radiator.

A sequence of photographs of the flare were obtained in runs 13 and 14 and are shown in Figures 3-19 and 3-20, respectively. In Figure 3-19, the frame speed is 6,300 frames/sec so that the time between exposures is 0.16 msec. In Figure 3-20, the frame speed is 4600 frames/sec and the time between exposures 0.22 msec. In Figure 3-15, the total sequence is approximately 1.3 msec in duration; in Figure 3-20, the duration is 0.66 msec. Photometric data show, however, that the duration of the flare is on the order of 15-20 msec for a hard target. Thus, it appears that the photographs in Figures 3-19 and 3-20 show the impact flash rather than a flame due to the flare. The sequence of photographs indicate that for a soft target the impact flash is more prolonged and less intense than for a hard target.

A spectrum of the flare in firing 11 is shown in Figure 3-21. The spectral lines shown on the edges are used for calibration. Due to an error, the calibration spectra are superimposed on the spectra of the flare, shown in the center portion, and should be disregarded. The spectrum shows Aℓ0, Na, Li, and possibly iron. It appears that these emissions are caused, in part, by excitation of target material.

Samples were taken of the atmosphere in the range tank following each firing. An analysis of these samples revealed only CO and $CO_2$ which indicates a fairly complete combination of the CTF into solid forms.

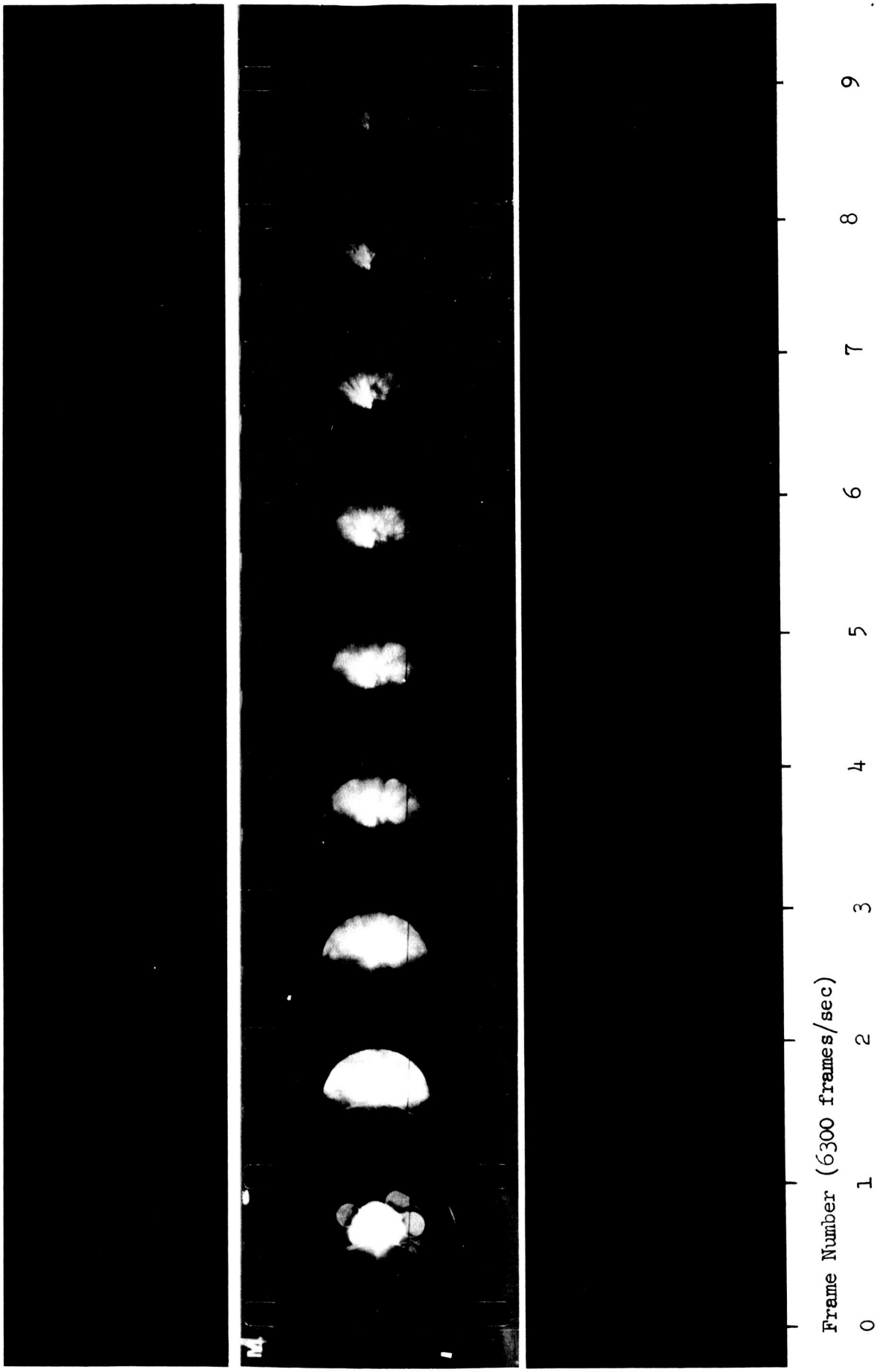


Figure 3-19 Photographs of Flare in Firing No. 13 (Dust Target)

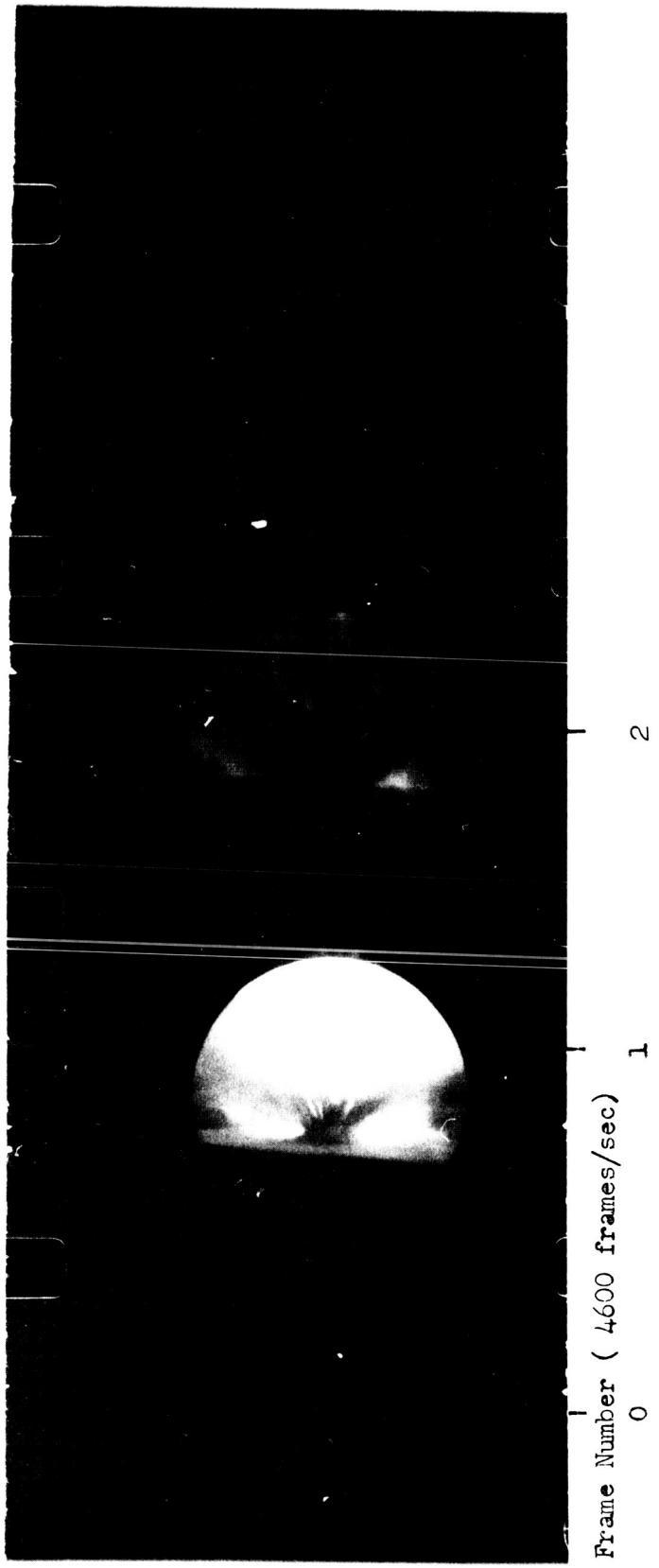


Figure 3-20 Photographs of Flare in Firing No. 14 (Solid Granite Target)

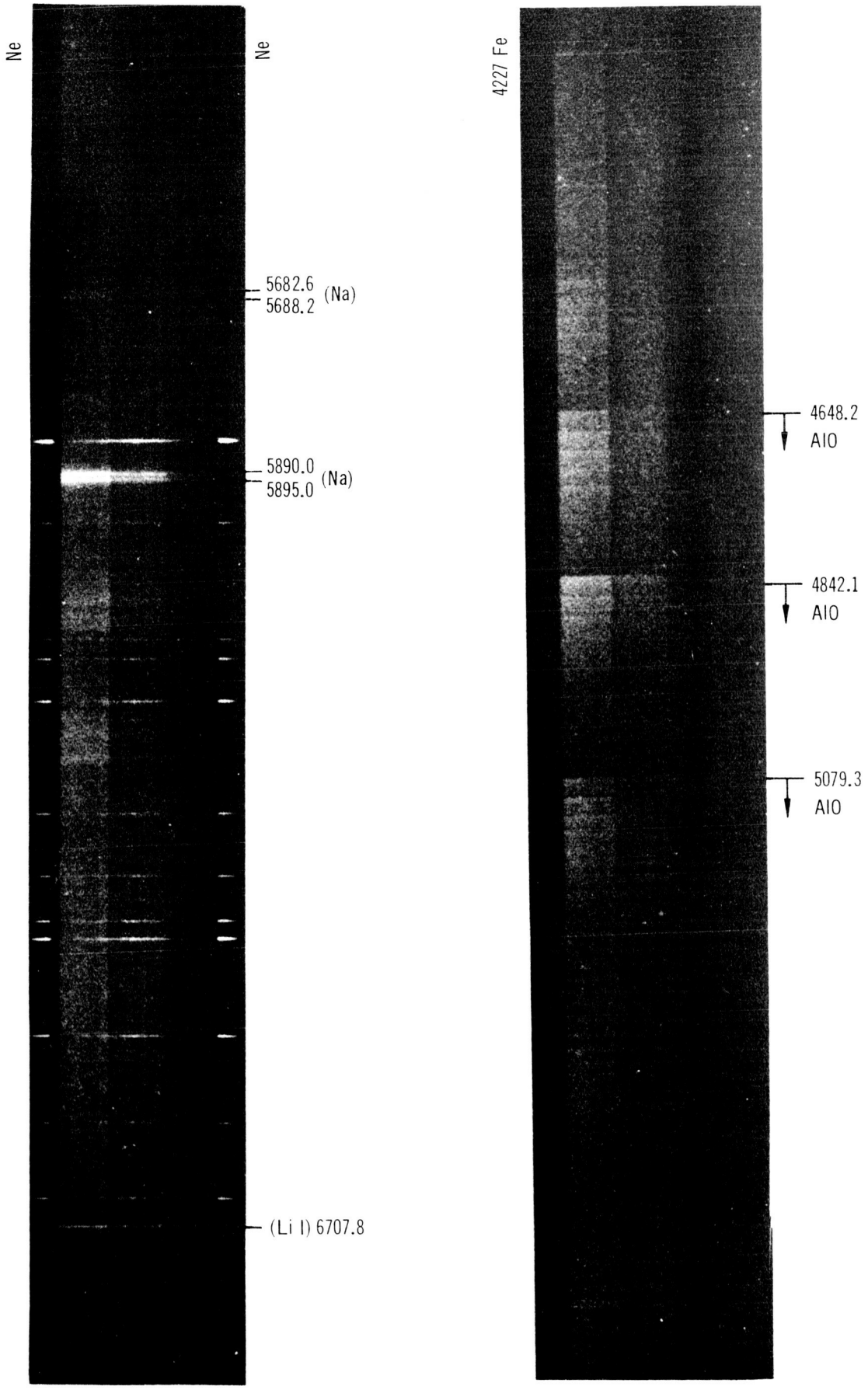


Figure 3-21 Spectra of Flare in Firing No. 11

## 3.4 SPECTROSCOPIC TESTS

### 3.4.1 Summary

The objective of these tests was to obtain vacuum spectrograms of simulated lunar soil (some containing up to 10% hydrogen-containing molecules) when excited by the combustion of a CTF-Al-flare model. These spectra were to be analyzed to verify that various soil models are distinguishable (i.e., approximate relative abundances of soil constituents are determinable) and that the presence of hydrogen can be detected.

In order to accomplish this objective three main problem areas were recognized and solved. They were: (1) containment of reactants, (2) ignition of reactants, (3) purity of reactants, i.e., as nearly as possible keeping out initially that what you are looking for in the soil, e.g., Si and Fe in the aluminum and HF in the CTF. These three problem areas were solved by experimentation and evaluation in the following way.

Several series of small pure (99.99+%) aluminum ampules containing CTF, aluminum powder and admixed simulated lunar soils (granite, gabbro, and serpentine, the latter containing more than 10% in hydrogen-containing molecules) were prepared and initiation attempted (see Table 3-7 and Figs. 3-22, -23, and -24). Most of these failed for reasons ranging from ampule leaks and ignition failure to spectrograph speed adjustment problems. The vacuum system constantly performed well. 40 to 70 microns were obtained in the chamber within a few minutes and held throughout each attempt.

The final spectroscopic test series (Series 14, Table 3-8) was successful in that 11 of 12 pyrex ampules were fired and 9 spectrograms were obtained. This was considered adequate for comparisons to be drawn. Pyrex ampules were made for this series since preliminary tests, where spectrograms were obtained, revealed no silicon lines or bands. Definite spectral differences are discernible between the calibration shots without admixed soils, and those with soil. Also there are obvious spectral differences between the soils. Light intensity differences are also apparent at the three gabbro quantity ratios (1, 5, 25). Gabbro was finally used for the dilution tests because larger

| Series | Environment | Ampule Type | Ignition Method |
|---|---|---|---|
| 1 | Air | .030 in. wall cyl. 5/8" tubing crimped on ends, 99.99+% pure aluminum | Both ends clamped in mount 1000A/6V D.C. Heating |
| 2 | Air | Same | One end clamped in mount. Sharp point electrode of pure Al arced at 1000A/6V D.C |
| 3 | Air | Same | Same |
| 4 | Air | Same | Same |
| 5 | Vacuum of 70μ | Same | Same |
| 6 | Vacuum of 70 μ | Same | Same |
| 7 | 4-Vacuum 40μ | Same | Same |
| | 1-Air | Same | Same |
| 8 | Vacuum of 40μ | Same | Same |

Table 3-7

COPIC TEST SERIES* ATTEMPTED

| CTF | Fuel | Soils | Results |
|---|---|---|---|
| NaF scrubbed and fractionally distilled | Tubing itself | None | All ampules leaked CTF- non ignited |
| Same | Tubing itself | None | Blew up holder - some spectra obtained w/CENCO spectrograph |
| Same | Cup around electrode containing fine impure Al wool | None | Two flares - one spectra obtained w/CENCO spectrograph |
| Same | Cup around electrode containing coarse pure Al wool | Yes | One good spectra showing soil involvement w/CENCO |
| Same | Same except one seeded with Lithium fines | None | Failed to ignite |
| Impure | Impure fine Aluminum dust inside ampule | None | Two detonations no |
| Same | Pure<300$\mu$ aluminum powder inside ampule | 2 w/o<br>2 with | No ignition |
| Same | Impure Al dust inside ampule | None | Detonation spectra overexposed (started using Meinel Stellar Spectrograph) |
| Same | Impure fine aluminum dust inside ampule | 1-None )<br>1-gabbro )<br>1-granite )<br>1-serpentine) | No ignition<br><br>Detonated and blew up vacuum chamber Spectra obtained showing soil involvement. |

| Series | Environment | Ampule Type | Ignition Method |
|---|---|---|---|
| 9 | Vacuum 70μ | Same 5/8" tube | Same |
| 10 | Vacuum 70μ | Same with small clamp on free end | Same |
| 11 | - | .015" wall- 5/8" cyl. tubing crimped on ends 99.99% pure Al | - |
| 12 | Vacuum 40μ | .030 in wall, cyl 5/8" tubing with local center section thinned to .015" wall thickness, crimped on ends, 99.99+% pure Al | Both ends clamped in mount. 1000A/6V D. heating |
| 13 | Vacuum 40μ | Pyrex glass, vacuum sealed after filling. | Platinum wire heating coil inside ampule. Variable power D.C. heating. |

* A series of seven shots, using as pure materials as possible, were

(1) Two calibration shots consisting of 10 gms CTF and 4 gms Al

(2) A shot consisting of 1 gm gabbro, 10 gms CTF, and 4 gms Al

(3) A shot consisting of 1 gm granite, 10 gms CTF, and 4 gms Al

(4) A shot consisting of 1 gm serpentine, 10 gms CTF, and 4 gm

(5) A shot consisting of 5 gms serpentine, 10 gms CTF, and 4 gr

(6) A shot consisting of 25 gms serpentine, 10 gms CTF, and 4 g

However, a complete program of shots was not successfully complet

Table 3-7 (cont)

| CTF | Fuel | Soils | Results |
|---|---|---|---|
| NaF scrubbed only | Pure < 300μ aluminum powder inside ampule | None | Delayed burning after expansion. Blew up bell jar |
| Same | Same | 2-None 5-with | No ignition |
| - | - | - | Flares split. Crimped ends failed to seal properly |
| Same | Same | 2-None | Thin center section arc vaporized without igniting contents |
| Same | Same | None | Ignition coil burnt out without igniting ampule contents |

planned as follows:

powder.

powder.

l powder.

s Al powder.

ns Al powder.

ms Al powder.

ed for all of the 13 preliminary series.

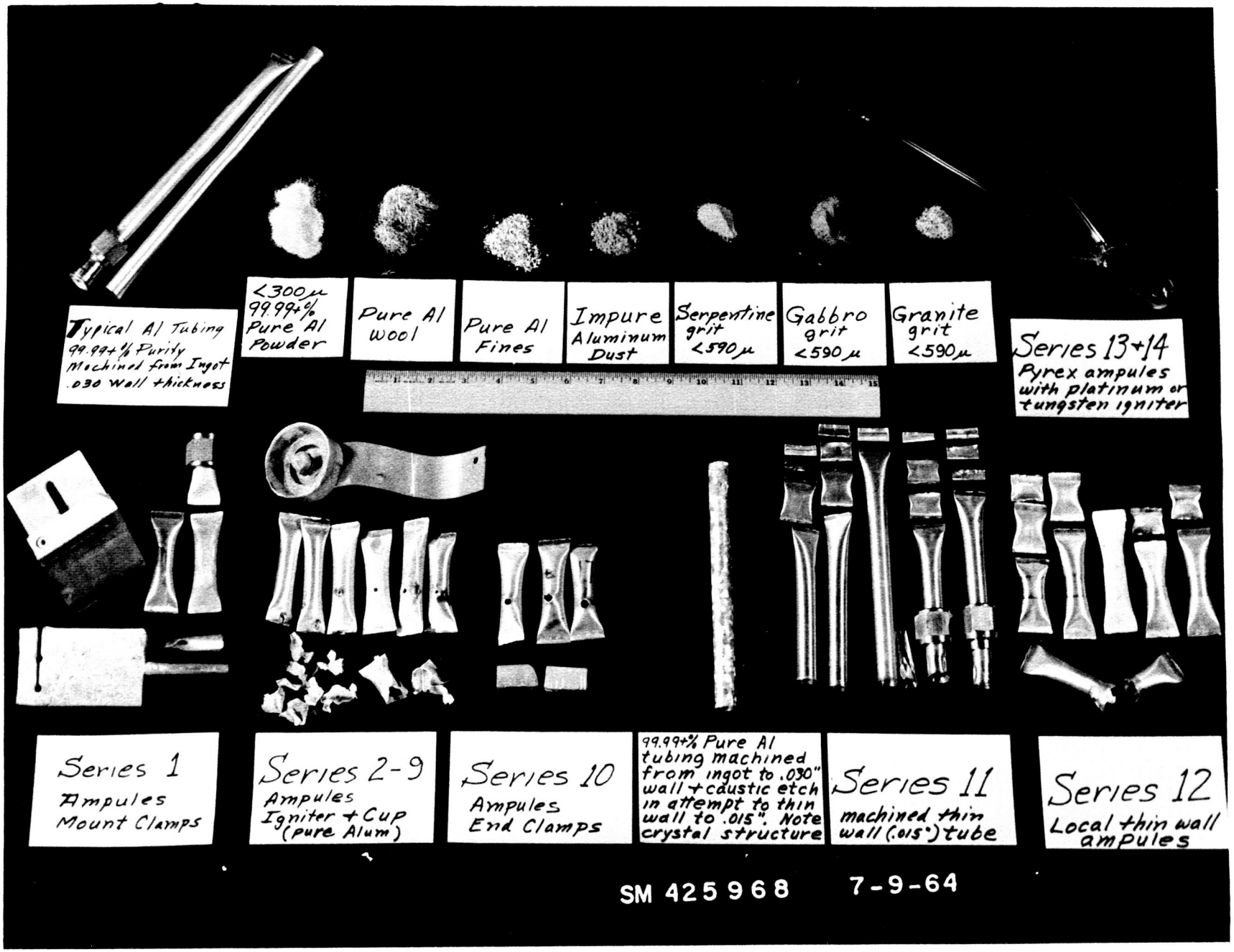


Figure 3-22 Spectroscopic Test Components

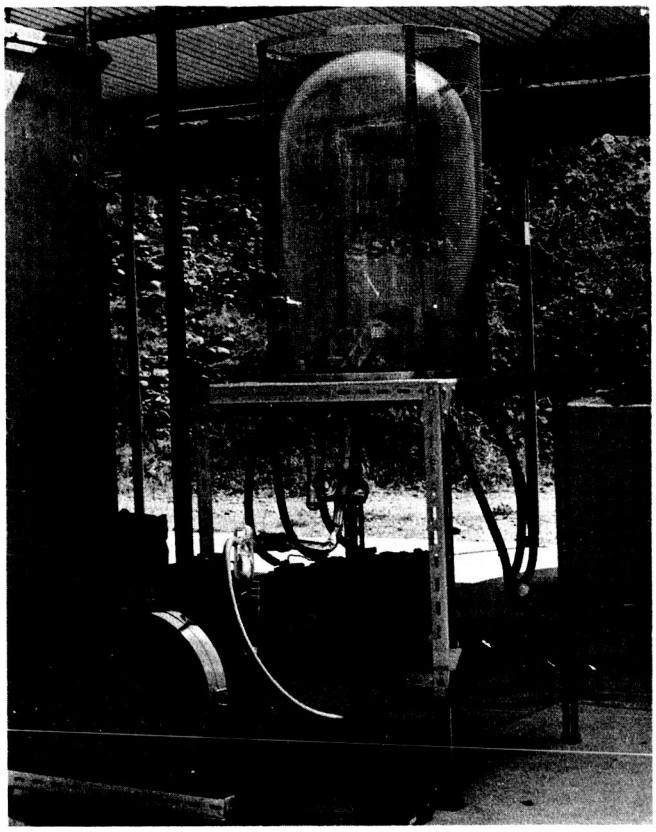

Figure 3-23 General Spectroscopic Test Setup

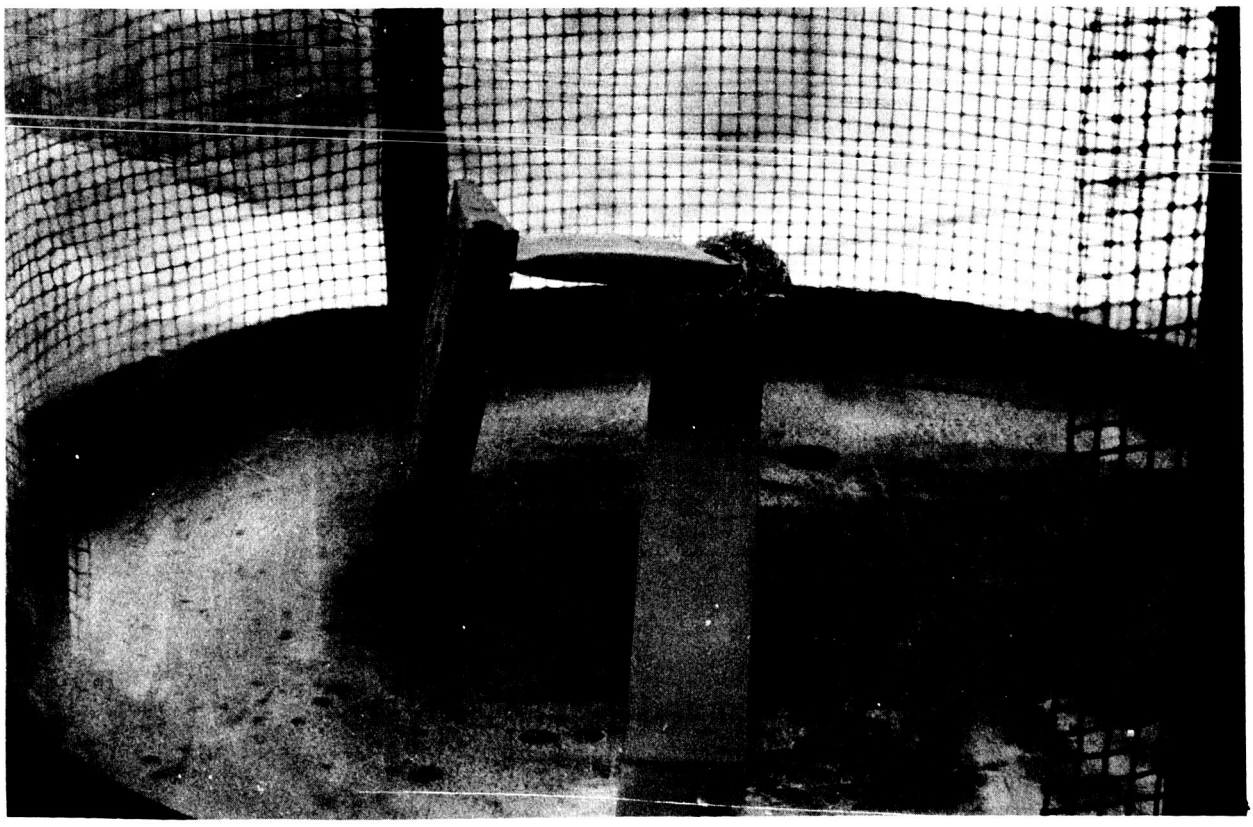

Figure 3-24 Spectroscopic test setup In Vacuum Chamber - Test Series 2-9

Tab

FINAL SPECTRO

Test Conditions: Container - Pyrex Glass Ampule
Ignition - Tungsten filament inside ampule
Pressure - 40 to 70 microns

| Spectrogram 32 (Calibration) | Spectrogram 37 (Calibration) | Spect Soil-no (< 590μ) C |
|---|---|---|
| Al- < 300μ powder 99.99+% purity & passivated 4 grams<br><br>CTF-NAF scrubbed & fractionally distilled 10 grams | Al- < 300μ powder 99.99+% purity & non-passivated 4 grams<br><br>CTF-NAF scrubbed but non-distilled 10 grams | Al- < 300μ purity but n 4 grams<br><br>CRF-NaF s non-distille |

| Spectrogram 42 (Calibration) |
|---|
| Al- < 300μ powder 99.99+% purity & passivated 4 grams<br><br>CTF-NaF scrubbed & fractionally distilled 10 grams |

ble 3-8

SCOPIC TEST SERIES

| rogram 39<br>n-passivated<br>ranite-1 gram | Spectrogram 38<br>Soil-non-passivated<br>(< 590 μ) Gabbro-1 gram | Spectrogram 33<br>Soil-passivated<br>Serpentine (< 590μ) 1 gram |
|---|---|---|
| powder 99. 99+%<br>on-passivated | Al- < 300μ powder 99. 99+%<br>but non-passivated 4 grams | Al- < 300μ powder 99. 99+%<br>purity & passivated<br>4 grams |
| crubbed but<br>d 10 grams | CTF-NaF scrubbed but<br>non-distilled 10 grams | CTF-NaF scrubbed &<br>fractionally distilled<br>10 grams |
| | Spectrogram 40<br>Soil-non-passivated<br>(< 590μ) Gabbro 5 grams | Spectrogram 35<br>Soil-non-passivated<br>( < 590μ) Serpentine 1 gram |
| | Al- < 300μ powder 99. 99+%<br>purity but non-passivated<br>4 grams | Al- < 300μ powder 99. 99+%<br>purity & passivated<br>4 grams |
| | CTF-NaF scrubbed but<br>non-distilled 10 grams | CTF-NaF scrubbed but<br>non-distilled 10 grams |
| | Spectrogram 41<br>Soil-non-passivated<br>( < 590μ) Gabbro 25 grams | Spectrogram 34<br>Soil-non-passivated<br>( < 590μ) Serpentine 1 gram |
| | Al- < 300μ powder 99. 99+%<br>purity but non-passivated<br>4 grams | Al- < 300μ powder 99. 99+%<br>purity & non-passivated<br>4 grams |
| | CTF-NaF scrubbed but<br>non-distilled 10 grams | CTF-NaF scrubbed but<br>non-distilled 10 grams |

than 1 gram quantities of serpentine caused chemical reaction and heating during ampule filling and was therefore considered dangerous to handle.

No OH or H features were observed since the spectrograph did not extend into the primary field of interest.

### 3.4.2 Test Setup

All ampules were loaded and fired at the Douglas Astropower test site. The preliminary test setup for series 1 thru 13 is shown in Figures 3-23 and -24. The spectrograph was located approximately 9 ft from the flare. The ampules were held in position by an aluminum fixture which gripped the crimped ends (see Figure 3-24). Storage batteries and electrical leads through the test plate were utilized for initiation. A bell jar, 18 in. x 30 in., was used for all vacuum tests; only the base plate and fixtures were used for the air tests.

In series 13, the pyrex ampule was suspended between the terminals by its platinum ignition wire.

In the final series (14) the pyrex ampule (at approximately 77° K) was placed on one of the bent over terminals and allowed to warm up until the integral tungsten wire caused ignition of the contents. Since some shots were performed in daylight, and ampule warm-up time varied between 15 and 45 minutes, the entire test setup was wrapped in an opaque covering which allowed the spectrograph to be open until the flare occurred.

### 3.4.3 Aluminum and Pyrex Ampules Preparation, Loading and Handling, and Safety Experiment

#### 3.4.3.1 Aluminum and Pyrex Ampules Preparation Procedures

Aluminum test sample preparation for Project ELF consisted of filling a number of ampules of high purity aluminum tubing with CTF, in some instances the ampules contained finely divided aluminum admixed with soil. The tubing was cleaned and passivated before filling. The ampules were formed from the tubing by a remote-control crimping machine. The CTF was initially purified by NaF scrubbing and fractional distillation before being

placed in the ampules; however, later in the preliminary series NaF scrubbed CTF was used to save time.

Although failures were experienced throughout the procedure, most of the basic problems were solved. Figure 3-22 indicates a great deal in this regard.

The pyrex ampules were fabricated from standard pyrex stock by glass blowing techniques. All seals were made in the same manner and vacuum checked. The ampules were configured to provide a CTF fill stem, a soil-aluminum fill stem, and two igniter wire stems. The igniter wire was installed and sealed before the components to be tested were filled. In series 14 the ampules were not passivated due to the reactivity of the gaseous CTF and tungsten. After filling with soil and aluminum the stem was sealed off. After filling with CTF (at about 77° K) glass blowing techniques were again employed to make the final seal. Only one ampule had to be disposed of before firing due to a leak.

3.4.3.2 Loading and Handling

Several techniques of filling the ampules were investigated before an acceptable one was chosen. The technique chosen involved no prepassivation of aluminum powder admixed with soil before placement in the ampule. Because no hydrogen phenomena was discovered in the first soil test (Spectrogram 33) of the final series, as well as the long time required to prepare the fractionally distilled CTF (8 hrs. for 10-15 ml), the ampules were then filled with NaF scrubbed CTF. The transfer of CTF was accomplished by warming the calibrated 300-gm CTF (NaF scrubbed) glass storage vessel and immersing the ampule in $LN_2$. Before sealing off the aluminum ampule, it was warmed to approximately room temperature to allow the solid CTF to melt away from the crimp area. In the case of pyrex, the ampule remained in the $LN_2$ while the fill stem was sealed off by melting, a sufficient distance away from the solid CTF. It was then allowed to cool and then lowered into the $LN_2$ bath where it was stored until firing.

3.4.3.3 Safety Experiments

During the course of events the wisdom of carrying around a mixture of Al and solid CTF at $LN_2$ temperatures was questioned, consequently three standard impact tests were run on a frozen ampule. No ignition or detonation occurred under 360 ft-lb/in$^2$ of impact (maximum obtainable from the apparatus).

3.4.4 Instrumentation

The spectrograph used in these tests was the same one used in the Douglas Light-Gas-Gun Tests. The spectrograph was a Cassegrainian mounted grating (600 lines per mm) type. It had a dispersion of approximately 120Å/mm. The wavelength region which was employed in test series 0 thru 8 was 4200Å - 6700Å. In test series 14 this region was changed to 3200Å - 5400Å. The camera employed a folded Schmidt system and Kodak 103a-0 and 103a-F plates. A step filter, permitting passage of approximately 100%, 10%, and 1% of the incident light, covered the slit proving three different, simultaneous exposures. A Stokes vacuum gauge was employed for all environment measurements.

3.4.5 Experimental Results

Only cursory evaluation was made of the few spectrograms obtained in the preliminary series of tests. This was because there were not enough in any one series to make comparisons. However, the available spectrograms were examined and used to determine that some soil constituents were being excited and that Silicon was not one of them. This allowed series 14 to be undertaken with the pyrex ampules suggested earlier in the program.

Figures 3-25, -26, and -27 show the spectra from the final test series and Table 3-8 gives the particulars on ampule loading and treatment. Table 3-9 presents the relative densities of lines and bandheads as a result of examination of the spectrograms taken of the final series of shots. All numbers in this table are very low because of the noisy and grainy background of the fast 103a-F film which had to be used because of the limiting millisecond exposure time. The graininess of the emulsion is evident in the microdensitometer

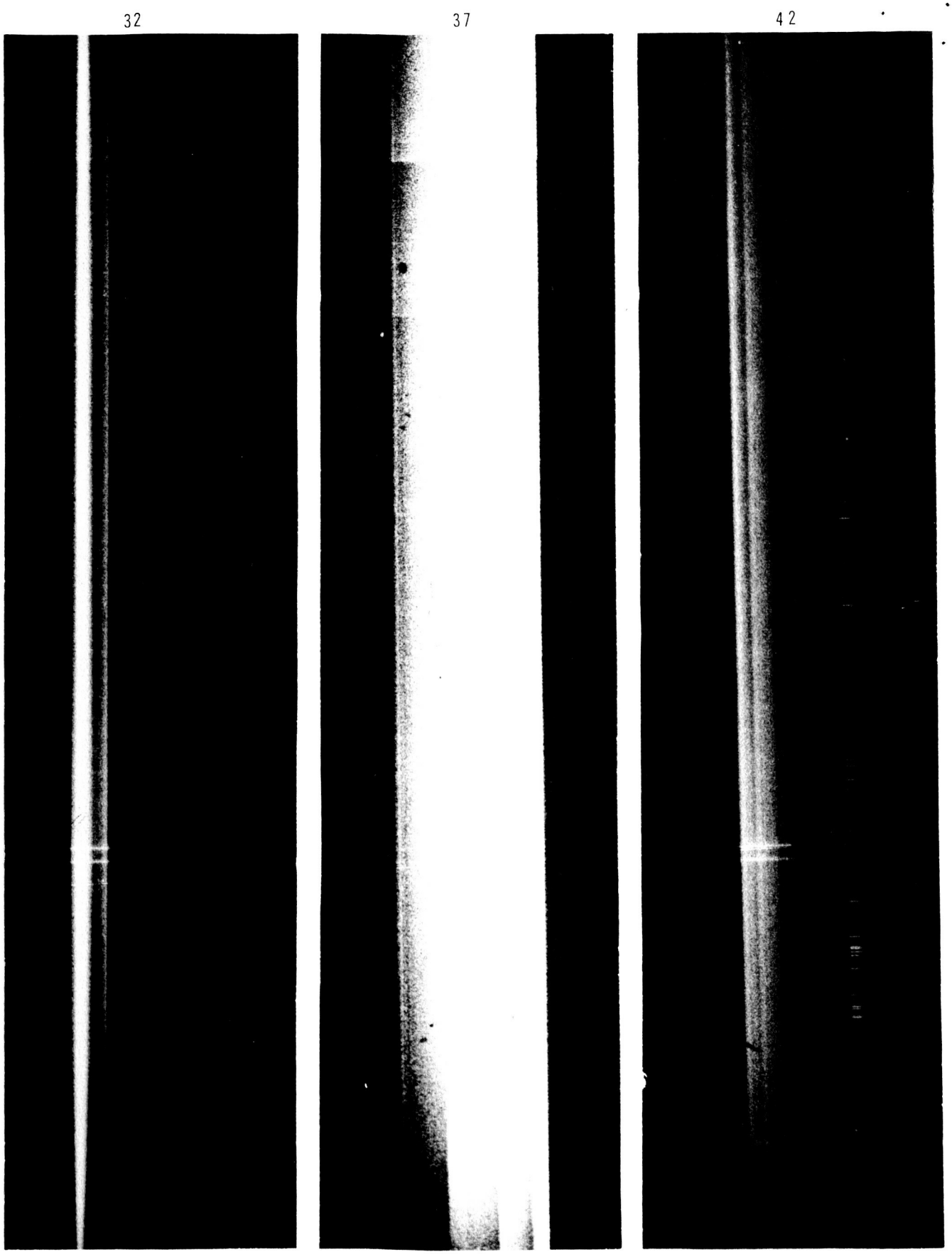


Figure 3-25 Spectrogram Comparison, Calibration Shots Dac Test Series 14
Best Print Of Each Used (Different Exposure Times)

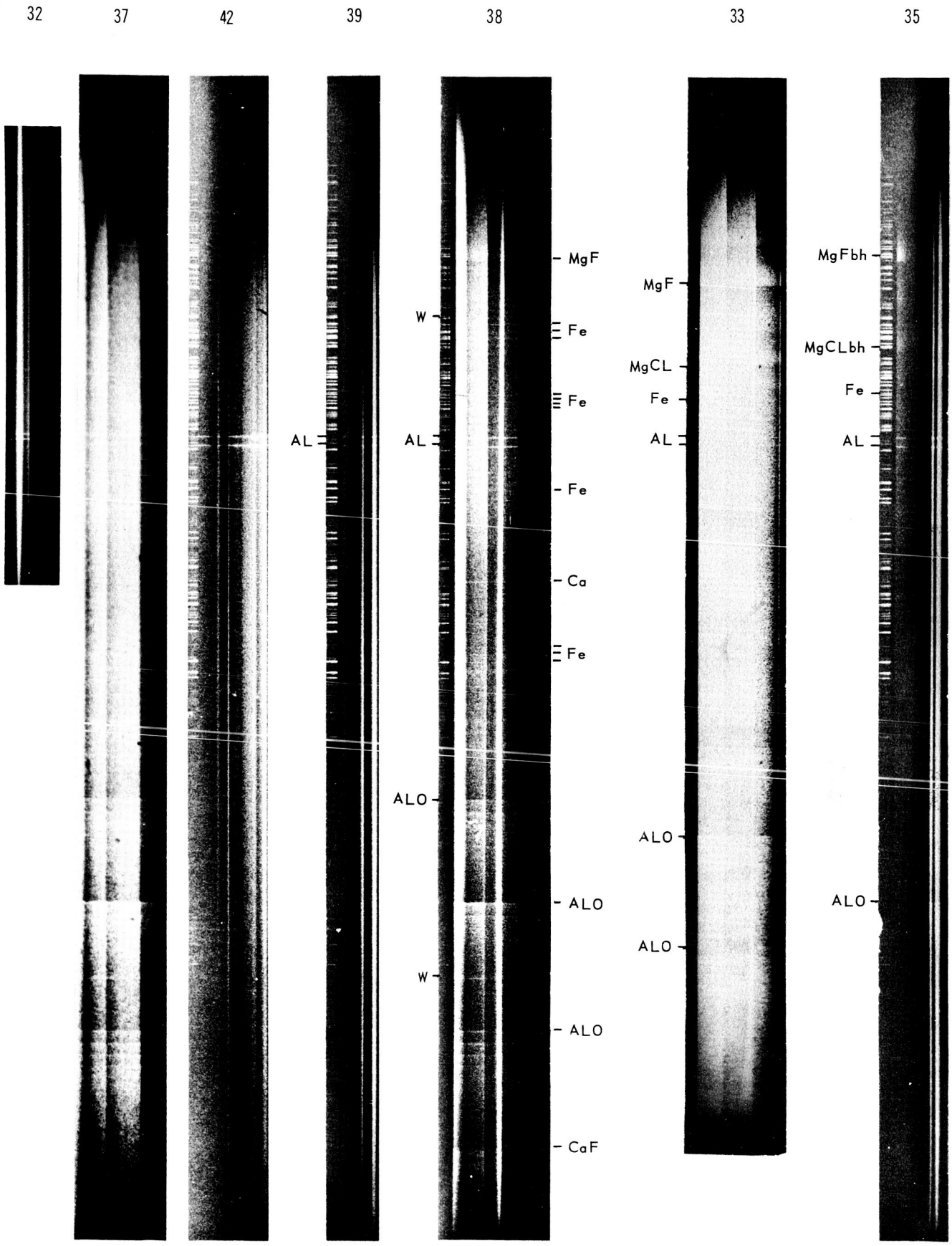


Figure 3-26 Spectrogram Comparison Calibration Shots & Soils Dac Test Shots

Best Print Of Each Used (Different Exposure Times)


| FILTER/CONTRAST | EXPOSURE TIME | DEVELOP TIME | ENLARGER LENS SETTING |
|---|---|---|---|
| #4/4 | 45 SEC | 2 MIN | F8 |

Figure 3-27 Spectrogram Comparison Gabbro Ratio Shots (Intensity) Dac Test Series 14

Table 3-9

RELATIVE DENSITIES OF LINES AND BANDHEADS

103a-F film---$\gamma$ = 0.6---normalized to Al 3962 plus background.

| Spectrogram # | 32 | 33 | 35 | 37 | 38 | 39 | 40 41 42 |
|---|---|---|---|---|---|---|---|
| Line | | | | | | | |
| Al 3962 | 0.63 | 0.11 | 0.28 | not analyzed | 0.25 | 0.28 | not analyzed |
| Fe 3737 | - | 0.09 | 0.13 | | 0.03 | - | |
| MgCl bh | - | 0.16 | 0.11 | | 0.08 | - | |
| MgF bh | - | 0.35 | 0.23 | | 0.05 | - | |
| Al0 bh 4842 | 0.04 | 0.13 | 0.05 | | 0.15 | - | |

All values corrected for background after normalization

traces. One of the problems caused by excessive graininess is the difficulty in picking out faint lines above the background. In this program, the problem was very great, not only because of the faintness of the lines, but also because the 2300Å wide spectrum is compressed into one inch of emulsion. These factors enable the human eye using a print, to be superior to the densitometer using the negative plate, for picking out significant features of these spectra.

As a result of the problems indicated above, only a few lines which could be positively identified were analyzed. Using a combination of densitometer traces and positive prints of the spectrograms, the major features are shown in Table 3-10.

In comparing different shots, it was first established that exposure and plate processing conditions were very nearly the same for all shots. Differences between calibration shots, 32, 37, and 42, were small. Possibly, there is more oxygen present in 37 due to the non-passivated aluminum sample. There is no difference except background in calibration shots, 32, 37, 42, and granite shot, 39, which contained impure CTF. The serpentine, 33, and gabbro, 38, shots are quite different from calibration shots, 32, 37, 42, showing much more structure. Major differences between gabbro, 38, and serpentine, 33, are in the background; serpentine, 33, being overexposed. Qualitatively, both 33 and 38 show the Al doublet, the MgF bands, the MgCl bands, the tungsten line (from the initiator) and the AlO bands. In addition, the gabbro shot, 38, shows a great number of iron lines, a calcium line at 4226.7Å, and CaF bands. Assuming the shots used here are representative and reproducible it should be quite easy (qualitatively) to distinguish between granite, serpentine, and gabbro using iron and calcium lines and MgCl, CaF and MgF bands as the basis.

No OH or other hydrogen features were observed because the spectrograph did not reach into the primary field of interest, i.e., 3060Å.

No Si or K lines were found.

The major difference between shots, 33 and 35, both serpentine, is the overexposure of 33 which prevents analysis for faint structure. The AlO bands are not visible on 35.

Table 3-10

SPECTRAL FEATURES SPECTROGRAPHICALLY IDENTIFIED

| Spectrogram No. | Soil | Features Present |
|---|---|---|
| 32 | None | Al doublet (3944.03 and 3962.53) |
| 33 | Passivated Serpentine 1 gram | Al doublet, MgF bands (3594.2) MgCl band (3777), W line (4982.6), AlO bands (4842.1, 4648.2, 5079.3) |
| 35 | Non-passivated Serpentine 1 gram | Al doublet, MgF bands, MgCl bands, Fe line (3859.9) |
| 37 | None | Al doublet, AlO bands, W line |
| 38 | Gabbro - 1 gram | Al doublet, MgF bands, MgCl bands, AlO bands CaF bands (5292.3) W line, Ca line (4226.7) Fe lines (3859.9, 3737.1, 3734.9, 37.19.9, 3820.4) 3 unidentified lines (Probably Fe at about 4370 |
| 39 | Granite - 1 gram | Al doublet, AlO bands (very faint) |
| 40 | Gabbro - 5 grams | Al doublet, Ca line, AlO bands |
| 41 | Gabbro - 25 grams | Al doublet, Ca line, MgF bands, MgCl bands, Fe as in 38 |
| 42 | None | Al doublet |

In general, the increase in quantity of gabbro in shots, 38, 40, and 41, reduced the intensity of the spectra and the number of lines and bands excited, except that the MgCl and MgF bands suddenly reappear in 41. Calcium line and Al doublets persist in all three shots.

For a comparison of lines on a photographic emulsion, it is necessary to correct for background and "gamma" (see Table 3-9). The gamma of an exposure is defined as the slope of the straight-line portion of the plot of the image density versus the log of exposure of the film. The density of a photographic image is the log of the opacity. The opacity is the reciprocal of the transmission of the image (in a densitometer). Thus D = log Op = log (1/T) = -log T, where D is density, Op is opacity, and T is time. Although the gamma correction is a function of wavelength, it is not a strong one. It is apparent that for 103a-F film (a film of high sensitivity, especially for long exposures as in astronomical work) the majority of structure falls on the linear portion of the "D-log E" curve. Data have been normalized with respect to the Al 3962 line and corrected for background using the average background below and above the line or bandhead in question. The gamma used was 0.6 in Table 3-9.

In establishing the light intensity trends in the three gabbro shots (see Figure 3-27) the following procedure was used:

All but a narrow strip of each spectrogram negative image in the same step region (continuum) was masked off, resulting in a one to one correspondence with flare region. Light transmission intensity was then measured on a relative scale at two wavelength regions with a sensitive cadmium sulfide cell. The following results were obtained:

| Spectrogram No. | % Soil Dilution Ratio | Gabbro Ratio | Relative Intensity at 4000Å (normalized) | Relative Intensity at 4200Å (normalized) |
|---|---|---|---|---|
| 38 | 6.7 | 1 | 1.0 | 1.0 |
| 40 | 26 | 5 | .62 | .54 |
| 41 | 64 | 25 | .08 | .07 |

It is anticipated that this procedure will be adapted to lines and bands and checked with the analysis of additional microdensitometer runs on 40 and 41 at a later date.

# Section 4
# ANALYSES

Presented in this part of the report are the results of four analyses which were conducted during the ELF feasibility study. The following is included:

1. Information concerning the probable lunar surface characteristics, which was of great assistance in selecting the most advantageous simulated soils for the experiments enumerated in Section 1
2. A discussion of several observational considerations on the feasibility of observing and recording the actual ELF impact event
3. A presentation of the Deep Space Net capabilities for tracking and predicting the impact time and position
4. A theoretical hydrodynamic evaluation of the impact event.

## 4.1 ANALYSIS OF LUNAR SURFACE CHARACTERISTICS

The purpose of this analysis was to present current thinking as to the physical and chemical nature of the lunar surface early in the ELF program so that the experiments could be conducted with the best possible selection of simulated lunar soils. The soils finally selected for the spectroscopic tests were granite, gabbro, and serpentine in finely divided form. The soils used for the impact tests were chosen mainly from a physical structure standpoint, for example, solid granite, gabbro, serpentine, and quartz; finely divided sand of the granite, gabbro, and serpentine; and powdered garnet dust. (For details see Appendix.)

## 4.2 OBSERVATIONAL CONSIDERATIONS

In this section, the results of analyses designed to answer the following questions are presented:

1. How can we observe the ELF event?

2. What can we expect to see?

3. How can we detect and record the information?

### 4.2.1 Observing Stations

The ELF event will be observed by existing telescopes located at observatories in the Southwest United States. Some preliminary contacts have been made by Dr. A. B. Meinel, Director of the Steward Observatory in Tucson, Arizona, to obtain expressions of interest from other astronomers and other observatories concerning their participation during the observation phase. Although no specific commitments have been sought at this early date, the preliminary discussions have indicated a high degree of interest and there is a good possibility that some of the largest telescopes may be available for the event. Among those contacted thus far are Dr. A. J. Deutsch, who is associated with the Mt. Wilson and Palomar Observatories, and Dr. W. Livingston of the Kitt Peak National Observatory.

The time window permitted for observing the event will be discussed in a later section, but it should be noted here that the observing time will be restricted to a period of several hours during the early phase of the new moon. The time window limits the geographical area from which the event may be recorded. The time is shown in Figure 4-1, which also illustrates the many potential participants, their location in the Southwestern United States, and the telescopes existing at these locations.

Participation by a number of observatories is desirable in the event of adverse weather at one or more of the sites. A minimum of five observatories should be involved in order to obtain sufficient geographic spread and to observe the event with different types of instrumentation. It is possible that each observatory may have more than one instrument available for observation.

### 4.2.2 Signal and Noise Intensities

Before the various detection and recording techniques are discussed (Section 4.2.3), it is appropriate to consider some of the critical parameters which will have a vital effect on the feasibility of detecting and recording the ELF event. These parameters include the radiant intensity of the flare

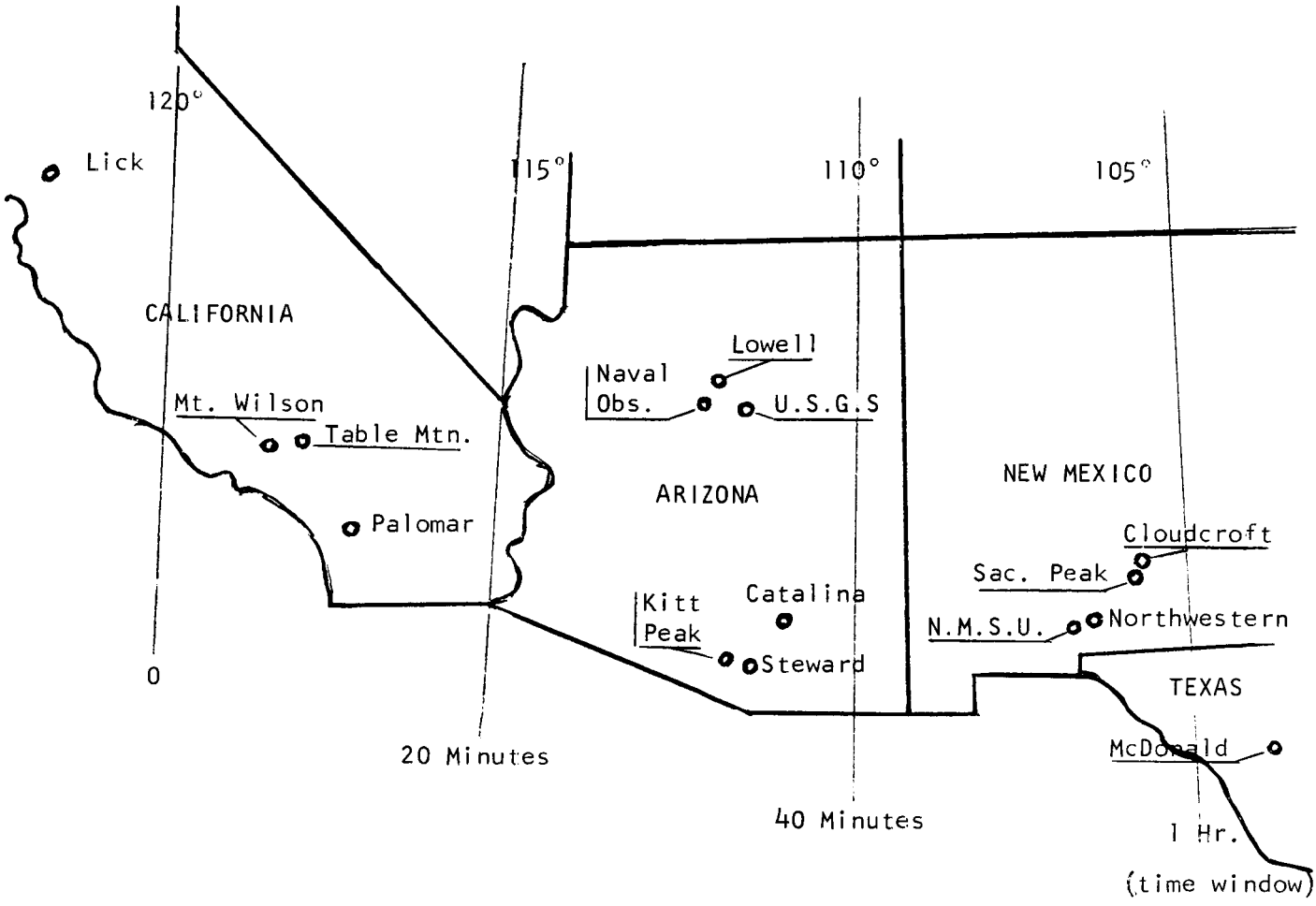


| OBSERVATORY | LOCATION | TELESCOPES Aperture Dia. |
|---|---|---|
| Lick | Mt. Hamilton, Calif. | 120", 36", 24" |
| Mt. Wilson | Pasadena, Calif. | 100", 60" |
| Table Mountain | Pomona, Calif. | 24" |
| Mt. Palomar | Rincon, Calif. | 200", 48", 20" |
| Naval Observatory | Flagstaff, Ariz. | 60", 42" |
| Lowell | Flagstaff, Ariz. | 69", 40", 24", 21" |
| U.S.G.S. | Flagstaff, Ariz. | 30" |
| Kitt Peak Ntl. | Tucson, Ariz. | 84", 36", 16", 16" |
| Steward | Tucson, Ariz. | 36" |
| Catalina | Tucson, Ariz. | 29", 21" |
| New Mexico State | Los Cruces, N.M. | 24" |
| Northwestern | Organ, N.M. | 24" |
| Sac. Peak | Alamogordo, N.M. | 16" |
| Cloudcroft | Cloudcroft, N.M. | 48" |
| McDonald | Ft. Davis, Texas | 82", 36" |

Figure 4-1 Observatories

signal, the background intensity reflected from the large surface, signal-to-background ratio considerations, electronic noise in the detection apparatus, and the instrument signal-to-noise ratio. It is important to differentiate between background noise (or background intensity) and electronic noise. The former will represent an average signal level which is essentially constant for the duration of the flare. Since the flare will produce a signal at the detector which is being viewed against an essentially constant background, the flare should be detectable as long as it represents a reasonable percentage of the total background energy. Experience indicates that an RMS signal to dc background ratio of the order of 0.2 will be adequate for flare detection. The consideration of electronic noise in the detector-preamplifier equipment is also of great importance since it will limit the ability to detect faint sources. These considerations are discussed in more detail below.

4.2.2.1 Signal Intensity

Optical signal intensity (total irradiance at the telescope aperture) can be expressed as follows:

$$H_s = \frac{\text{radiant energy of flare}}{\text{burn time}} \times \frac{1 \text{ sphere}}{4\pi \text{ steradians}}$$

$$\times \frac{\pi}{4} \times \frac{(\text{dia. of aperture})^2}{(\text{lunar distance})^2}$$

$$H_s \propto \frac{\text{radiant energy}}{\text{burn time}} \times \frac{\text{solid angle subtended by aperture}}{\text{unit solid angle}}$$

Definition of the flare irradiance was based on an extrapolation of experimental results. This extrapolation was performed as follows: in static tests, light intensity was measured for 50-, 500-, and 5,000-gm flares. While the data are not conclusive, it appears that a linear relationship between flare mass and light intensity would be appropriate for use in estimating the characteristics of a full-scale flare. A value for flare radiant energy of 0.30 watts-sec/Å, which is appropriate for the 4,500 to 6,500 Å wavelength region, was chosen on the basis of data obtained in the impact

tests. An average value of flare irradiance was determined to be 20 watts/Å, based on an event duration of 15 msec. Based on a linear relationship between this value (for 16.4 gm. of reactants) and the full-size (100 lb of reactants) flare, the full-size flare would have an irradiance of 55,000 watts/Å.

A 60-inch (151 cm) diameter telescope subtends an angle of

$$\frac{\pi}{4} \times \frac{(151)^2 \text{ cm}^2}{(3.84 \times 10^{10})^2 \text{ cm}^2} = 1.2 \times 10^{-17} \text{ steradian; therefore,}$$

$$\text{irradiance H} = \frac{55. \times 10^3}{4\pi} \frac{\text{watts/Å}}{\text{steradian}} \times 1.2 \times 10^{-17} \text{ ster}$$

$$= 5.3 \times 10^{-14} \text{ watts/Å}$$

In the next section, the best viewing conditions are determined to be four days after new moon, at the end of astronomical twilight. Figure 4-2 shows the altitude of the moon and the number of air masses through which the signal must pass as a function of the number of days after new moon. (This figure is for the period 30 May to 5 June 1965. The data can also be considered valid for April 1965. In addition, the data are representative for the October 1965 period except that the conditions described would occur 2 hours before dawn rather than at sunset and 2 hours after sunset.) From this figure, the number of air masses four days after new moon at the end of astronomical twilight is approximately 2. Assuming a transmission factor of 0.36 per air mass, absorption by the atmosphere will modify the peak irradiance to be $5.3 \times 10^{-14} \times 0.36 = 1.9 \times 10^{-14}$ watts/Å.

4.2.2.2 Background Intensity

Background noise is contributed by energy reflected from the Earth-lighted (dark) portion of the moon and by scattered moonlight. During the first three or four days after the new moon, the greatest contribution is from the dark portion. The intensity of this noise is an inverse function of the absorption by the atmosphere, through which it is transmitted. Absorption is nearly a

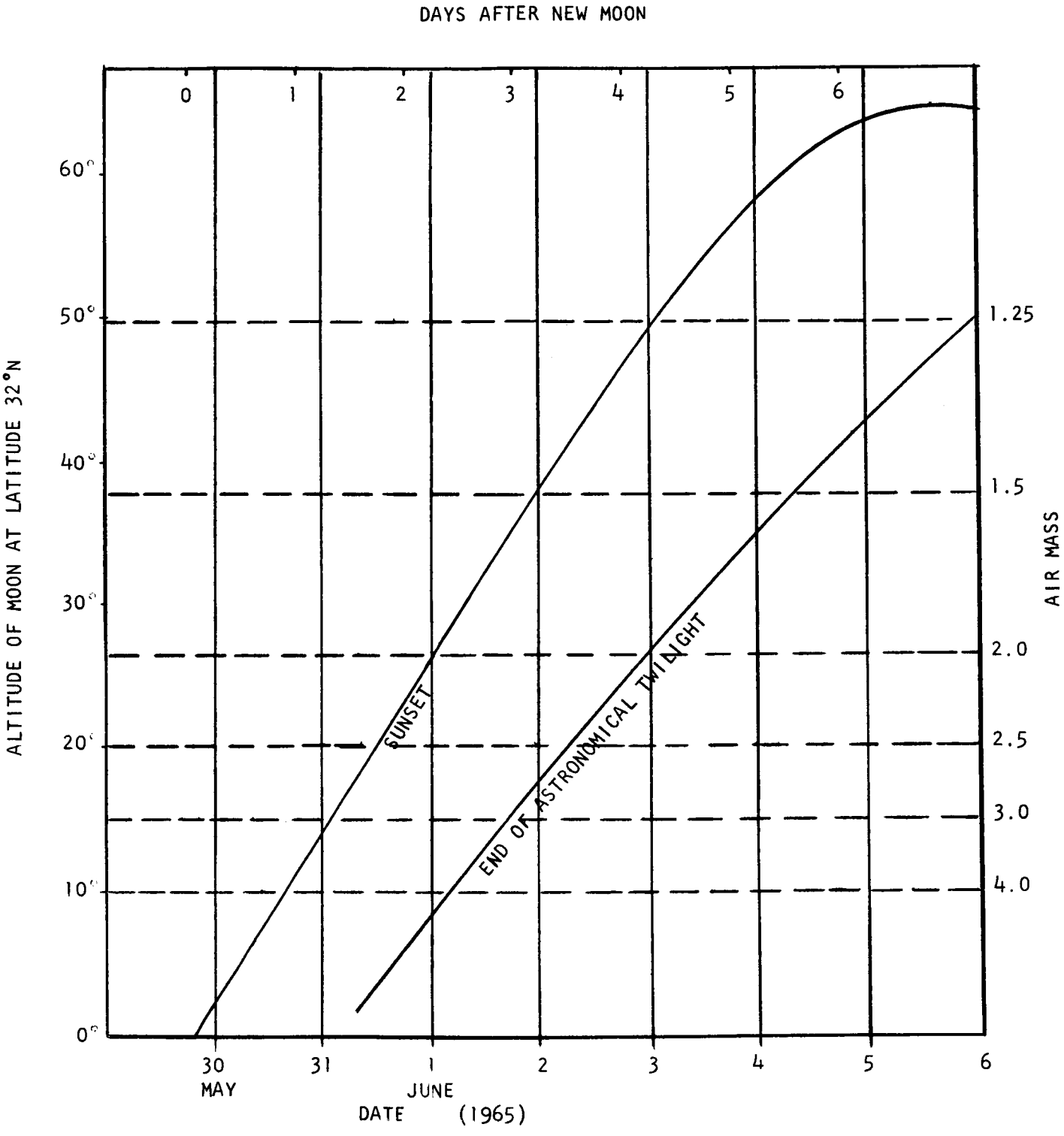


Figure 4-2 Altitude Of Moon At Sunset And End Of Astronomical Twilight 5/30 – 6/5/1965

cosine function of the angle of elevation ($\emptyset$) of the moon since this angle defines the number of air masses through which the signal passes.

Background noise contributed by scattering in the atmosphere of energy from the lighted portion of the moon, which is actually outside the field of view, is a function of the atmospheric transmission as well as the area of the lighted portion, and several other factors. Because of the complex nature of this function, computed values were not considered applicable, and measured values were used. The measurements were made by Dr. Walter Fitch of the University of Arizona. Data derived from this experiment is plotted in Figure 4-3.

An expression for background energy at the aperture is as follows:

$$H_{bg} \propto \frac{\text{irradiance}}{\text{unit area}} \times \frac{\text{angular field of view x area of aperture}}{}$$

Signal from the flare is subject to the same absorption function as is the Earth-shine signal. A plot of percentage of transmission of the flare signal vs. days after the new moon (based on values at the time of the end of astronomical twilight, 2 hours after sunset) is included in Figure 4-3. The most advantageous signal-to-background ratio occurs at the time when the slopes of these two curves are equal, which is approximately four days after the new moon. The value of four days after the new moon will be used for computation purposes throughout this report.

A field of view described by an ellipse having axes of 12 km and 60 km (associated with a $3\sigma$ probability of impact) represents a solid angle of view of:

$$\frac{\pi}{4} \times \frac{12 \times 60 \times 10^{10} \text{ cm}^2}{(3.84 \times 10^{10} \text{ cm})^2} \times 3.85 \times 10^{-9} \text{ steradians}$$

$$1 \text{ steradian} = 4.2 \times 10^{10} \text{ sec}^2$$

$$3.85 \times 10^{-9} \text{ steradians} \times 4.2 \times \frac{10^{10} \text{ sec}^2}{\text{steradian}} = 160 \text{ sec}^2$$

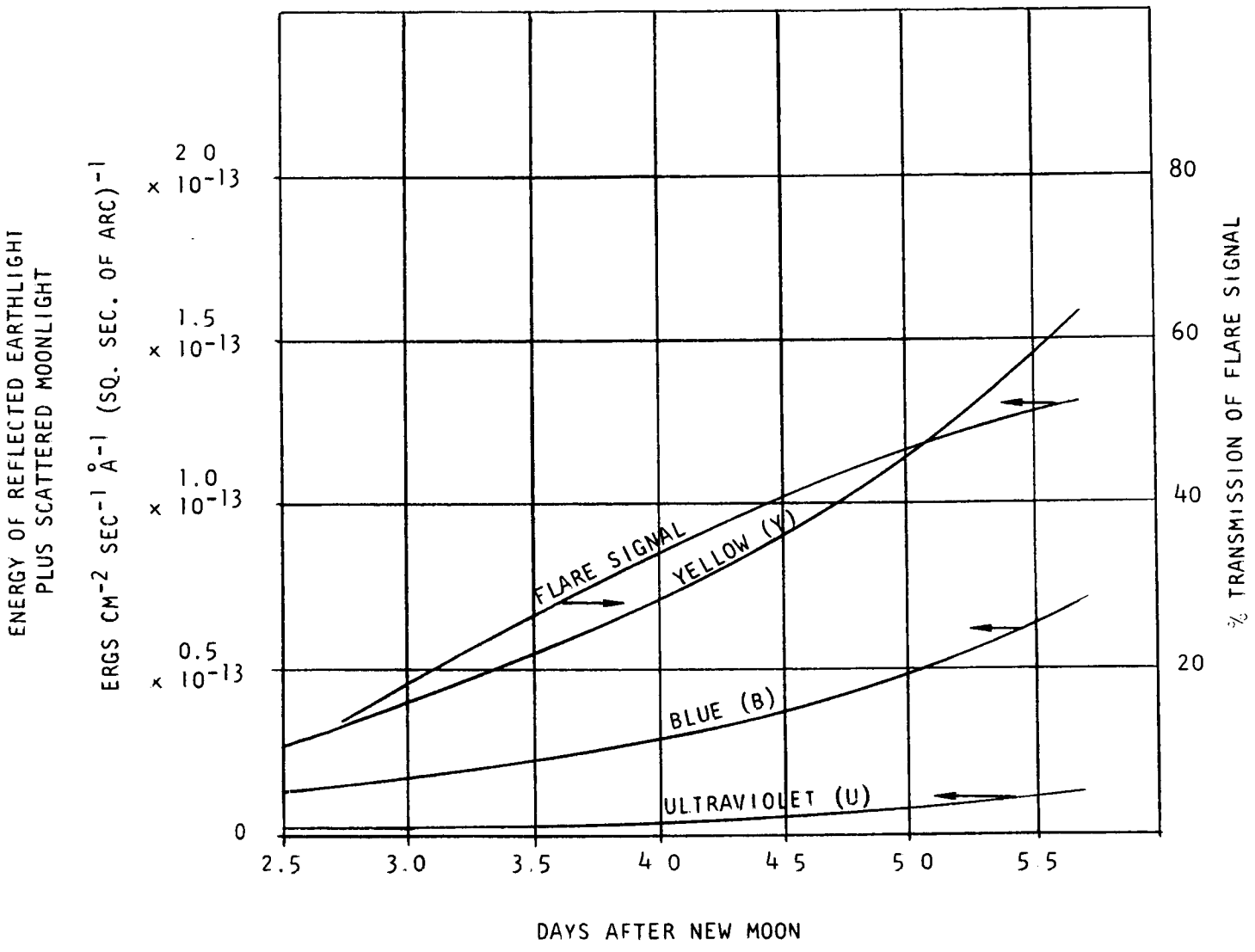


Figure 4-3 Graph Of The Observed Illumination On The Dark Face Of The Moon As A Function Of The Time After New Moon

The peak background intensity was observed to be $7.0 \times 10^{-14}$ ergs $cm^{-2}$ $sec^{-1}$ (sq sec of arc)$^{-1}$ 4 days after new moon (see Figure 4-3).

Thus, background intensity =

$$\frac{\text{irradiance}}{\text{unit area}} \times \text{angular field of view} \times \text{area of aperture}$$

$$= 7 \times 10^{-14} \frac{\text{ergs}}{\text{sec} \times \text{Å} \times \widehat{\text{sec}}^2} \times 160\ \widehat{\text{sec}}^2 \times 1.80 \times 10^4\ \text{cm}^2 \times \frac{\text{watt-sec}}{10^7\ \text{ergs}}$$

$$= 2.03 \times 10^{-14}\ \text{watts/Å}$$

4.2.2.3 Optical Signal-to-Background Ratio

Optical signal-to-background ratio can be expressed as:

$$\frac{H_s}{H_{bg}} \propto \frac{\dfrac{\text{Flare radiant energy}}{\text{burn time}} \times \dfrac{\text{solid angle subtended by aperture}}{\text{unit solid angle}}}{\dfrac{\text{irradiance} \times \text{area of aperture} \times \text{angular field of view}}{\text{unit area}}}$$

$$\frac{H_s}{H_{bg}} \propto \frac{\text{flare radiant energy}}{\text{background irradiance} \times \text{burn time} \times \text{field of view}}$$

$$\frac{\text{signal}}{\text{background}} = \frac{H_s}{H_{bg}} = \frac{1.9 \times 10^{-14}}{2.03 \times 10^{-14}} = 0.94$$

Since the ability to direct a telescope is limited to approximately $\pm 1\ \widehat{\text{sec}}$, this inaccuracy must be added to the target area to allow a minimum $3\sigma$ probability of observing the hit. An angle of $1\ \widehat{\text{sec}}$ with its apex on the earth subtends an arc 1.87 km long on the moon. If twice this dimension is added to each axis, the target area becomes $\frac{1.574 \times 6.374}{1.2 \times 6.0} = 1.36$ times larger than the area described as a $3\sigma$ target. The effect of this change is to reduce the signal-to-background ratio accordingly. The signal-to-background ratio becomes $\frac{0.94}{1.36} = 0.69$. This will not materially affect performance of the system since ratios as low as 0.2 can be readily interpreted by either photographic or electronic recording means.

In the use of either recording technique, steps must be taken to prevent the background signal from saturating the signal-processing equipment.

Since the background signal is consistent in character, (steady-state) it can be rejected in the electronic recording devices by high-pass filtering techniques (ac coupling). No directly analogous technique is available in the case of the photographic record. However, the detrimental effect of integration of the background signal over the exposure time can be minimized by moving the film past the aperture during the time window. The portion of the film that witnesses the event is thus only exposed to the background light during the period of the event, and records what is nearly the true signal-to-background ratio.

4.2.2.4 Equipment Noise Level

In the case where electronic means are employed, the electrical signal-to-noise ratio becomes significant. The signal is contributed by the light energy from the flare, while the noise component is principally the noise equivalent power (NEP) of the photomultiplier tube. Since the noise signal is similar in character and frequency to the light signal expected from the flare, a probable minimum signal-to-noise ratio is on the order of 2.

4.2.2.5 Signal-to-Noise Ratio

Whenever the light signal is dispersed for purposes of spectral analysis, the signal received by the transducer is described by the spectral irradiation ($H_\lambda$) multiplied by the spectral window (resolution) of the transducer. This product, when compared to the NEP of the transducer, describes the electrical signal-to-noise ratio. An analysis of the signal discussed in Section 4.2.2.1 is as follows:

Optical signal into aperture $H_\lambda = 1.9 \times 10^{-14} \frac{\text{watts}}{\text{Å}}$

Efficiency of optics = 0.3

Signal to transducer $H_\lambda = 1.9 \times 10^{-14} \times 0.3 = 5.7 \times 10^{-15} \frac{\text{watts}}{\text{Å}}$

Assuming a 10Å minimum-resolution window,

$$\text{Signal through window} = 5.7 \times 10^{-15} \frac{\text{watts}}{\text{Å}} \times 10\text{Å} = 5.7 \times 10^{-14} \text{ watts}$$

$$\text{NEP of photomultiplier tube 1P21 at 25°C} = 1.9 \times 10^{-15} \text{ watts}$$

$$\text{S/N (1P21 tube)} = \frac{5.7 \times 10^{-14}}{1.9 \times 10^{-15}} = 30.$$

This is entirely adequate since a S/N ratio of 2 is considered usable.

### 4.2.3 Instrumentation

A number of potential recording techniques that could be used to detect and observe the flare were analyzed with the expectation that some of them would not prove to be feasible. The techniques which were evaluated included: (1) direct photographic recording of the event to obtain a time-integrated spectrograph of the flare radiance, (2) spectrographic recording using an image-intensifier technique to ensure adequate exposure of a low-intensity flare, (3) nonscanning multichromator approach using multiple sensors in a single dispersion instrument to provide time-resolved outputs from fixed spectral intervals, (4) photoelectric detection with a rapid-scan monochromator to obtain time-resolved spectra of the event, and (5) simple photomultiplier observation of the integrated spectrum to provide a time-resolved output of the total radiation from the flare.

The possibility of adapting or modifying existing instrumentation at various observatories has been considered, and it appears feasible to use existing spectrographic equipment for direct photographic recording of the event. Observation of the flare requires fairly rapid time response with little possibility of integration because of the brief duration of the event. Thus, most other types of instrumentation must be tailored for this application, although, in some cases, it may be possible to use detector assemblies that have been provided with new electronics.

4.2.3.1 Direct Photographic Recording

In this section an analysis of direct photographic recording of the flare event is presented.

Predicted flare yield = $5.5 \times 10^4$ watts/Å

(average over 3,500Å - 6,500Å spectral range)

Solid angle subtended by 60 in (152 cm) aperture:

$$a = \frac{\pi}{4} \times \frac{(1.52 \times 10^2)^2}{(3.84 \times 10^{10})^2} = 1.29 \times 10^{-17} \text{ steradian}$$

Transmission through 2 air masses = 0.36. Irradiation at aperture =

$$0.36 \times \frac{5.5 \times 10^4 \text{ watts}}{\text{sphere - Å}} \times \frac{1 \text{ sphere}}{4\pi \text{ ster.}} \times \frac{1.29 \times 10^{-17} \text{ ster.}}{} = 2 \times 10^{-14} \frac{\text{watts}}{\text{Å}}$$

Since the diameter of the fireball image was determined to be smaller than the minimum resolvable element of the film, (Kodak 1-0 has a resolution of from 69 to 95 lines per mm) assuming a minimum increment to be $(0.02 \text{ mm})^2 = (2 \times 10^{-5} \text{ m})^2 = 4 \times 10^{-10} \text{ m}^2$.

Assuming that the dispersion of the spectrum is such that 10Å spans 0.02 mm of film, the energy available to develop a minimum increment of film $= 2 \times 10^{-14} \frac{\text{watts}}{\text{Å}} \times 10\text{Å} = 2 \times 10^{-13}$ watts.

$$\text{Irradiation of the film} = \frac{2 \times 10^{-13} \text{ watts}}{4 \times 10^{-10} \text{ meters}^2} = 5 \times 10^{-4} \frac{\text{watts}}{\text{meter}^2}$$

$$= 5 \times 10^{-4} \frac{\text{watts}}{\text{M}^2} \times 685 \frac{\text{lumen}}{\text{watt}} = .3425 \frac{\text{lumen}}{\text{meter}^2}$$

$$= 0.3425 \text{ meter-candles}$$

From Kodak Photographic Notebook (Scientific and Technical Data, Section P-9 Page 4d):

Kodak Film 1-0 Relative Sensitivity ($S_A$) = 50

$$S_A = \frac{1}{\text{meter candle - sec}} \text{ to expose to a density of 0.6}$$

$$\therefore t = \frac{1}{0.3425 \text{ meter - candle} \times 50} = \frac{1}{17} = 0.06 \text{ sec}$$

Since density vs. exposure is a log function, our 0.01 sec exposure time should produce a density of 0.2 to 0.3. This is readily measurable by a micro-densitometer.

The optics required for direct photography can be identical to the arrangement used with the image intensifier tube, as described in Section 4.2.3.2. In the direct photographic approach, the film is located at the optical focal plane, as shown in Figure 4-4.

The following performance specifications are applicable to the instruments:

| | |
|---|---|
| Sensitivity (threshold) | $10^{-15}$ watt-sec |
| Spectral resolution | 5 Å |
| Wavelength accuracy | 5 Å |
| Photometric accuracy | 3% |
| Recording means | Photographic |
| Dynamic Range | 100 |
| Calibration means | Tungsten lamp and neon source |

Cost and lead time estimates are as follows:

| Item | Cost | | Time |
|---|---|---|---|
| Optics and Mechanics | | | |
| Design (complete) | $20,000 | | 4 Months |
| Design (modification)* | | $ 4,000 | |
| Purchase parts | 4,000 | 4,000 | 3 Months (lead time) |
| Fabrication and test | 16,000 | 16,000 | 3 Months |
| Calibration | 1,000 | 1,000 | 1 Month |
| Installation | 1,000 | 1,000 | 1 Week |
| Total | $42,000 | $26,000 | 8 Months |

*Note: Modification required to adapt design of optics used for image intensifier version.

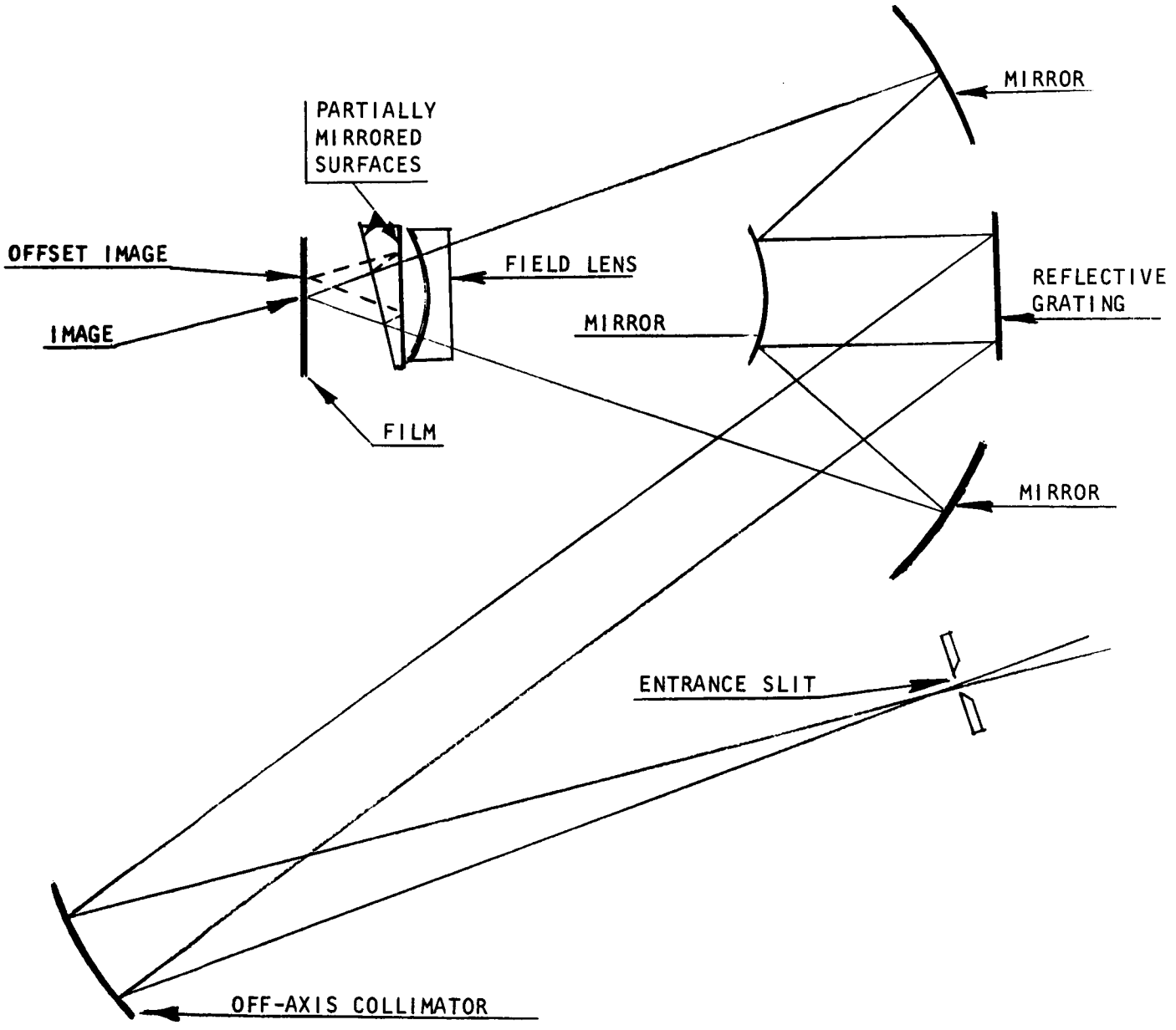


Figure 4-4 Meinel Spectrograph (Direct Recording)

4.2.3.2 Image-Intensifier Spectrograph

In case of a low-intensity impact event and the possible marginal performance of direct spectrographic recording of the event, serious consideration should be given to the application of electronic image-intensifier techniques to enhance the recorded spectrograph.

With present state-of-art components and techniques, an instrument could be constructed enabling an event to be recorded which has 1 to 10% of the intensity required for direct photographic recording. This approach is applicable where the signal-to-noise and signal-to-background levels are adequate, but the absolute magnitudes are insufficient to permit proper recording with reasonable telescope apertures and suitable film emulsions.

High-resolution image-intensifier tubes require strong, uniform magnetic focusing fields which, in turn, impose use of somewhat bulky focus coils around the tube. As a result, the photocathode is usually recessed from the mechanical interface with the tube assembly. This has been a nagging problem to the user since conventional spectrographic instruments have not been designed with sufficient focal plane relief to allow use of such novel detection devices. The high optical speed desired for maximum sensitivity, and the relatively large field of view required to image the spectrum on a plate has frequently been obtained in conventional instruments by the use of fast Schmidt-type camera optics, with the focal plane located between the imaging mirror and the refractive corrector plate.

This approach dictates that the focal plane apparatus be small with respect to the total camera aperture in order to minimize obscuration of the aperture. This is not a serious problem for photographic recording, since the photographic plate and plate holder can be conveniently small. It restricts the flexibility of the instrument for use with other recording techniques,

however. The relatively large bulk and the recessed focal surface of the image-intensifier highlights the need for a new optical configuration that provides an accessible focal plane with good relief from the structural interface.

Dr. A. B. Meinel has proposed an ingenious adaptation of reflective microscope optics to achieve the necessary focal plane relief. His design consists essentially of an inverted cassegrain reflective system, as shown in Figure 4-5, wherein the primary mirror is a small convex element, and the secondary is a large concave surface. Since the system is entirely reflective, except for a small field flattener at the focal surface, it is not restricted to use in any particular wavelength interval, and is completely adaptable to a variety of detection devices, of which the image-intensifier tube is one example. The configuration lends itself to a highly flexible, modularized instrument suitable for a variety of spectrographic applications.

As shown in Figure 4-5, mirror M1 collimates the energy from the telescope, matching the dispersion module to the light-gathering apparatus. This mirror would be interchangeable to permit efficient matching to a variety of telescopes with different focal ratios. The collimated light is diffracted from a plane replica grating and reflected from primary mirror M2. It is then reimaged by secondary mirror M3 to form a spectrum at the focal surface. Complete flexibility in operating wavelength is achieved by selection of gratings with appropriate dispersion constants (lines per millimeter) and orientation of the grating angle to be compatible with the blaze angle. Order separation is achieved by addition of an appropriate fore prism or wedge to introduce a slight dispersion normal to that provided by the grating. The various orders will then be arrayed one above the other at the focal surface.

The output of the image tube will be transferred to photographic film by a 1:1 transfer lens. The transfer system will include two partially reflecting surfaces at a slight angle to one another to provide multiple images at the film with decreasing intensities. Thus, if the exposure is in error due to

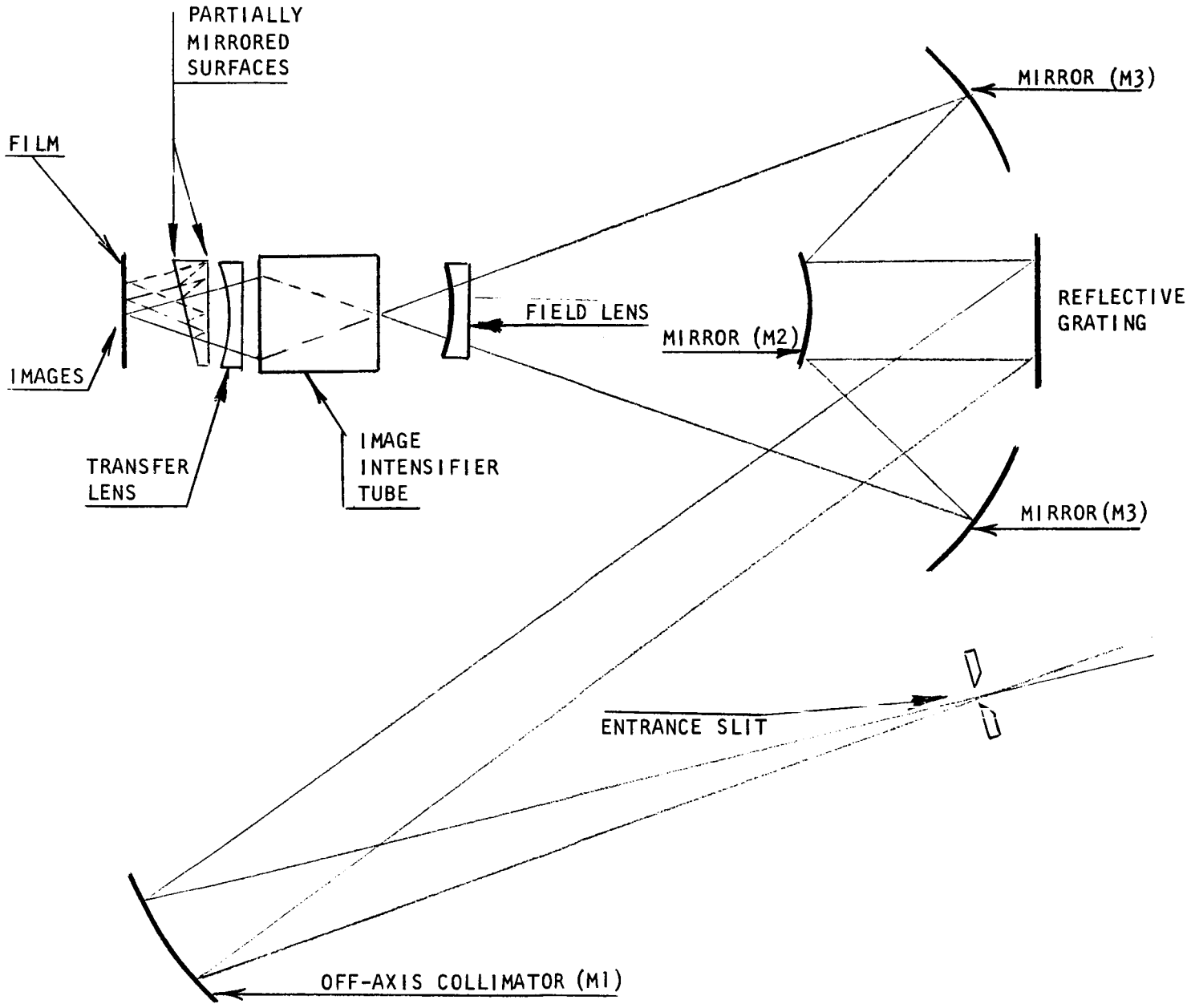


Figure 4-5 Meinel Spectrograph (Image Intensifier)

higher than expected radiant intensity from the flare, saturation of the straight-through image will not result in total loss of information since lower intensity images will be provided by diversion of approximately 10% of the light flux into the multiple reflecting paths. Graded images having relative intensities of 100, 10 and 1 would thus provide an extremely high dynamic range for this recording technique.

The following performance specifications are applicable to the instrument:

| | |
|---|---|
| Sensitivity (threshold) | $10^{-16}$ watt-sec |
| Spectral resolution | 5Å |
| Spectral range | 3,000Å to 6,000Å |
| Wavelength accuracy | 5Å |
| Photometric accuracy | 5% |
| Recording means | Photometric |
| Dynamic range | 1000 |
| Calibration means | Tungsten lamp and neon source |

Cost and lead time estimates are as follows:

| Item | Cost | Time |
|---|---|---|
| Optics and mechanics | | |
| Design | $20,000 | 4 Months |
| Purchase parts | 5,000 | 3 Months (lead time) |
| Fabrication and test | 25,000 | 4 Months |
| Electronics | | |
| Design | 3,000 | 1 Month |
| Purchase | 15,000 | 6 Months (lead time on tube) |
| Fabrication and test | 5,000 | 1 Month |
| Calibration | 2,000 | 1 Month |
| Installation | 1,000 | 1 Week |
| Total | $76,000 | 10 Months |

4.2.3.3 Multi-Channel Spectrometer

A fixed image, multi-channel spectrometer is displayed schematically by Figure 4-6. In this instrument a series of exit slits and their respective individual detectors witness preselected portions of the spectrum. An analysis of the performance of this instrument is as follows:

Assuming the signal conditions described in Section 4.2.2.5, we have an irradiance of $5.7 \times 10^{-14}$ watts at the transducer. If the transducer (photomultiplier tube) has a quantum efficiency of 10%, photon yield at the transducer is

$$N = 5.7 \times 10^{-14} \text{ watts} \times 4 \times 10^{18} \frac{\text{photons}}{\text{watts-sec.}} \times \frac{0.01 \text{ sec.}}{\text{event}} \times 0.1$$

$$= \frac{230 \text{ photons}}{\text{event}}$$

Output signal from the transducer can be recorded by a tape recorder for playback into a strip chart recorder, or directly into a high-speed strip chart recorder. Either technique will provide a time-resolved record of the event at preselected portions of the spectrum.

The following performance specifications are applicable to the instrument:

| | |
|---|---|
| Sensitivity (threshold) | $10^{-13}$ watts |
| Spectral resolution | 10Å |
| Spectral range | 3000Å to 9000Å |
| Wavelength accuracy | 5Å at 3000Å to 15Å at 9000Å |
| Photometric accuracy | 10% |
| Recording means | Electronic |
| Dynamic range | 100 |
| Calibration means | Tungsten lamp and neon source |

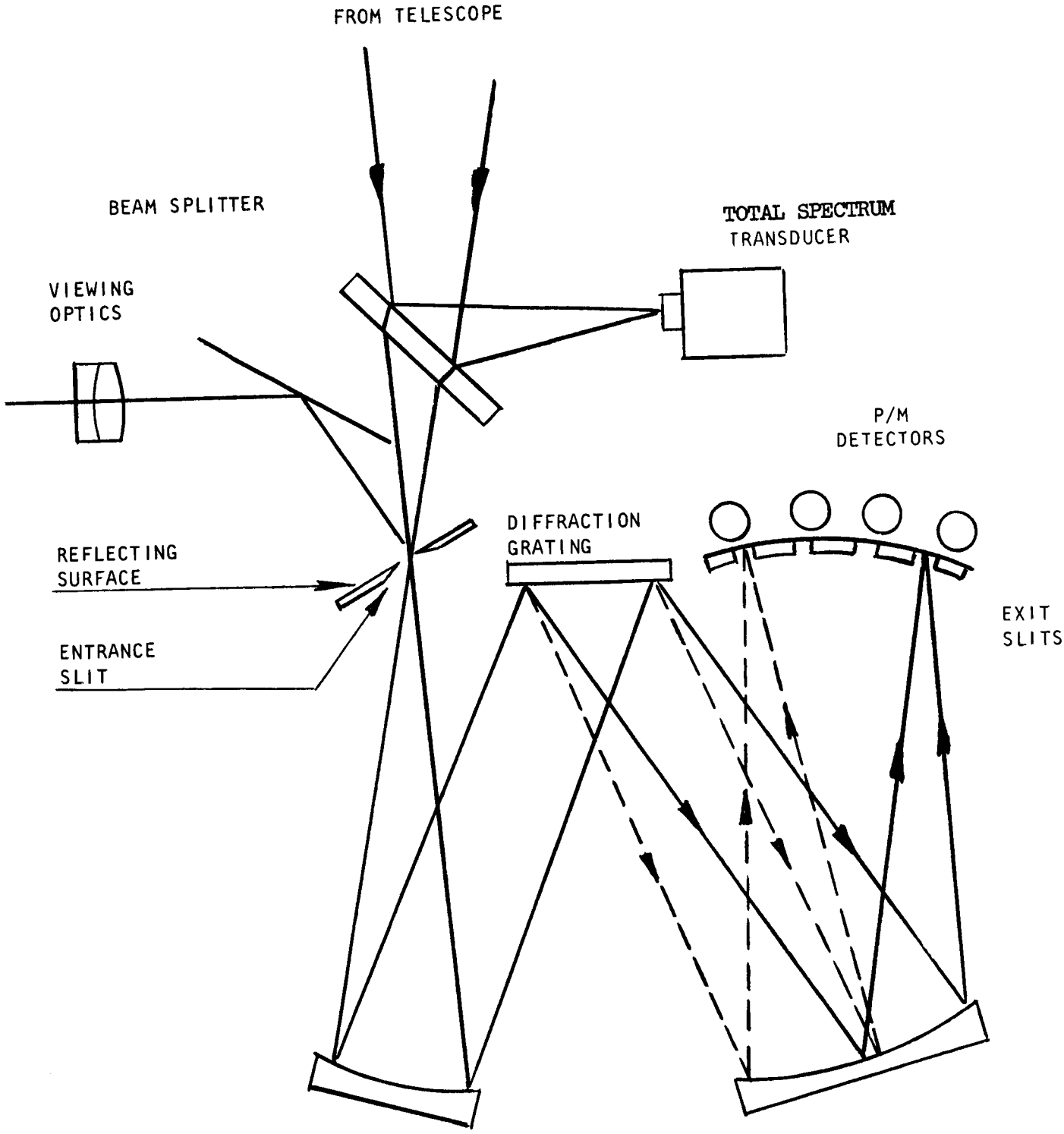


Figure 4-6 Multi-Channel Spectrometer

Cost and lead time estimates are as follows:

| Item | Cost | Time |
|---|---|---|
| Optics and mechanics | | |
| Design | $15,000 | 4 Months |
| Purchase parts | 5,000 | 3 Months (lead time) |
| Fabrication and test | 20,000 | 4 Months |
| Electronics | | |
| Design | 3,000 | 1 Month |
| Purchase parts | 2,000 | 1 Month |
| Tape recorder (leased) | 6,000 | |
| Fabrication and test | 5,000 | 2 Months |
| Calibration | 2,000 | |
| Installation | 1,000 | 1 Week |
| Total | $59,000 | 8 Months |

4.2.3.4 Scanning Spectrometer

Some effort has been expended in the study of various concepts that allow time-resolved coverage of the complete spectrum. They are all defeated by the limited light available. In order to provide coverage of the complete spectrum with one exit slit and one transducer, the spectrum must be scanned across the slit. For time resolution to be meaningful, it is necessary to scan the spectrum at least 10 times during the event. In the case of an 0.01 sec. burn time, a scan frequency of 1,000 cps is required. Considering a 10Å spectral resolution, the following extension of the analysis presented in Section 4.2.3.3 is valid.

$$N = \frac{230 \text{ photons}}{\text{event}} \times \frac{\text{event}}{10 \text{ scans}} \times \frac{\text{scan}}{300\text{Å}} \times \frac{10\text{Å}}{\text{increment}}$$

$$= \frac{0.077 \text{ photons}}{\text{increment}}$$

Since this yield is at least two orders of magnitude below a usable quantity, any upgrading due to larger collecting optics or any compromise of other parameters is to no avail.

4.2.3.5 Time-Resolved, Total Spectrum Recorder

A single channel transducer can be used to record the nondispersed signal from the event. Such a device would consist of a photomultiplier tube and a field stop placed at the focal plane of a telescope. Output signal from the tube would be recorded either on magnetic tape or on a high-speed strip chart recorder.

Since this transducer witnesses the total spectrum, large collecting optics are not necessary to provide a sufficient quanta. An extrapolation of the analysis presented in Section 4.2.2.1 indicates the following yield from a 20-in. aperture:

$$N = 230 \frac{\text{photons}}{\text{increment-event}} \times \frac{3000\text{Å}}{\text{spectrum}} \times \frac{\text{increment}}{10\text{Å}} \times \frac{(20)^2}{(60)^2}$$

$$= 7700 \frac{\text{photons}}{\text{spectrum-event}}$$

This instrument provides time-resolved information related to the total spectrum. Its value lies in the analysis of the burn rate of the flare and thereby of the physical composition of the lunar surface. This information will also be a valuable adjunct to the spectral photographic and photoelectric information.

Economic considerations suggest that this instrument be used in conjunction with the multi-channel spectrometer. The two instruments share a common telescope and tape recorder. A partially silvered mirror (beam splitter) diverts part of the light energy (10%) into the total spectrum recorder. A schematic description of this concept is included in Figure 4-6.

The following performance specifications are applicable to the instrument:

| | |
|---|---|
| Sensitivity (threshold) | $10^{-15}$ watts |
| Spectral range | 3000Å to 7000Å |
| Photometric accuracy | 10% |
| Recording means | Electronic |
| Dynamic range | 100 |
| Calibration means | Tungsten lamp |

Cost and lead time estimates are as follows:

| Item | Cost | Time |
|---|---|---|
| Optics and Mechanics | | |
| Design* | $2,000 | 1 Month |
| Purchase parts | 1,000 | 3 Months (lead time) |
| Fabrication and test | 2,000 | 1 Month |
| Electronics | | |
| Design | 1,500 | 1 Month |
| Purchase parts | 1,000 | 1 Month |
| Fabrication and test | 500 | 1 Month |
| Total | $8,000 | 6 Months |

*Note: All costs are based on use of the technique described where telescope and recorder are shared with multichannel spectrometer. Elapsed time considerations can be absorbed in the estimate offered for the multichannel instrument.

## 4.3 IMPACT PREDICTION CONSIDERATIONS*

Of vital importance to the acquisition of flare data is the coordination required during the experiment to provide accurate pointing and impact-time information to the participating observers. It is most desirable to be able to predict the impact area with a high degree of accuracy, since this will permit a minimum field of view for the recording devices and therefore a low background-noise level. In addition, it is desirable to have an accurate time prediction to minimize the impact-time window and reduce the recording interval and the attendant exposure of photographic devices to the background signal. The tracking activity must be sufficiently coordinated with the observing sites (1) to permit timely positioning of the participating equipment in order to observe the predicted impact area on the lunar surface and (2) to permit recording of the event beginning at a time interval of less than 1 min. (preferably 10 sec. prior to impact).

* Information presented in this section concerning the Deep-Space Net was provided by Dr. E. Rechtin, T. W. Hamilton and J. J. Rennilson of the Jet Propulsion Laboratory, California Institute of Technology.

### 4.3.1 Prediction Accuracy

In order to determine the position and time of flare impact on the lunar surface, the Deep-Space Net would track the spacecraft, determine its orbit, and predict the impact conditions. Tracking would be continuous and commence 5 to 30 min. after injection.

Position-prediction errors are assumed to be normally distributed with a mean value of zero. The standard deviation of longitude error is approximately 10 km, while the standard deviation in latitude error is approximately 2 km. These values apply for moderate ( $< 45°$) lunar impact angles and no mid-course correction. For high-impact angles, such as in the case of a grazing impact, or where a mid-course correction is employed, the theoretical prediction errors would be higher. The values given are conservative, however, in that they are based on the assumption of a massless moon; hence the focusing effect of the moon's gravitational field is not considered. The values above are appropriate for the Spring 1965 time period. For a later period, the uncertainties would be reduced, due primarily to a change from L-band to S-band equipment. The impact position is known within the above accuracy of 4 or 5 hours before impact; thus accuracy does not improve substantially in the last 4 or 5 hours before impact.

Impact-time prediction accuracies, however, improve sharply as lunar impact is approached. Two hours before impact the standard deviation in time error is 3 sec. One hour before impact the standard deviation is down to 1 sec. Again, a normal distribution is assumed with a mean error of zero.

The accuracy with which lunar impact conditions are known was determined by a statistical analysis of the estimated errors involved in tracking and orbit determination. Experience with Ranger has provided confidence in the prediction capabilities.

### 4.3.2 Coordination of Tracking Facility and Observatories

Impact position and time data are provided in celestial coordinates and GMT. On previous Ranger missions, communication of this data has been performed by means of direct dialing. However, due to the importance of this information

in observing a lunar flare, open, direct telephone lines between the tracking facility and observatories appear to be warranted near the time of the impact event.

### 4.3.3 Tracking Facility Availability

Personnel of the Deep-Space Net Program Office have indicated, on an informal basis, that the Deep-Space Net would be available to support the ELF program during the spring or fall of 1965.

### 4.3.4 Tracking-Facility Modifications

The accuracy with which the position and time of lunar impact can presently be predicted are adequate for successful observation of the flare event. Thus, the requirements of this program can be satisfied without the necessity for modifying the Deep-Space Net.

## 4.4 THEORETICAL IMPACT EVALUATION

The work summarized in this section represents some of the effort of Shock-Hydrodynamics and was designed to assist Douglas in establishing:

1. The probable distribution of the chemically reactive material, as a function of time, during and after impact of the ELF on the lunar surface.
2. The nature and extent of the mixing of the flare materials with the lunar surface during impact.
3. The effects of variation of flare configuration upon the mixing process.

Since the lunar surface may range in consistency from a powdery, low-density, ash-like structure to a hard granite-like structure, it is necessary to design a CTF container which will prove satisfactory performance as a flare throughout this range of possible surfaces. It was recognized from previous analyses of impact phenomena and experimental results, that a compact, high-density, CTF container impacting upon the soft lunar surface would penetrate to a great depth in moderate density structure before CTF combustion took place. As a result, the light generated by combustion in this case would be absorbed in the lunar material and only a very small fraction, if any, would propagate

back to the earth. Use of a compact CTF container is therefore not recommended. The optimum container against a soft surface would be a flat plate, whose low areal density minimizes penetration.

On the other hand, if the lunar-dust layer is thin, then the impact, in effect, occurs upon a hard rock surface. In this case, a plate-shaped container, of the more compressible CTF, would largely rebound before adequately mixing with the lunar surface.

Therefore, in order to assure satisfactory mixing of CTF and hard-surface material and to obtain satisfactory visibility for the CTF reaction in powdery-surface material, the CTF container must be so designed as to contain elements of both high and low areal density.

### 4.4.1 Triorthogonal Disc

To accomplish these purposes, we proposed a triorthogonal disc configuration as a carrier; the research reported here largely concerns the evaluation of portions of such a carrier.

The advantages of the triorthogonal disc configuration are as follows:

1. If the nature of the lunar surface impacted is powdery, there is a sufficiently large cross-sectional area of CTF available to resist deep burial prior to mixing and combustion.
2. If the surface impacted is very hard, there is always some portion of the disc structure oriented so as to give at least modest penetration. The probability of occurrence of the various orientations has been computed and the results are summarized below.
3. The geometrical relations existing between the three orthogonal discs and the target are such as to provide high velocity jetting in the case where all of the plates are obliquely oriented upon impact. Such jetting accomplishes additional mixing and will therefore contribute usefully to the spectral output of lunar constituents.

### 4.4.2 Summary of Results

The considerations are evaluated in a series of four computations, in which two models of the lunar surface, 90% and 0% porous hard rock, were considered and which were designed to bracket the spectrum of possible cases. The first model corresponds to a powdery and soft surface and the second

to a hard rock, somewhat harder than the common terrestrial rocks such as granite, basalt, gabbro, or quartz.

Simulated impacts at normal obliquity of thin CTF plates in two orientations against these two targets were studied. The first orientation was with the plate impacting flat on the lunar surface, i.e., plate surface normal to velocity. The second orientation was with the plate surface canted at 26 1/2° with the velocity. The impact velocity is taken to be 3.11 km/sec. (10,200 fps) which is the best current estimate of the anticipated impact velocity on the lunar surface.

A detailed discussion of the results is presented in an accompanying report prepared by Shock-Hydrodynamics, a subcontractor. A brief summary of the salient features is presented here.

#### 4.4.2.1 Case I

Case I is a study of a CTF disc which impacts flat upon the soft model of the lunar surface.

Its performance is as anticipated; 782 $\mu$sec. after impact the CTF has penetrated only about 40 cm, and its downward velocity has been reduced to about 0.2 meters/msec. It is confined in a cavity about 80 cm in diameter which remains open at the top. Ample surface opening is maintained for the mixture of CTF, lunar dust, and luminous combustion products to escape from the crater.

#### 4.4.2.2 Case II

Case II is a study of the impact of a canted CTF plate upon the soft model of the lunar surface. The study indicates that the same physical phenomena occur as in Case I, but that the penetration depths are magnified by the secant of the cant angle. Therefore, small cant angles are desirable for optimum performance. The probability analysis indicates that one plate will always be canted at angles less than 54° 44' so that satisfactory performance is assured for the case of a soft lunar surface.

#### 4.4.2.3 Case III

Case III is a study of a CTF disc which impacts flat upon the hard model of the lunar surface. The study indicates that the plate largely rebounds after a very short time and only the peripheral portion of the plate becomes involved with the lunar surface to any extent. This phenomenon is considered to provide minimum performance of the flare. Fortunately, the probability study indicates that the occurrence of such an orientation, for any one of the three triorthogonal discs, is quite unlikely.

#### 4.4.2.4 Case IV

Case IV is a study of a CTF plate canted at 63° 26' which impacts on the hard model of the lunar surface. A jet of lunar rock is produced which will always encounter a facing CTF plate and enhance the mixing between flare material and lunar constituents. In addition, the flare material which first contacts the lunar rock shatters it, and subsequently additional CTF is diverted into the shattered region. As a result, good mixing is attained between the flare material and lunar constituents. The canting also provides enhanced penetration, which results in good contact being maintained. Based on these results, a plate canted at this angle is expected to perform satisfactorily as a flare, and increasing the cant angle will improve performance even further.

### 4.4.3 Probability Analysis

The probability analysis indicates that the cant angle will be greater than 63°26' with a probability of 95%. In all cases, at least one plate will be canted at an angle greater than 54° 44'. Therefore, we conclude that the flare will perform satisfactorily also against the hard lunar surface model.

### 4.4.4 Conclusions

From the studies carried out, the feasibility of obtaining a satisfactory impact of the triorthogonal flare configuration on the lunar surface seems to be shown, no matter what the nature of that surface. Moreover, since the time scales for mixing and the amounts of lunar material mixed with the flares vary with the character of the lunar surface, this type of flare will apparently satisfactorily distinguish between at least the two extreme lunar surface models.

## Section 5
## DISCUSSION OF RESULTS

Detail discussion will be found in the individually reported sections; however, some of the salient points are summarily discussed herein.

### 5.1 EXPERIMENTS

The question of compatibility of flare structural materials with CTF has been answered to some degree in that massive aluminum of several types withstood the temperature and vibration environment expected for the flare. It must be remembered that dynamic structural similarity was not necessarily obtained; therefore, similar tests should be performed on the end item flare in the future to assure that accelerated corrosion rates of aluminum do not take place in a CTF environment. There also remains some developmental work in the seal area since several failures occurred during the testing.

The combustion test results have indicated several things fairly clearly, namely that a slightly aluminum-rich-mixture ratio gave the best performance, and when extrapolated to lunar flare size, it should give adequate light yield to be observed from earth. Also, the question of configuration has been answered to the extent that finely divided aluminum wool gave performance equal to that of powder, indicating that either could be used in at least two different ways in the practical design of a flare. The soil penetration tests, as well as some of the spectroscopic tests discussed later, confirm the fact that light yield decreases with an increase in depth (or soil dilution) which reemphasizes the importance of having a low areal-density flare to minimize this effect. The vacuum compatibility tests at Amoco were inconclusive since not enough successful tests were accomplished; however, as discussed later, the Douglas light-gas-gun tests in a low-pressure environment gave results consistent with the light-yield efficiency of the Amoco air tests.

Results obtained in the light-gas-gun impact tests indicate that flare initiation does occur when impacting a hard or soft target at lunar impact speeds. These results are, however, limited to a single model configuration and the soft target evidence is limited to fastax photographs and spectrographic results, since an electrical failure prevented taking photometric data on that one test. The light yield obtained in the hard impact test is comparable with the light yield obtained in static tests and indicates a good efficiency for the conversion of chemical energy to light energy (approximately 1/2%). Since this efficiency is comparable to the efficiency achieved in static tests, it is evident that there was nearly complete combustion of the reactants in the impact tests and that the reactants remained in the vicinity of the impact for the duration of the flare. The assignment of a temperature to the flare is somewhat meaningless because the radiation is not characterized by a graybody distribution except possibly between 4500Å and 6500Å. Considering just this region the peak temperature appears to be quite high--roughly 5000°K. A comparison of the fastax sequences indicate that physical structure, i.e., hard and soft targets, is discernible because of impact flash duration differences. The theoretical impact analysis discussed later, confirms this point.

It has been proven that the light-gas-gun/ballistic range facility can be used to effectively simulate flare impact. By performing tests in this facility it is possible to duplicate actual lunar impact velocities. Also tests can be performed at low-ambient pressures. In addition, various flare configurations can be tested. Also, projectiles containing CTF can be launched without detrimental effects.

The spectroscopic tests indicate a fairly-high degree of soil involvement and considerable excitation of soil constituents by a near stoichiometric-mixture-ratio of finely divided aluminum and CTF under low-ambient pressures. Differentiation between calibration shots and soil shots is easily made as well as between soils, indicating clearly the feasibility of the concept based on this one series of tests. Part of this same series was to evaluate the effect of soil dilution upon light intensity and the three gabbro shots do clearly establish that increasing soil involvement does decrease the intensity of the flare. Even though photometric data were not required for this series, there was sufficient

light emitted from all reactions to obtain interpretable spectrograms. It was also observed that the light emitted during each of these shots which were conducted in broad daylight, was bright enough to penetrate the heavy black material covering the vacuum chamber.

## 5.2 ANALYSES

Based upon an extrapolation of experimental data, there is sufficient light to enable the lunar flare to be detected above the relatively constant background intensity. Spectroscopic observation of the event using direct photographic techniques appears feasible and could be accomplished with some modification to existing instrumentation. Other types of measurements are also feasible but require new instrumentation. In the case of electronic instrumentation, the signal-to-noise ratio is entirely adequate. The measurements that can be made in addition to direct spectroscopy are:

1. Time resolved photometric recording in fixed spectral intervals.
2. Time resolved photometric recording of the total radiation.
3. Spectroscopic recording which utilizes an image intensifier technique to ensure adequate exposure in the event of a low intensity flare.

At least five observatories, located throughout the southwest U.S., will be needed to observe the event. The interest which several astronomers have expressed in observing the event indicates that at least this many observatories could be available, and it appears further that some of the largest telescopes could be used.

The function of predicting where and when the flare would impact the lunar surface would be performed by the Deep Space Net. This prediction can be made with sufficient accuracy using existing equipment consequently modifications to improve accuracy are not warranted for this program.

The several questions surrounding the actual impact event, relating to optimum payload design, probable distribution of the chemically reactive materials and the nature and extent of the mixing of the flare materials have been analyzed by high-speed computer methods. The results indicate that the triorthogonal configuration has the greatest probability of successfully meeting all the requirements of near-surface reaction against both hard and soft targets. The light-gas-gun test results also confirm the findings of this theoretical analysis.

# Section 6
# CONCLUSION

The ELF concept is feasible insofar as it can be determined from the limited scope and extent of this study.

## Section 7
## RECOMMENDATIONS

Since the scope of the ELF feasibility study was limited to some extent, the following recommendations are made for additional studies which would increase the confidence level and the probability of success of the program:

1. Additional impact analysis should be carried out to determine the impact phenomena due to edge-on collision of a jack-type projectile with a hard lunar surface.
2. A radiation transmission evaluation of the expected lunar flare should be made to determine the degree of absorption and transmission that occurs during combustion and expansion of the products in a vacuum.
3. Investigate the effects of the required lunar-lighting conditions (new moon or old moon) and of the relative location of the cooperating observatories with respect to the launch site on the earth-lunar flight mechanics for a thrust-augmented Delta from AMR and also determine the sensitivity of the trajectories considered to various possible errors (vector velocity, launch time, etc.).
4. Undertake a statistical investigation to establish the total probability of impacting the lunar surface within the desired area, taking into account defilade effects. This would also involve studying the statistical effects of adding a mid-course correction to the system.
5. Undertake additional study of the feasibility of special photometric and spectrographic recording equipment to be used in the cooperating observatories.
6. Test additional small size experimental flares under closely controlled configuration and instrumentation restraints to establish the reproducibility of test results in air.
7. Test additional small size experimental flares under closely controlled configuration and instrumentation restraints to establish the luminosity and light yield to be expected at different levels of vacuum.
8. Fire the best model simulations of the actual lunar flare in the Douglas Aeroballistic range using the 3-1/2 in. gun in order to obtain more information concerning initiation on impact, efficiency of combustion, and efficiency of light yield in relation to three different simulated lunar soil porosities.
9. Experimentally determine the velocity of sound and bulk modulus of chlorine trifluoride.

10. Attempt to accelerate simulated lunar surface material to collide with a model flare by the line-wave-generator (mousetrap) method in order to obtain impact initiation and penetration information on a better simulation of the actual lunar flare.

11. Undertake an analytical and experimental study of the factors influencing the initiation of the aluminum-chlorine trifluoride reaction. The factors to be studied include the effects of different degrees of containment, the configuration of the reactive aluminum, and the conditions under which various initiation devices (such as contaminants) operate satisfactorily.

12. In connection with the reproducibility tests formerly mentioned, investigate the use of actinometry to define the amount of energy which the chemical reaction radiates in the violet and ultraviolet ($\lambda < 4300$Å).

13. Perform detailed analysis of spectrograms, taken both from previous experiments and during this follow-on phase, in order to identify atomic and molecular spectra and relative abundance of products.

14. Make formal contacts with astronomers in various specific observatories in the southwestern United States in order to begin a definition of the specific observational problems associated with each ELF-candidate telescope.

15. Coordinate with personnel of the Goldstone tracking facility to ensure that the communication link with the observatories is properly implemented.

It is further recommenced that NASA implement plans for an ELF flight-demonstration program as soon as possible.

Appendix

# PRELIMINARY ANALYSIS OF LUNAR SURFACE CHARACTERISTICS FOR THE ELF FEASIBILITY STUDY

## A. 1 INTRODUCTION

The purpose of this study is to present current thinking as to the physical and chemical nature of the lunar surface for use in the Early Lunar Flare (ELF) feasibility study. Several possible surface models are outlined, and preliminary analyses are made of those which represent significantly different surface conditions.

Data and interpretations are presented in two sections. First, possible physical characteristics are outlined, and from these a representative range of surface models is selected. Particular models are then chosen for consideration during the ELF study on the basis of their presenting significantly different impact situations. Second, possible chemical characteristics are considered. Information is presented concerning the elements which may be present and detectable as well as elements whose detection would provide the greatest information as to the surface mineralogical composition. In addition, consideration is given possible surface models which represent significantly different chemical situations.

The lunar surface is by no means homogeneous either laterally or in depth. Therefore, each surface model presented in this study must be considered to represent a crude and highly oversimplified estimate of the conditions which may exist over some unknown fraction of the lunar surface. The models presented are not equally likely to represent lunar conditions. However, since none can presently be excluded, it is necessary to consider all, at least initially, in the determination of the ELF feasibility.

A number of somewhat exotic hypotheses as to nature of the lunar surface have appeared from time to time. These include such concepts as the presence of subsurface ices, carbides, organic material, and free radicals. These possibilities are not specifically considered since the range of physically different impact situations treated should bound any effects produced by the presence of such materials. However, some of these possibilities are noted, for obvious reasons, in the second section where the chemical characteristics of the lunar surface are considered.

## A.2 PERTINENT PHYSICAL CHARACTERISTICS

The visible lunar surface is believed to be composed primarily of granular material and/or of slag-like highly porous rock. Only a relatively small amount of material having a bulk density comparable to that of normal terrestrial rock can be exposed at the surface, though such material is likely to predominate at some unknown depth.

Investigators championing the granular model agree upon little else. Estimates of the average grain size range from a few microns to a few hundred microns or so. Estimates of the layer thickness range from a few millimeters to a kilometer. The porosity of the layer is generally believed to be high, perhaps in excess of 90% at the surface, with the porosity decreasing with depth. It is believed that this surface layer is underlain directly by a poorly-sorted mixture of rock fragments, by highly fractured incompetent rock, by competent rock, by a highly porous material, or by some combination of these. In the granular layer itself the grains are thought to exist in three forms: (1) an unbonded state where the only mutual attraction is due to weak Vander Waals' forces, (2) in a bonded state produced by the deposition of sputtered material or material vaporized during meteorite impact, or (3) in a bonded state produced through the action of normal atomic bonding forces.

Investigators championing the slag model believe the slag to be formed by the cooling in vacuo of molten material produced primarily during meteorite impact. They believe the surface and near surface material to be highly vesicular, with a porosity possibly in excess of 90%. The porosity is expected to decrease with depth, with the slag-like material grading eventually into competent rock.

A number of hypotheses concerning the possible behavior of the lunar surface have been formulated. These range from predictions that the surface is so tenuous that any solid object placed or impacted upon it would penetrate to great depth, to predictions that the surface should pose no particular bearing problems. It should be noted that most investigators favor the latter case.

A representative cross-section of the various surface models covering the range of postulated surface behavior is given in Table A-1.

In this feasibility study it is desirable to choose a set of surface models which will cover the range of possible lunar surface conditions and which also can be used for experimental and theoretical studies. Of particular interest is the choice of models which represent significantly different impact situations. Four criteria are suggested as the basis for choosing the pertinent surface models:

1. Depth and time of penetration and deceleration history.
2. Amount of surface material involved in flare reaction.
3. Amount and characteristics of ejecta (important as regards observation of flare).
4. Degree of burial by surface material (also important as regards observation of flare).

### A. 2. 1 Penetration

At the expected lunar impact velocity the only physical parameter determining the impact behavior, insofar as depth and time of penetration, and deceleration history are concerned, is bulk density (or porosity). Thus, the extreme models for penetration are model D and those models in which an $\approx 90\%$ porosity extending to depth is assumed, in particular Models A and B (fine grained). Model B, (fine grained) has been proposed by Gold and Hapke (Cornell University). They have made estimates, based in part upon laboratory experimental data, of the bulk density (and porosity) to be expected as a function of depth below the lunar surface. In doing this they have assumed

Table A-1

LUNAR SURFACE PHYSIC

| | Single Layer Models | | | |
|---|---|---|---|---|
| | A | B | C | D |
| Type Model | Porous Slag | Deep loose granular layer | Deep adhering granular layer | Competent roc covered by ne ligibly thin granular laye |
| Grain Size | --- | Fine, 1-50$\mu$ with average of $\sim 10\mu$, to coarse with average of $100\mu$ or greater | Same as B | --- |
| Grain Shape | --- | Generally irregular | Same as B | --- |
| Porosity | Possibly greater than 90% at surface decreasing with depth | Same as A if fine grains but only $\sim$ 60-70% at surface if coarse grains | Same as B or less | Small except i thin surface covering laye |
| Bearing Capacity | Low, some sinkage | Very low if fine grained to medium if coarse grained | Low to medium | Very high |

CAL MODELS

| | Multiple Layer Models | | |
|---|---|---|---|
| | E | F | G |
| ck g- r | Loose granular (< 1 meter) grading into rock fragments and competent rock | Cemented granular (< 1 m.) grading into rock fragments and competent rock | Slag (< 1 meter) over competent rock |
| | Same as B in granular layer | Same as E | --- |
| | Same as B in granular layer | Same as E | --- |
| n r | Same as B in granular layer; porosity of lower layer dependent on type of material present | Same as E | Same as A in slag layer; small in rock layer |
| | Low to medium but with good support given by underlying layer and no excessive sinkage | Low to medium with underlying good support | Low with underlying very good support |

an $\approx$ 1-50$\mu$ grain diameter, with the average size being $\approx 10\mu$ and a material density of 3.5g $cm^{-3}$. Their data are as follows:

| Depth (cm) | Porosity (%) | Bulk Density ($g/cm^{-3}$) |
|---|---|---|
| 0 | 90 | 0.35 |
| 1 | 89 | 0.38 |
| 10 | 86 | 0.49 |
| 100 | 80 | 0.70 |
| 500 | 73 | 0.94 |
| 1000 | 70 | 1.05 |

No such calculations have been performed for Model A. However, for this model, the porosity should decrease with depth at least as fast as given in this table. For Model D the bulk density can be considered to be about the same as the material density ( $\cong 3.5$ $g/cm^{-3}$).

A.2.2 Surface Materials

The minimum amount of mixing between surface and flare material will probably occur for Model D. The maximum amount of mixing will probably occur for Model B (fine grained) though other models may approach or equal this model.

A.2.3 Ejecta

From the studies conducted by NASA Ames and others it appears that more ejecta are emitted from impacts into granular than bulk material. However, the precise effects of porosity, grain size and degree of bonding upon the amount and behavior of ejecta are not known. Due to this uncertainty we consider two separate possibilities, as follows:

1. If penetration for Model B (fine grained) is not excessive then the minimum amount of ejecta would be produced from Model D. (Model B (fine grained) would then produce the maximum amount with possibly Models C, E and F producing comparable amounts. Model B (fine grained) would present as serious a case as any since the bulk of the ejecta would be composed of grains of size approaching the wavelength of visible light).
2. If penetration for Model B (fine grained) is excessive this model would produce the minimum amount of ejecta. Models such as B (coarse grained), E and F in which either the porosity is significantly less than 90% or the surface material is underlain by a more competent sublayer could provide maximum ejecta.

Though uncertainty exists as to which case may be applicable, both can be covered to a reasonable degree by studying Models B (fine and coarse grained) and D.

### A.2.4 Burial

Maximum burial should occur for Model B (fine grained) with Model A falling close to this. Minimum burial should occur for Model D.

The results of this discussion are given in the following table. The double arrows indicate surface models which may be roughly equivalent.

| | Penetration | Mixing | Ejecta | Burial |
|---|---|---|---|---|
| Upper Extreme | A ⟷ B (fine) | B (fine) others? | B (coarse) ⟷ C, E F or B (fine) | B (fine) |
| Intermediate | E, B (coarse) | E | --- | B (coarse) |
| Lower Extreme | D | D | D or B (fine) | D |

It can be seen from this table that to obtain a reasonable certainty that the extreme impact situations are covered in the ELF feasibility study only Models B (fine grained), B (coarse grained) and D need be investigated (Model B (coarse grained) needs to be considered only as regards ejecta).

## A.3 PERTINENT CHEMICAL CHARACTERISTICS

Chemical models of the lunar surface representing the range of current thought are given in this section. Preliminary analysis of these models is made to determine those which represent significantly different cases insofar as elemental composition is concerned. In addition, note is made of those elements whose detection could provide the greatest amount of information as to the surface and near surface mineralogy.

In this preliminary study, average elemental compositions are used for all models. Considerable compositional variations can be expected within each model listed, especially for those representative of terrestrial igneous and sedimentary rocks. Meteorites are somewhat less variable in this respect,

and the tektites appear to be least variable of all. Obviously the use of average compositions has serious drawbacks, particularly since the ELF will represent essentially a "point" sampling and there is no reason why the surface composition at this point need represent an "average" composition. However, the use of average compositions is of value, particularly during the initial feasibility studies, in presenting the elements which may or may not be present, and in indicating approximately the relative abundances of these.

In the tables to follow, representing the possible surface models, the numerical values given are the weight percentages of the oxides and, in parentheses following, of the elements. Trace elements are not listed because the chance of their being detected through use of the ELF is much less than that of major elements. Moreover, they have less diagnostic value than do the major elements.

A number of investigators believe that the lunar surface is composed primarily of material analogous to terrestrial igneous rock. Table A-2 gives the composition of various terrestrial igneous rocks. Most of these investigators favor the ultrabasic (peridotite) to basic (basalt) composition though some believe differentiation may have occurred to the extent that intermediate (diorite) and/or acidic (granite) rocks are present. The average igneous rock column shown is not an average of the four preceding columns but represents a long-accepted estimate of the average composition of the outer ten miles of the earth's crust. It is very close to being one part average granite to one part average basalt and could represent lunar surface composition if only a small to moderate amount of differentiation has occurred.

Other investigators believe the lunar surface to be of meteoritic composition. The average meteorite composition is shown in Table A-3. It approximates that of chondrites which are estimated to make up over 80% of all meteorites. Note that the chondrites (and achondrites also), though usually thought of as stones, do commonly contain a significant proportion of nickel-iron and troilite phases and therefore cannot be regarded as pure silicate phase. The division of the average meteorite into the three phases shown in the table is probably most convenient for the purposes of the study. However, the three phases are not necessarily to be associated with particular classes of meteorites;

Table A-2

TERRESTRIAL IGNEOUS ROCKS

| Oxide (Element) | | Granite (Acid) | Diorite (Intermediate) | Basalt (Basic) | Peridotite (Ultra-basic) | Average Igneous |
|---|---|---|---|---|---|---|
| $SiO_2$ | (Si) | 71.6 (33.4) | 55.5 (29.9) | 14.1 (22.9) | 42.0 (19.6) | 59.4 (27.7) |
| $Al_2O_3$ | (Al) | 14.5 ( 7.7) | 17.0 ( 9.0 | 15.7 ( 8.3) | 4.7 ( 2.5) | 15.4 ( 8.2) |
| $Fe_2O_3$ | (Fe) | 1.5 ( 1.1) | 2.7 ( 1.9) | 5.4 ( 3.8) | 8.1 ( 5.7) | 3.1 ( 2.2) |
| FeO | (Fe) | 1.1 ( 0.9) | 4.8 ( 3.7) | 6.4 ( 5.0) | 5.6 ( 4.4) | 3.3 ( 2.6) |
| MgO | (Mg) | 0.9 ( 0.5) | 4.4 ( 2.6) | 6.2 ( 3.7) | 25.5 (15.3) | 3.5 ( 2.1) |
| CaO | (Ca) | 2.0 ( 1.4) | 7.3 ( 5.2) | 9.0 ( 6.4) | 6.4 ( 4.6) | 5.1 ( 3.6) |
| $Na_2O$ | (Na) | 3.0 ( 2.2) | 3.6 ( 2.7) | 3.1 ( 2.3) | 0.8 ( 0.6) | 3.8 ( 2.8) |
| $K_2O$ | (K) | 4.1 ( 3.4) | 2.4 ( 2.0) | 1.5 ( 1.2) | 0.2 ( 0.2) | 3.1 ( 2.6) |
| $H_2O$ | (H) | 0.8 ( 0.1) | 0.9 ( 0.1) | 1.6 ( 0.2) | 6.4[b] ( 0.7)[b] | 1.2 ( 0.1) |
| Other oxides | | 0.5 | 1.4 | 2.0 | 0.4 | 2.1[c] |
| | (O)[a] | (48.8) | (45.5) | (44.2) | (46.1)[b] | (46.0) |
| Total | | 100.0 | 100.0 | 100.0 | 100.0 | 100.0 |

[a]Does not include O in "other oxides."

[b]Probably in error; more likely 1-2% $H_2O$ at most. Therefore, H 0.1-0.2%, O 41.3-42.2%

[c]Includes trace C (0.03%).

Table A-3

METEORITES

| Oxide (Element) | Average Silicate Phase | Average Troilite Phase | Average Nickel-Iron Phase |
|---|---|---|---|
| $SiO_2$ (Si) | 35.3 (16.5) | | |
| $Al_2O_3$ (Al) | 2.9 ( 1.5) | | |
| $Fe_2O_3$ (Fe) | 0.1 ( 0.1) | | |
| FeO (Fe) | 13.0 (10.1) | | |
| MgO (Mg) | 19.7 (11.8) | | |
| CaO (Ca) | 2.6 ( 1.9) | | |
| $Na_2O$ (Na) | 0.8 ( 0.6) | | |
| $K_2O$ (K) | 0.2 ( 0.2) | | |
| FeS (Fe) | | 7.4 (4.7) | |
| (S) | | (2.7) | |
| Fe (metallic) | | | 14.0 |
| Ni (metallic) | | | 1.3 |
| Others | 2.3[b] | 0.3[c] | 0.1[d] |
| (O)[a] | (31.9) | | |
| Total | 76.9 | 7.7 | 15.5 |

All three phases:

Total Fe: 28.9%

Total Ni: 1.6%

[a]Does not include O in oxides of "others."

[b]Ti, Mn, P, Ni, Cr, Co; in part as oxides.

[c]Mn, P, Ni, Cr, Co.

[d]Co.

the composition of each phase is calculated from its composition and abundance in all meteorite classes.

According to some students of the moon, the tektites are objects blasted from the lunar surface as a result of meteorite impacts. Their composition may, therefore, represent that of the lunar surface. The average tektite composition is shown in Table A-4. The single set of values given is probably truly representative of this material since tektites do not show great chemical variation despite their occurrence in widely scattered areas of the earth.

Table A-4
TEKTITES

| Oxide (Element) | | Average[a] | |
|---|---|---|---|
| $SiO_2$ | (Si) | 74.4 | (34.7) |
| $Al_2O_3$ | (Al) | 13.1 | ( 6.9) |
| FeO[b] | (Fe) | 4.5 | ( 3.5) |
| MgO | (Mg) | 2.1 | ( 1.3) |
| CaO | (Ca) | 1.9 | ( 1.4) |
| $Na_2O$ | (Na) | 1.3 | ( 1.0) |
| $K_2O$ | (K) | 2.1 | ( 1.7) |
| Other Oxides | | 0.9 | |
| | (O)[c] | | (48.9) |
| | Total | 100.3 | |

[a]Based on averages of 10 moldavites, 2 bediasites, 38 tektites from the Southeast Asia and Malaysia fields, 9 australites, and 3 Ivory Coast Tektites.

[b]All Fe Calculated as FeO.

[c]Does not include O in "other oxides."

At least one recent theory holds that the lunar maria may consist of sediments deposited in oceans that once existed on the moon. To allow for this possibility the compositions of the common terrestrial sedimentary rocks are shown in Table A-5. These are probably the least applicable to the ELF study, not only because the hypothesis is more improbable but also because such sediments, even if they exist may not resemble those of the earth.

## A.4 CONCLUSIONS

The following comments are in order:

1. In all cases the elements of importance number no more than twelve; in many cases fewer than this. Differences in rock type are therefore expressed as changes in relative proportions of a small group of elements rather than as the presence or absence of certain key elements. Oxygen is the most abundant element, silicon is next (except for the average meteorite, as noted in the next comment). For the most probable lunar surface rocks these two elements can be expected to make up the bulk of the constituents--almost 50% of the average meteorite and 60% to over 80% of the others.
2. In the average meteorite, iron is the second most abundant element, being almost equal to oxygen, the two together making up some 60% of the constituents. However, the silicate phase recalculated to 100% is nearly identical to peridotite; in fact, the average meteorite can be regarded as ultra-basic igneous rock diluted with iron. Thus, should the ELF impact an area of the moon composed largely of the silicate phase, meteorite and ultra-basic would be indistinguishable. The two can be distinguished chiefly by the iron content in meteorite compositions close to the average, or with more plentiful nickel-iron and troilite phases.
3. The various stages of differentiation in the igneous rock series are characterized by clear and distinct chemical changes. In going from ultra-basic to acidic there is an increase in silicon, potassium and oxygen and a decrease in iron, magnesium, and, except for a reversal in the ultra-basic end, calcium.
4. The average tektite is very similar to the average granite. It contains somewhat more iron and magnesium and somewhat less sodium and potassium than the granite. This difference is not great enough to distinguish the two on the basis of the ELF results but may be of significance in the experimental materials used in the feasibility study. There is also a difference in water content, the tektites containing much less than 0.1% water on the average, but this difference is probably not detectable in the ELF project. It should also be pointed out that, again except for water, tektites are close in composition to some common terrestrial sandstones which differ significantly from the average sandstone shown in Table A-5.

Table A-5

TERRESTRIAL SEDIMENTARY ROCKS

| Oxide (Element) | | Average Shale | Average Sandstone | Average Limestone | Average Sediment[a] |
|---|---|---|---|---|---|
| $SiO_2$ | (Si) | 58.1 (27.1) | 78.3 (36.5) | 5.2 ( 2.4) | 58.0 (27.1) |
| $Al_2O_3$ | (Al) | 15.4 ( 8.2) | 4.8 ( 2.5) | 0.8 ( 0.4) | 13.4 ( 7.1) |
| $Fe_2O_3$ | (Fe) | 4.0 ( 2.8) | 1.1 ( 0.8) | 0.5 ( 0.4) | 3.5 ( 2.5) |
| FeO | (Fe) | 2.5 ( 1.9) | 0.3 ( 0.2) | -- -- | 2.1 ( 1.6) |
| MgO | (Mg) | 2.4 ( 1.4) | 1.2 ( 0.7) | 7.9 ( 4.7) | 2.7 ( 1.6) |
| CaO | (Ca) | 3.1 ( 2.2) | 5.5 ( 3.9) | 42.6 (30.4) | 5.9 ( 4.2) |
| $Na_2O$ | (Na) | 1.3 ( 1.0) | 0.5 ( 0.4) | 0.1 ( 0.1) | 1.1 ( 0.8) |
| $K_2O$ | (K) | 3.2 ( 2.7) | 1.3 ( 1.1) | 0.3 ( 0.2) | 2.9 ( 2.4) |
| $H_2O$ | (H) | 5.0 ( 0.6) | 1.6 ( 0.2) | 0.8 ( 0.1) | 3.2 ( 0.4) |
| $CO_2$ | (C)[b] | 2.6 ( 0.7) | 5.0 ( 1.4) | 41.5 (11.3) | 5.4 ( 1.5) |
| Other oxides | | 2.3[d] | 0.5 | 0.2 | 1.9[e] |
| | (O)[c] | (49.0) | (51.9) | (49.7) | (49.0) |
| Total | | 99.9 | 100.1 | 99.9 | 100.1 |

[a]Based on approximately 80% shale, 12% sandstone, 6% limestone.

[b]C in $CO_2$ only.

[c]Does not include O in "other oxides.

[d]Includes 0.8% C.

[e]Includes 0.7% C.

5. The sedimentary rocks differ from the igneous rocks chiefly in having less sodium and more carbon and water. The low sodium is due to the fact that in the geochemical cycle of rock breakdown the sodium is retained in the sea and not completely returned to the sediment. The higher carbon content is due to life-derived organic matter and limestone. The increased water results from the formation of hydrated and OH-bearing minerals in the course of weathering, transportation, and deposition; some is also present in organic hydrocarbons. Thus, the differences are the result of the presence on earth of oceans, rivers and atmosphere, and for this reason the sediments are the lease likely of the groups shown in the tables to occur on the moon. In any case, except for these differences, the average sedimentary rock is very close in composition to the average igneous rock inasmuch as terrestrial sediments are derived ultimately from the breakdown of igneous rocks. Note that the average shale, too, is similar to the average igneous rock; it is estimated to be the most abundant sediment type and hence dominates the average.

6. Water content is very low in all groups except the sediments. Because of the abundance of oxygen, water must be detected by measurement of hydrogen, the weight percentage of which is almost an order of magnitude lower than that of molecular water. An exception to this is one type of carbonaceous chondrite, in which water contents of as much as 20% were measured. However, carbonaceous chondrites of all types are rare on earth, and, in addition, it is possible that much if not all of this water was picked up in the terrestrial environment rather than being indigenous to the meteorites. It is probably safest to count on very little water being present in material of meteoritic composition.

   Possible lunar sources of water are surface ice in permanently shadowed zones, subsurface deposits probably in the form of ice, ice-filled fissures or cracks near the surface, and OH- and water-bearing minerals. However, none of these sources are likely to contribute water to the flare. Permanently shadowed zones with surface ice, if they exist at all, can exist only in the polar regions, whereas impact will occur in a near-equatorial zone. Subsurface deposits can contribute only if they are shallow enough to be within the penetration and excitation depth of the flare and if they exist essentially at the point of impact. Depths, of course, are unknown and could be within that of the impact. And the areal proportion of the ice-filled fissures, if they exist, will be low. The low water content of the rocks shown in the tables (excluding the sediments) shows that primary OH- and water-bearing minerals do not contribute significantly in this regard. For example, the micas and amphiboles, the major OH-bearing mineral species of igneous rocks can comprise as much as 20% of the rock (although commonly it is less than this) but contain only some 2% of water by weight. Secondary minerals, such as serpentine, the zeolites, and the clay minerals, contain more water--in the range of 10% to 20%--but are formed in the terrestrial environment by hydration due to weathering ground water circulation, and hydrothermal alteration, processes that probably do not occur on the moon. In summary, ELF should

be designed on the assumption of very low water content of the lunar surface materials.

7. In one recent study it has been estimated that organic matter could have been formed in the past and could still exist on the moon. Organic matter can be detected in the ELF project mainly by measurement of carbon abundance, although other elements, such as hydrogen, oxygen, nitrogen, and sulfur, would be present. Carbon is virtually absent in all the groups listed in the tables except the sediments, in which case its presence (to the extent of about 1% to 2%) is due to organic activity. Again, the carbonaceous chondrites are an exception in that they may contain up to 3.5% but, as has been mentioned, they are extremely rare on earth and presumably as rare on the moon. In the study it is estimated that as much as 10 $gm/cm^2$ of organic matter could have been formed on the moon and could be localized at a depth of a few tens of meters. This may well be below the depth of impact of the ELF payload. However, if mixing has occurred as a result of meteorite impact, this 10 $gm/cm^2$ of organic matter may be dispersed through the lunar surface material to a depth not exceeding a few tens of meters, according to the study. In this case, if a depth as little as 10 meters and a bulk density of the lunar surface material as low as 0.3 $gm/cm^3$ are assumed, a maximum of (10 x 100)/(0.3 x 1000) = 3% of organic matter can be present. Presumably this would be in the form of carbon compounds of unspecified composition but perhaps 1% or so could be estimated for the maximum carbon content if organic matter is present under the conditions set forth in the study. This is within the range of sedimentary rocks and also well within the range of the carbonaceous chondrites so that the carbon measurement might not unambiguously demonstrate the presence of organic matter. Hydrogen, because of its low atomic weight, would constitute a smaller proportion than carbon. The presence of nitrogen, especially in combination with carbon and hydrogen, would strongly indicate organic matter, but its proportion by weight would be enough less than that of carbon to make detection difficult if not impossible. Oxygen and sulfur, of course, are present in the rocks and meteorites and are not unique to organic matter. Therefore, it is unlikely that under the conditions assumed in the study this 3% of organic matter can be observed in the ELF experiment.

8. Loss of atoms can occur as the result of sputtering by low energy solar particles if these particles can strike the surface. This process may or may not affect the composition of the lunar surface materials as measured in the ELF experiments, depending upon the degree to which accretion and mixing rates counter-balance that of sputtering. Data from sputtering experiments point to rates such that some 17 cm of thickness may have been lost from the surface of the moon since its origin. These data also indicate that oxygen may be removed preferentially, leaving the surface enriched in cations. Thus, if no material is assumed to have been added to the lunar surface during the lifetime of the moon the zone of enrichment could extend no more than a few atom layers in depth and the change in composition would be negligible. At the other extreme, if the rate

of accretion of new material is assumed to have just balanced the rate of oxygen removal, the cation-enriched zone could attain a thickness of about 17 cm. This is a maximum figure, and since such a perfect balance of rates is highly improbable a more reasonable estimate may be in the neighborhood of 8 to 10 cm. Therefore, if the depth of impact and excitation of the ELF payload is large compared to this, say of the order of one meter or more, the composition change would be negligible. For shallower depths, however, the cation abundances would increase relative to that of oxygen, but in this case the relative proportions of the cations would remain about the same as in the parent rock provided the cation sputtering rates are not too different one from the other.

9. Other processes that may affect the composition of the surface materials are metamorphism, meteor slag formation, and medium to high energy solar and cosmic radiation. None is likely to alter significantly the compositions listed in the tables. Terrestrial metamorphic processes generally involve redistribution of the chemical elements of the rock so that new minerals are formed at the expense of the old without greatly changing the bulk chemical composition. The local melting involved in the formation of slag, as envisioned by the meteor slag theory, would possibly also result in change of mineral facies but no great change in bulk chemical composition. Some volatiles may be lost in the process but the compositions shown in the tables are also essentially volatile-free. Solar and cosmic rays of medium and high energy have been estimated to affect at most a very thin layer of the surface--insignificant from the point of view of the ELF.

## A.5 SUMMARY

The chemical elements of highest abundance are estimated to be oxygen, silicon, iron, aluminum, magnesium, and calcium. Those of greatest diagnostic value are silicon, iron, magnesium, calcium, and potassium for distinguishing rock types, hydrogen for detecting water or water-bearing materials, and carbon and nitrogen for detecting organic matter. These tables and comments are intended as guidelines for initiating the compositional aspects of the ELF study.